POLITECNICO DI MILANO

Department of Civil and Environmental Engineering

Doctoral Programme in Environmental and Infrastructure Engineering

XXXV Cycle - 2023

IMPACTS OF CLIMATE CHANGE ON HYDROLOGICALLY DRIVEN PASTURE DYNAMICS IN MOUNTAIN CATCHMENTS

Supervisor and Tutor:

Prof. Daniele Bocchiola

The Chair of the Doctoral Programme:

Prof. Riccardo Barzaghi

Doctoral Dissertation of:

Francesca Casale Matr. 940423

ABSTRACT

The aim of this thesis work was the assessment of the potential effects of climate change upon the productivity of pasture in Italian Alps, focusing on Valtellina valley and the Gran Paradiso National Park in Valle d'Aosta region. To do so, some agro-climatic indices, related to climate and water availability, were introduced to summarize the effects. A pasture model *Poli-Pasture* was developed here as module of the existing hydrological model *Poli-Hydro*, and it was used for the simulation of plants growth. Two different configurations in pasture modelling were used for the two case studies. *Poli-Pasture* was corrected for the case study of Gran Paradiso National Park with a module, based on *CoSMo* model, for the simulation of inter-specific competition.

Starting from the information of collected samples in the study areas in fulfilment of the IPCC MOUPA project, some species were chosen, among the most abundant in Italian pastures, as reference for the simulation of pasture productivity. In particular, *Trisetum flavescens* and *Nardus stricta* were considered as index species in Valtellina valley, in a low altitude belt and in a high altitude one respectively, while *Trifolium alpinum*, *Dactylis glomerata, Nardus stricta* and *Festuca rubra* were considered representative of the pasture community in Gran Paradiso National Park, in the same altitude belts (here two species for altitude belt).

After the calibration of the model and the simulation for the present period, the model was used, for both cases, to project pasture productivity until the end of the XXI century, using the scenarios of the Fifth and Sixth Assessment Reports of IPCC, and considering a large number of global circulation models, specifically 3 for AR5 and 6 for AR6.

In response to the increase of temperature, the model projected a potential increase of pasture productivity, with some exceptions in low altitudes, in particular in Valtellina valley (until -31% for AR5 under 1100 m asl in the period 2041-2050). In Valtellina valley under AR5 the increase of total productivity is projected between +38% and +173% respectively for RCP 2.6 at the middle of the century (2041-2050) and RCP 8.5 at the end of the century (2091-2100), while under AR6 the increase ranges between +62% and +210% for SSPs 2.6 and 8.5 at the end of the century. In the area of Gran Paradiso National Park under AR6 the increase of annual productivity ranges between +81% and +116% for SSP 7.0 at the middle of the century and SSP 8.5 at the end of the century. Here in low altitude belt the variation is contained, while in high altitude belt it is considerable. A large percentage increase does not correspond to a large increase in absolute value, considering an average fresh biomass productivity of 6.5 t/ha (12.9 t/ha in low altitude belt and 1.9 in high altitude belt) in Valtellina valley and of 3.6 t/ha (6.5 t/ha

in low altitude belt and 3.5 t/ha in high altitude belt) in Gran Paradiso area during the present period.

The large expected evapotranspiration demand in future was satisfied in practice in Valtellina, notwithstanding the decrease of precipitation, thanks to a better use of water availability. Differently, in Gran Paradiso area the lack of water availability from precipitation and snow melt could be a limitation to growth.

The result of the inter-specific competition simulation shows a larger presence of *Trifolium alpinum* (55%-59%) in low altitude belt and of *Nardus stricta* (71%-74%) in high altitude belt. In the future this condition will be exacerbated thanks to the better resistance of these species to high temperatures and drought conditions. Each species has a different nutritional value, so the general increase of biomass productivity is not related to an improvement of the value for pasture of bovines.

The results provide preliminary evidence of altitudinal shift of pasture lands and of potential livestock, and thereby economic development, in the valley at higher altitudes than now.

SINTESI

L'obiettivo di questo lavoro di tesi è l'analisi degli effetti potenziali dei cambiamenti climatici sulla produttività dei pascoli nelle Alpi italiane, in particolare in Valtellina e nel Parco Nazionale del Gran Paradiso, nella zona valdostana. Sono stati quindi introdotti alcuni indici agro-climatici, relativi alle condizioni climatiche e alla disponibilità idrica, per riassumere gli effetti. È stato utilizzato un modello con due diverse configurazioni nei due casi di studio. Per la simulazione della crescita vegetazionale, è stato sviluppato il modello *Poli-Pasture*, associandolo al modello idrologico già esistente *Poli-Hydro*. La modellazione pascoliva è stata eseguita con diverse configurazioni nei due casi di studio. *Poli-Pasture* è stato corretto nel caso studio del Gran Paradiso, con un modulo per la simulazione della competizione interspecifica, basandosi sul modello *CoSMo*.

Basandosi sulle informazioni raccolte dai campionamenti effettuati nell'ambito del progetto IPCC MOUPA, sono state scelte alcune specie, tra le più abbondanti nei pascoli italiani, come rappresentative per la comunità per la simulazione della produttività pascoliva. In particolare in Valtellina sono state utilizzate *Trisetum flavescens* e *Nardus stricta* rispettivamente per una fascia a bassa quota e una ad alta quota, mentre nel parco del Gran Paradiso sono state considerate *Trifolium alpinum* e *Dactylis glomerata* a bassa quota e *Nardus stricta* e *Festuca rubra* ad alta quota.

Dopo la calibrazione del modello e la simulazione nel periodo presente, il modello è stato utilizzato in entrambi i casi di studio per le proiezioni della produttività pascoliva fino alla fine del XXI secolo, utilizzando gli scenari del quinto e sesto rapporto di valutazione dell'IPCC e combinandoli con un considerevole numero di modelli di circolazione globale, in particolare 3 per l'AR5 e 6 per l'AR6.

In risposta all'aumento di temperatura le simulazioni mostrano un potenziale aumento della produttività, con alcune eccezioni a bassa quota in Valtellina (fino al -31% sotto i 1100 m slm per l'AR5 nel periodo 2041-2050). In Valtellina, per l'AR5, l'aumento potenziale di produttività totale varia tra +38% per il RCP 2.6 a metà secolo (2041-2050) e +173% per il RCP 8.5 a fine secolo (2091-2100), mentre per l'AR6 l'aumento va da +62% a +210% rispettivamente per gli SSPs 2.6 e 8.5 alla fine del secolo. Nell'area del parco del Gran Paradiso per l'AR6 l'aumento di produttività annuale varia tra +81% e +116% per il SSP 7.0 a metà secolo e il SSP 8.5 a fine secolo. Qui l'aumento a bassa quota è limitato, mentre è considerevole ad alta quota. L'aumento significativo in percentuale non corrisponde però ad un grande aumento in valore assoluto, considerando la produttività media nel periodo di controllo di 6.5

t/ha (12.9 t/ha a bassa quota e 1.9 t/ha ad alta quota) in Valtellina e di 3.6 t/ha (6.5 t/ha a bassa quota e 3.5 t/ha ad alta quota) nel parco del Gran Paradiso.

La grande richiesta evapotraspirativa in futuro viene in pratica soddisfatta in Valtellina, nonostante la riduzione delle precipitazioni, anche grazie ad un utilizzo più efficiente dell'acqua disponibile. Diversamente nell'area del Gran Paradiso talvolta la mancanza di disponibilità d'acqua risulta limitante per la crescita.

I risultati della simulazione della competizione inter-specifica mostrano una maggiore presenza di *Trifolium alpinum* (55%-59%) a bassa quota e di *Nardus stricta* (71%-74%) ad alta quota. In futuro queste specie saranno ancora più abbondanti grazie alla loro migliore resistenza a temperature elevate e a condizioni di siccità. Ogni specie ha però un diverso valore nutrizionale, quindi l'aumento complessivo di produttività non è collegato a un miglioramento del valore per il pascolamento dei bovini.

I risultati forniscono un'evidenza preliminare in futuro dell'innalzamento in quota delle aree pascolive, e uno sviluppo dell'allevamento a quote più elevate rispetto ad ora.

TABLE OF CONTENTS

FIGURE LIST

TABLE LIST

1   INTRODUCTION

Part of the work carried out in fulfilment of the thesis was developed under the umbrella of the project IPCC-MOUPA (*Interdisciplinary Project for assessing current and expected Climate Change impacts on MOUntain PAstures*), of Climate-Lab (the interdepartmental laboratory of Politecnico di Milano about climate change) in collaboration with Università degli Studi di Milano, funded by Fondazione Cariplo.

1.1   The IPCC MOUPA project

This project is focused on two study areas: one in Valtellina valley, specifically in the Dosdè valley, and the other one, Orvieille, in the area of Gran Paradiso National Park in Valle d'Aosta region.

The project is divided into six work-packages (WP). In general, the object of the project is to i) evaluate the past and present climatology of the study areas and project future climatic conditions, ii) model the pasture dynamics, iii) analyse the effects of climate change on the biodiversity and the fauna of pasture areas, iv) study the socio-economics effects of changes in pasture productivity, and v) define fragility indices to quantify the effects of climate change.

Figure 1: Logos of IPCC MOUPA project partners.

1.2 Climate change in mountain regions

Alpine regions are considered a hotspot for global warming; temperatures increased by +2°C since 1880, twice the global average (Rottler et al., 2019). This makes Alps particularly vulnerable to climate change, considering also the fragile equilibrium of the system and the existent anthropogenic and environmental pressures (Beniston & Stoffel, 2014).

Evidence of warming of alpine regions are related to glaciers retreat and to snow dynamics. In the last six decades the glaciers area was reduced of -30%, and recently the number of glaciers increased for the fragmentation of large glaciers into smaller ones (Baroni et al., 2015; D'Agata et al., 2020; Diolaiuti et al., 2011, 2012; Haeberli & Beniston, 1998). In the future a mass loss about 2 Gt of ice per year is expected (Paul et al., 2020). In the meanwhile the increase of temperature is causing a reduction of solid precipitation in winter and earlier snow melting in spring (Barnett et al., 2005). For these reasons changes in discharge occurred in the last century, in particular a shift of the peak runoff in earlier season, an increase of winter discharge above 1800 m asl (due to the increase of liquid precipitation instead of snowfall) and a decrease in spring and summer discharge (due to the reduction in snow cover and consequent snow melt and to the increase in evapotranspiration) (Bocchiola, 2014; Bocchiola et al., 2010; Soncini & Bocchiola, 2011).

Changes in runoff and snow cover timing and amount are affecting the hydrology of mountain and downstream areas, water resources exploitation for socio-economic purposes (i.e. hydropower production, agriculture, tourism) (Casale et al., 2021; Fuso et al., 2021), and alpine ecosystems.

In the alpine ecosystems, an important role is covered by pastures. In mountain areas, pastures and farming systems are paramount important activities for local communities, a source of income for local development, and a key feature of local ecosystems dynamics (Mazzocchi et al., 2018; Stendardi et al., 2022; Wanner et al., 2021). During 1990-2010, ca. 17% of the Italian alpine pastures were abandoned (Battaglini et al., 2014), with a consequent reduction of livestock animals (-30% during 1970-2000) (Battaglini et al., 2003). Only in Lombardia Region in the period 1970-2000, the 38% of the total pasture surface was lost (Boschetti et al., 2007).

Pasture management has positive effects on land sustainability, maintaining landscape and cultural value, supporting biodiversity and soil fertility, thereby reducing soil loss, and natural risks (Bellini, Moriondo, Dibari, Bindi, et al., 2023; Bernués et al., 2015; Dale & Polasky, 2007; Deléglise et al., 2019; Egarter Vigl et al., 2017; Gusmeroli, 2003). On the contrary, land abandonment brings about growth of shrubs, and grassland biodiversity loss,

increased erosion, wildfires and avalanches risk, loss of traditional productive activities and typical landscapes (Faccioni et al., 2019).

Modified climate and hydrology at high altitudes may influence soil moisture, vegetation growth, and in particular pasture dynamics, which heavily depends upon temperature and precipitation. Snow cover extent and duration also affect pasture growing seasonality, area availability and biomass (Van Der Wal et al., 2000; Zeeman et al., 2017). Higher temperature increases water demand, and possibly lower precipitation may lead to water stress (Addimando et al., 2015; De Silva et al., 2008). Pasture production, and growth rate may be influenced by extreme events, e.g. hot waves and intense precipitation (Cullen et al., 2009; Deléglise et al., 2019; Tubiello et al., 2007). So an uplift of Alpine pasture species is expected (Brunetti et al., 2009; Huber et al., 2013), and it may cause a loss of pasture/grassland habitats at the lowest altitudes, and habitat fragmentation (Briner et al., 2013; Dibari et al., 2020).

The expected change on the distribution and productivity of alpine grassland will affect ecological relationships between animal species, in particular between domestic and wild grazers for interference competition, and migration of birds and insects.

On the other hand, a correct management of pasture areas could mitigate soil deterioration related to over-grazing by livestock, cultivation of marginal soils and deforestation (Beniston, 2003).

1.3   An overview of the thesis work

For this thesis work these different aspects are evaluated. The study begins with the modelling of the pasture dynamics in two study areas: Valtellina Valley and Valle d'Aosta region. The modelling involves a hydrological model to simulate the soil water balance, coupled with a pasture model that considers both the conditions of a single index species for pasture and the inter-specific competition between pasture species. The hydrological model used here is the *Poli-Hydro* model, developed by Climate-Lab of Politecnico di Milano. The pasture model is called *Poli-Pasture* and it is developed specifically for this thesis work. *Poli-Pasture* initially considers a target species to simulate the pasture community, then it is modified and coupled with an adjustment of the *CoSMo* model, developed by Università degli Studi di Milano, to consider the interspecific competition. The two conditions and hypothesis of simulation are compared. After the calibration and validation of models, future projections are done considering different climate projections, developed by the coupling of different Global Circulation Model of the Fifth and the Sixth Assessment Reports of IPCC with the

Representative Concentration Pathways and the Shared Socio-economic Pathways of the correspondent Assessment Report.

The text is organized as follows: in the next chapter the state of the art of the pasture modelling is analysed, then in chapter 3 the study areas are presented, in particular Valtellina Valley and the area of Gran Paradiso National Park in Valle d'Aosta region; in chapter 4 utilized data for each study and in Chapter 5 all the developed models are reported; in that chapter the fragility indexes developed for the IPCC MOUPA project and the methodology to build climate projections are also presented; to conclude, in chapters 6 results and discussion are reported and in chapter 7 there is the conclusion of this work.

2 STATE OF THE ART KNOWLEDGE

Poli-Hydro is a hydrological model largely used by Climate-Lab of Politecnico di Milano for studies in high-altitude catchments to simulate the hydrological cycle (Aili et al., 2019; Bocchiola et al., 2018; Bombelli et al., 2019; Casale et al., 2020; Soncini et al., 2015, 2017; Stucchi et al., 2019). It is properly developed to simulate the cryosphere dynamic, using a T-index approach for the simulation of snow and ice melt and a specific tool for simulation of glaciers development and movement.

Poli-Pasture, developed here and already published, is a model for simulating grassland species growth. It is based on another model developed by Climate-Lab for the simulation of agricultural crop, namely *Poli-Crop* (Addimando et al., 2015; Bocchiola, 2015; Bocchiola et al., 2019; Nana et al., 2014). This is a simplified version of *CropSyst*, a widely used model for vegetation dynamic simulation, and the basis for a lot of other crop models (Stöckle et al., 1994).

In literature, a lot of models are available for the simulation of grassland dynamics, considering different matters, and with different levels of complexity. Moreover, the largest part of these models is used to simulate vegetation growth at the paddock level with a site-specific configuration. Few studies are available about the simulation of pasture dynamics in wide mountainous areas, and in particular in the Italian Alps, and for a long-term simulation. At the same time, it is difficult to find hydrological models that integrate a complete vegetation dynamics simulation for the water consumption (Fatichi et al., 2012).

For example the *WFM* model developed by (McCall & Bishop-Hurley, 2003) considers a large number of factors but it is used for studies in small areas, usually in New Zealand, and parameters are calibrated using the dominant species in the specific site (Beukes et al., 2008). Also the *SALUS* model, used in North and South America, is used generally for studies with a detailed spatial scale, and needs on-site biomass data for the calibration. The pasture growth, here as in other models, is based on the active radiation intercepted by leaf (Insua et al., 2019b, 2019a). Also the two models used by (Johnson, 2008; Johnson et al., 2008), *DairyMod* and *EcoMod*, and the *MoSt-GG* model (Ruelle et al., 2018) consider the water and nutrients availability, with possibility of irrigation and fertilizers use, and the grazing and the animal needs based on their physiology. They simulate both the grazing and the cut scenarios but they are used again at the paddock level, for simulation with resolution of few m^2. *ModVege* model (Calanca et al., 2016; Piseddu et al., 2022) simulates the mass flow on a daily time step under the hypothesis that the community behaviour can be explained by the mean traits of dominant

grasses. Few functional plant groups can be combined in different proportion in the area. The potential growth is proportional to the active radiation and the water limitation is simulated using a simple water balance. Also here the study area is a small designed experiment area.

Generally, ecohydrological models and vegetation models, for the specific simulation of pasture lands but also for other kinds of vegetation, can simulate the vegetation states and growth using water, energy, carbon and nutrients budget, but they consider small areas. This is principally due to the high complexity of the models and to the consequent computational load. Moreover, sometimes these models could not spatialize weather data in large areas and could not consider the effect of topography, in particular in mountain areas with a complex topography. The majority of these models do not consider more species in the area, but analyse the ecosystem in its entirety, without considering competition and mortality (Fatichi et al., 2016; Movedi et al., 2019).

The *T-C* model (Fatichi et al., 2012) is an ecohydrological model widely used for studies in the European Alps (Botter et al., 2021; Fatichi et al., 2014; Mastrotheodoros et al., 2019, 2020). The model is used both at the paddock and at the watershed scale. It uses in input spatialized climatic variables and considers water, energy and carbon budget. The vegetation growth is based on carbon accumulation. Water supply limitation is the most important factor of plant stress. The model considers two layers of vegetation in the same cell, usually high and low vegetation, which are constantly distributed during the simulation. Again some plant types are identified to collect all similar species and each of them could be used in a layer. In spite of the complexity of the model, different configurations can be chosen based on the aim of the simulation.

So, generally, pasture studies are site-specific or analyse specifically the behaviour of plants, they are unlikely focused on biomass productivity. Here, *Poli-Pasture* is a tool able to analyse a wide area, even though at the expense of the specificity of pasture species. *Poli-Pasture* is a distributed model thanks to the coupling with the hydrological model *Poli-Hydro*, specifically developed to consider high catchment climate and topography. For this reason it is different from other site-specific models that simulate the pasture growth in small areas without considering spatial variability.

Here, two large catchments, in Valtellina and in Valle d'Aosta, were pursued.

Moreover, after a first development of the model in Valtellina area, the coupling of *Poli-Pasture* with *CoSMo* model in Valle d'Aosta region makes *Poli-Pasture* able to simulate the inter-specific competition and the pasture plant ecosystem in the detail, not only as a community.

CoSMo here, for the first time, is used coupled to a distributed model, and not only to a site-specific vegetation model (Confalonieri, 2014; Movedi et al., 2019; Piseddu et al., 2022).

Poli-Hydro and *Poli-Pasture* are physically based and not empirical or data-driven. They are spatially distributed and developed specifically for the study of high-altitude catchments.

This pasture model is able to increase knowledge of pasture species growth and of climate change impacts therein in the Italian alpine regions, to aid the future management of pasture-related economic activities.

Other studies analyse effects of climate change in the European Alps, also without considering a specific modelling of pasture dynamics. For example (Deléglise et al., 2019) based the study on agroclimatic indicators, and (Zeeman et al., 2017) studied the effects of snow cover timing and volume on the carbon balance in soil and plant carbon usage during the growth, and as a consequence on pasture productivity. Someone had studied the effect of overgrazing on pasture and the consequent degradation, with changes in plant composition (Fragnière et al., 2022; Kurtogullari et al., 2020).

In fulfilment of this thesis work, different papers were used to develop and calibrate three models, *Poli-Hydro*, *Poli-Pasture* and *CoSMo*.

The calibration of *Poli-Hydro* was reported in (Carletti et al., 2022; Casale et al., 2021; Fuso et al., 2021; Maruffi et al., 2022) for what concerns the Adda catchment, specifically for Valtellina and Valchiavenna valleys, and in (Duratorre et al., 2020) for the area of Gran Paradiso National Park.

A paper was published relative to the results of the study on Valtellina valley (Casale & Bocchiola, 2022), in particular the calibration of *Poli-Pasture,* the analysis of effects of climate change and the results of agroclimatic indices.

The development of an adaptation of *CoSMo* model for the inter-specific competition simulation was based on the papers of (Confalonieri, 2014; Movedi et al., 2019), and developed for this thesis work.

Then the calibration of *Poli-Pasture* and *CoSMo* in the Valle d'Aosta region was the focus of a master degree thesis (Morgese, 2022).

3 THE STUDY AREAS

3.1 Valtellina Valley

One of the study area for the application of the pasture dynamic model is Lake Como watershed, namely the Valtellina Valley and Valchiavenna Valley, in the Central Alps of Italy, overlapping the Adda river and the Mera river watersheds (Figure 2).

The watershed covers an area of 3880 km^2, and an altitude range from 225 to 4000 m asl. The median altitude is 1940 m asl, the 55% of the area is above 1800 m asl and 17% above 2500 m asl. In Figure 3 the hypsographic curve is reported as reference for the behaviour of the watershed altitude.

118 km^2, equal to the 3% of the area, are covered by glaciers. Different glacier groups can be identified: in the East of Valtellina the Ortles-Cevedale group (39 km^2) (Baroni et al., 2015; Bombelli et al., 2019), the Dosdè-Piazzi group (4 km^2) (Diolaiuti et al., 2011; Soncini et al., 2017) and the Livignasco group (1.8 km^2) (D'Agata et al., 2018) are present, while in the centre of Valtellina there are glaciers on the South bank in the Orobie group, covering an area of 2.6 km^2, and glaciers on the North bank in the Bernina-Disgrazia group, namely Scerscen, Fellaria, Ventina, Disgrazia and Codera-Masino sector (Aili et al., 2019; D'Agata et al., 2018, 2020). In Northern Valchiavenna valley the group of Spluga-Val di Lei is present, covering an area of 3.4 km^2 (D'Agata et al., 2018; Fuso et al., 2021).

Pasture and grassland cover an area of 522 km^2 in the watershed, equal to the 13%. The distribution could be seen in Figure 4. A large spatial variability of pasture productivity can be seen, because of differences in altitude, so in temperature, soil fertility, precipitation and as a consequence, soil moisture conditions (Gusmeroli et al., 2005; Sabatini et al., 2008).

The Adda river is exploited for hydroelectric energy production, indeed twenty-seven dams are located along the river and its tributaries (Denaro et al., 2018). More than 50% of reservoir capacity is managed by A2A S.p.A. and Enel: the first one manages reservoirs in the Upper Valtellina, and the second one controls reservoirs in Valmalenco (in the central Valtellina) (Aili et al., 2019; Bombelli et al., 2019). These plants contribute overall to the 13% of the hydropower demand of Italy, and the electric energy is principally used in Lombardia region (Beniston & Stoffel, 2014; Coppola et al., 2014; European Environemntal Agency, 2009; Rottler et al., 2019). Also on the Mera river and on its tributary, the Liro river, nine hydroelectric power plants are present, divided between Italy and Switzerland, and managed by A2A S.p.A. in Italy and by EWZ in Switzerland.

The climate of the valley is classified as *Cfb* in the Köppen-Geiger classification (Peel et al., 2007), so Valtellina has a temperate climate with no dry seasons and with warm summer. Average yearly precipitation is around 1400 mmy^{-1}, 1422 mmy^{-1} below 2000 m asl and 1383 mmy^{-1} above 2000 m asl. However, precipitation is more abundant in the Western part of the valley, nearby lake Como (1137 mmy^{-1} at Morbegno), with respect to the Eastern part (670 mmy^{-1} at Livigno-Foscagno). Precipitation peaks in May and November. The mean annual temperature is +1.5°C above 2000 m asl and +5.0°C below 2000 m asl. It reaches 0°C at Livigno La Vallaccia (2660 m asl) and +14°C at Morbegno (230 m asl). Summer temperature peaks in July, around +23°C in Morbegno and +8°C in Livigno. Winter temperature reaches +3°C and -8°C respectively.
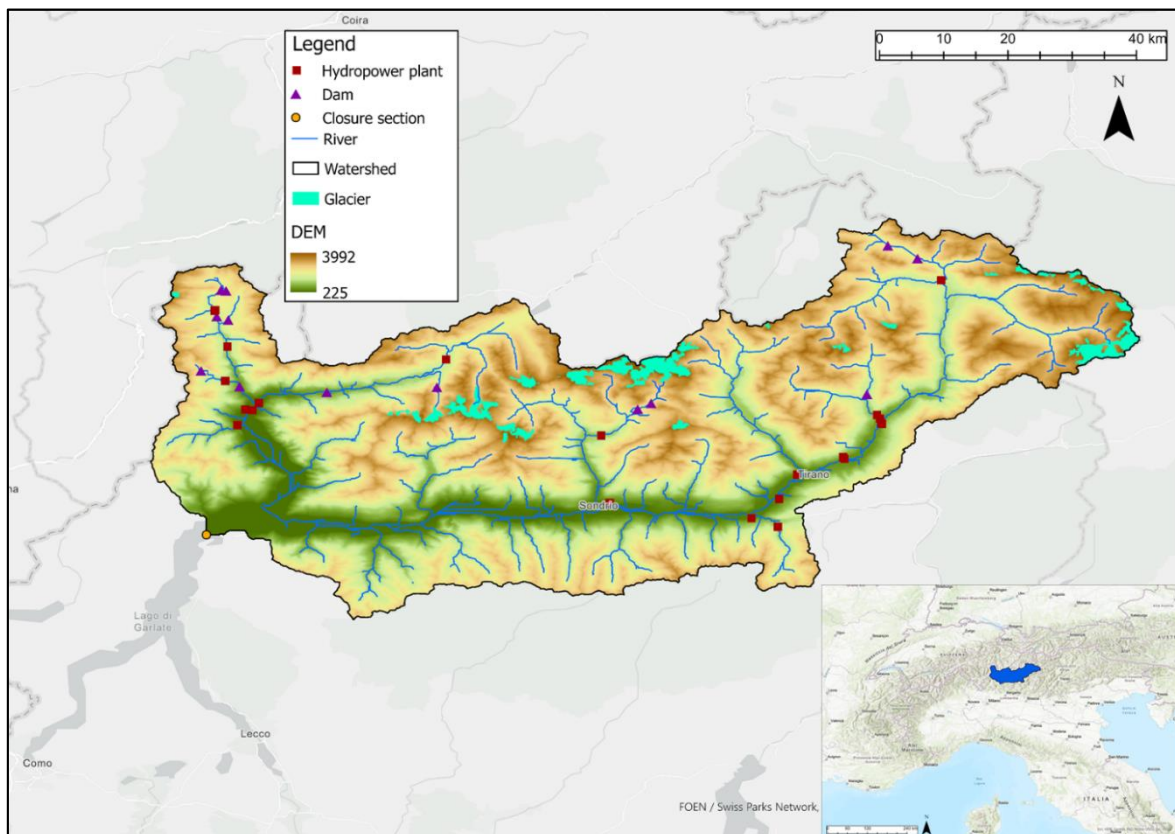
Figure 2: Study area: Valtellina and Valchiavenna valleys (Lake Como watershed, namely Adda and Mera rivers watersheds).
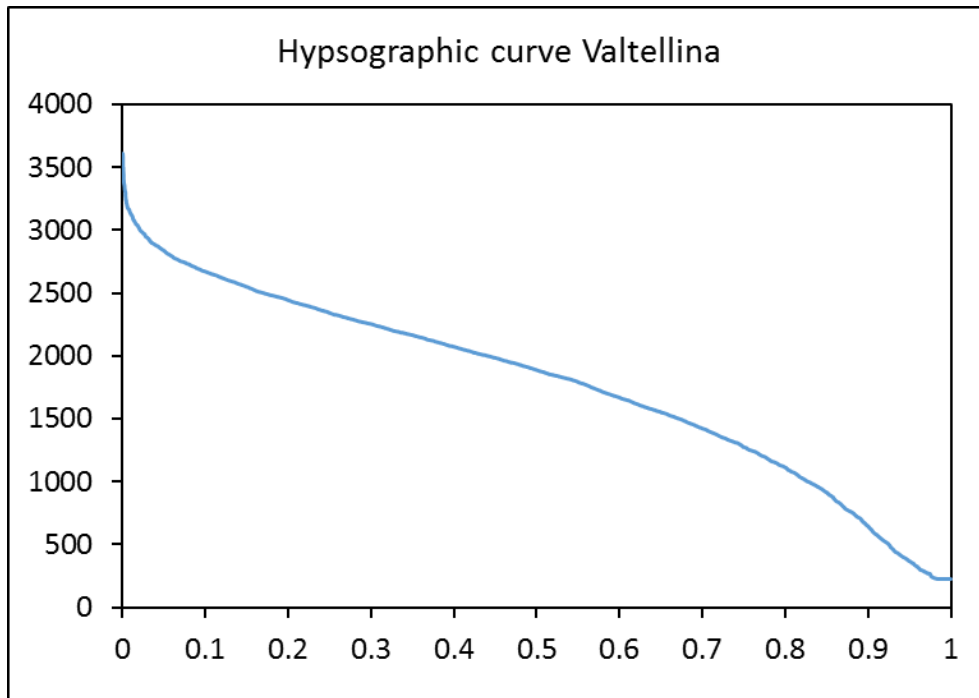
Figure 3: Hypsographic curve of Valtellina study area.
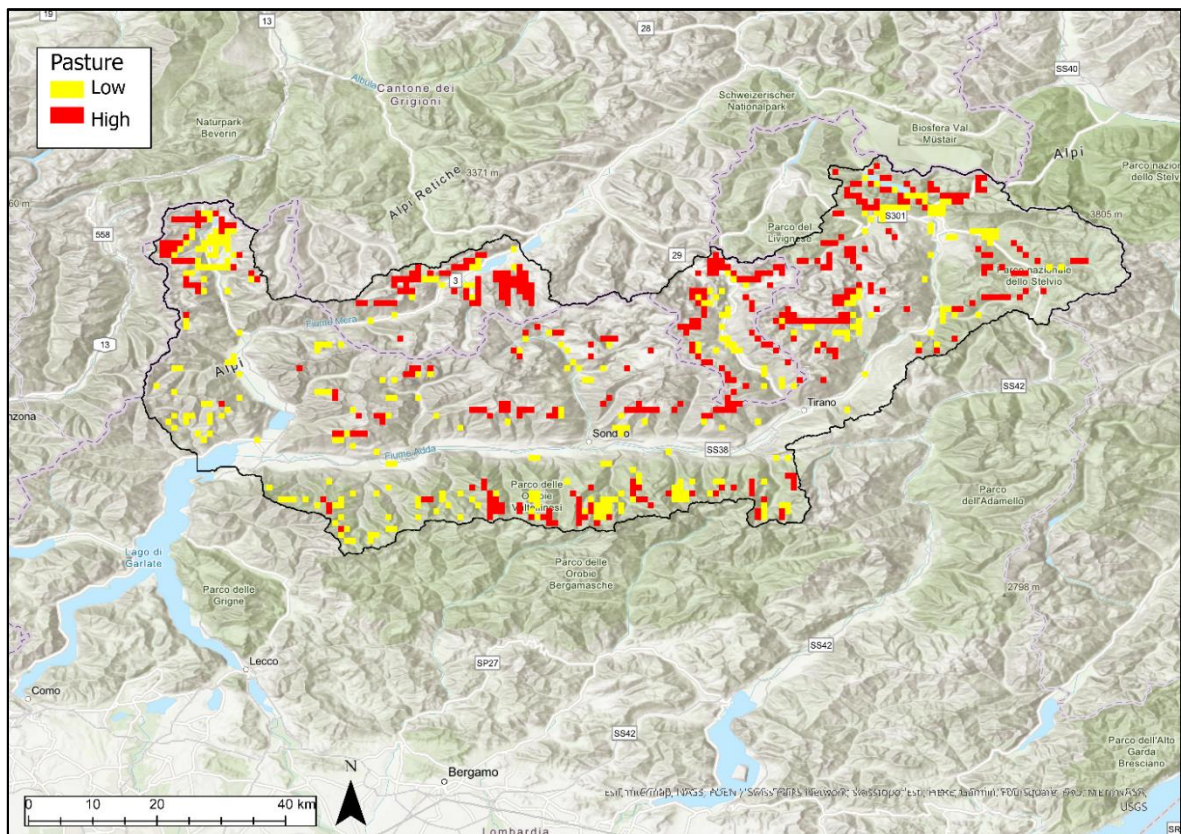
Figure 4: Pasture distribution in Valtellina Valley. In yellow pasture at low altitude, and in red pasture at high altitude.

3.2 Gran Paradiso National Park

The National Park of Gran Paradiso is the first national park established in Italy, it was born in 1922 and covers an area of 710 km^2 in Northern Italy (Filippa et al., 2022), of which 370 km^2 in Valle d'Aosta region and 340 km^2 in Piemonte region. For the aim of the study the focus is on the park area in Valle d'Aosta region (Figure 5). It occupies the area of three valleys, Valsavarenche, Cogne Valley, and Rhêmes Valley. The first one is crossed by the Savara river, with a length of 27 km, the second one is crossed by the Grand Eyvia river, and the third one by the Dora of Rhêmes. Three rivers flow into the Dora Baltea river, the principal river of Valle d'Aosta region and a tributary of Po river.

The study area considers three watersheds for a total surface of 350 km^2: the Grand Eyvia and the Savara rivers watersheds and the Nomen river watershed between the other two.

The park covers an altitude range between 800 m asl and 4000 m asl. The 50% of the area is above 2639 m asl; above 1800 m asl there is the 92% of the area, while above 2500 m asl there is the 61% (Figure 6).

Gran Paradiso Group is among the most glaciered areas in the North-Western Italian Alps, with 72 glaciers (Baroni et al., 2021). Based on information of the glacier cadastre of Valle d'Aosta region of 2005, in the study area of this work, 19.15 km^2 are covered by ice (Duratorre et al., 2020).

In Figure 7 the distribution of pasture is reported. It covers an area of 20 km^2, principally above 1800 m asl, correspondent to the 5.7% of the study area.

The climate here is classified as *Dfa* in the Köppen-Geiger classification, so cold, without dry season and with hot summer. Average annual temperature is -2.0°C above 1800 m asl and -0.4°C under this altitude, while annual precipitation is 944 mm/y above 1800 m asl and 684 mm/y under 1800 m asl.
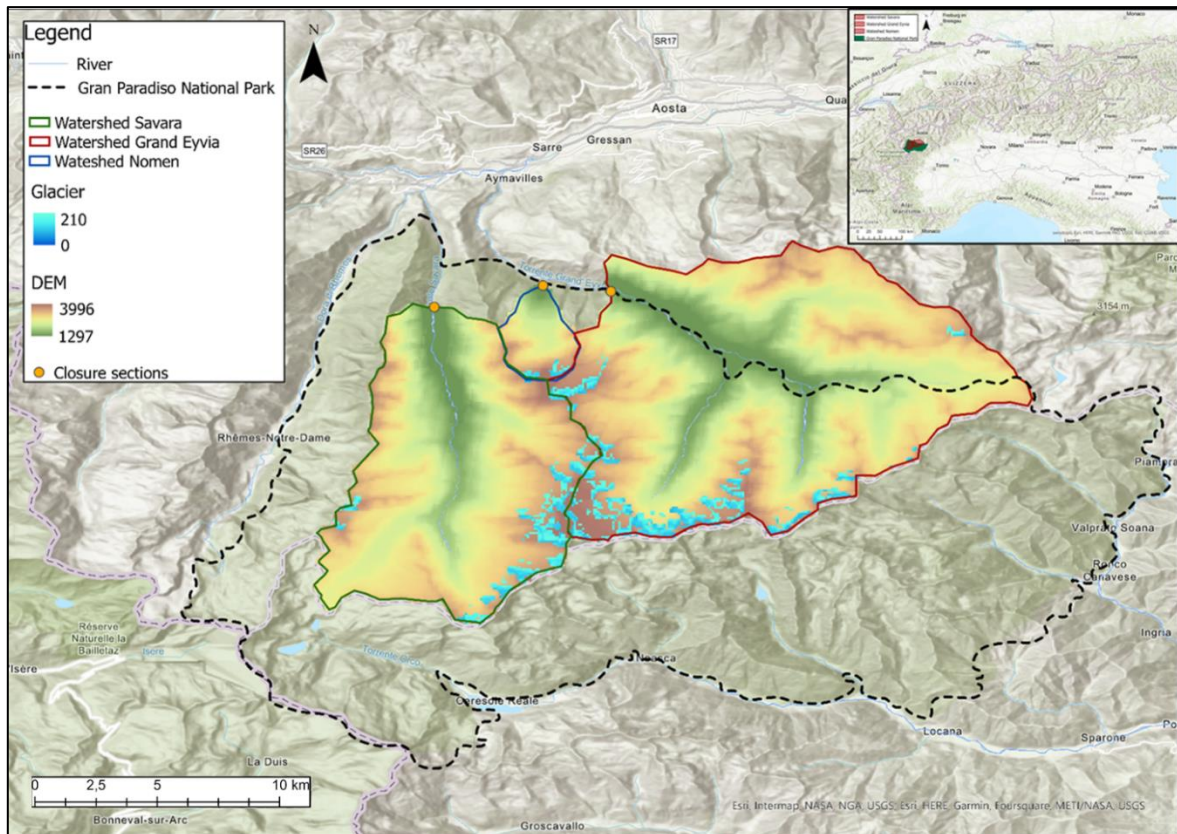
Figure 5: Study area in Valle d'Aosta region. Three watersheds and Gran Paradiso National Park boundaries are reported.
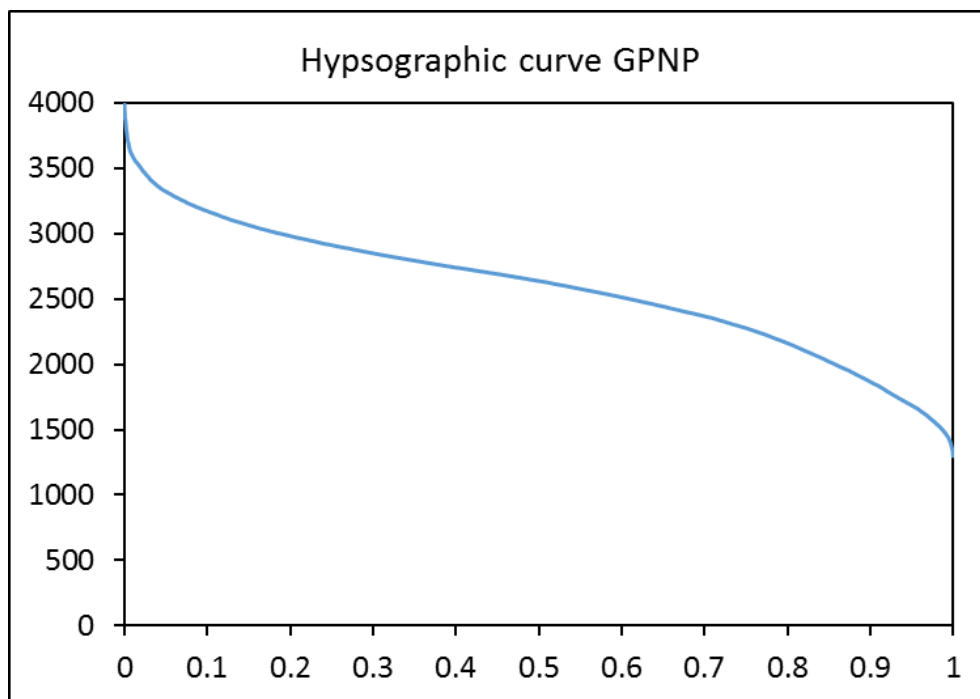
Figure 6: Hypsographic curve of Gran Paradiso National Park in Valle d'Aosta region.
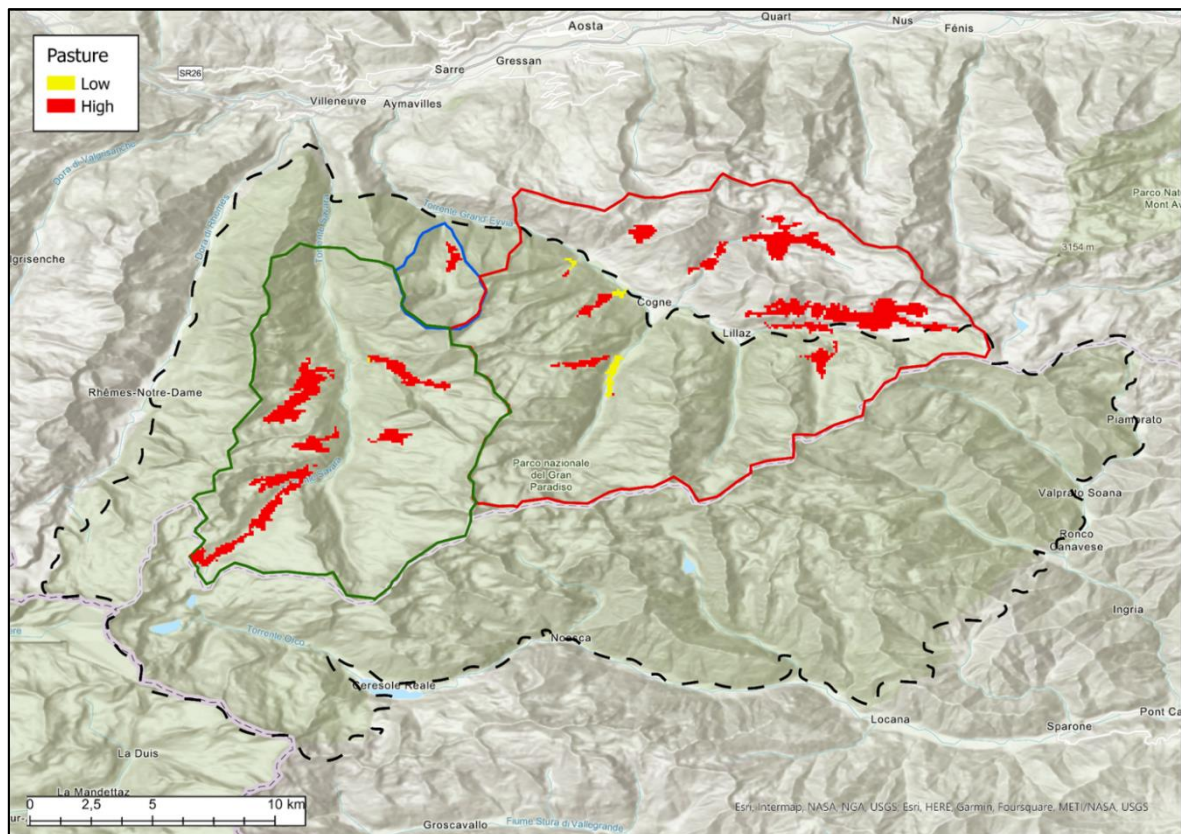
Figure 7: Pasture distribution in Gran Paradiso National Park. In yellow pasture at low altitude, and in red pasture at high altitude.

3.3 Pastures characteristics and management in the Alps

The alpine pasture is usually natural in high altitude areas, and it is exploited during summer for bovine, ovine and caprine pasture. In winter animals house in closed barns located in the valley, while during spring and early summer animals graze at low altitudes (1600-1800 m asl), and through a vertical transhumance they move upward at high altitudes during summer, in August (2500 m asl). The system is organized in mountain cottage and animals feed on grass. Pasture fertilization is through the natural distribution of animal faeces, and no chemical control is applied (Boschetti et al., 2007).

It is important to organize and control the pasture i) to maximize the feeding of animals and the energy efficiency in their production of milk and meat, ii) to maintain a good quality of grass, in terms of nutrient value and biodiversity, and iii) to reduce the soil erosion due to the animal treading (Gusmeroli, 2003). Usually the grazing for bovines is controlled and animals are gathered in defined areas, where grass is at the optimal growth stage, in which they can move for preferred grass. Animals, in this way, optimize their consumption, and it is possible to control the growth of good pasture species (Barcella & Gusmeroli, 2018; Gusmeroli, 2003).

For this reason, it is useful and largely used the rotational grazing system (Boschetti et al., 2007).

A controlled pasture guarantees: i) the utilisation of grass at the optimal stage, ii) improvement of the pasture with the control of bad species presence, iii) to divide animals in homogenous groups for necessities, iv) regular increase of nutritive elements in soil, v) maintenance of stable soil structure (Barcella & Gusmeroli, 2018).

The Dosdè valley has glacial origin and an average altitude of 2100 m asl. The soil is acidophilic and different phytocoenosis could be identified. 88 vegetal species are counted here: four endemic species, three species under total national protection and one species under regional protection.

The first phytocoenosis is characterised by three diagnostic species: *Nardus stricta*, *Plantago alpina*, and *Trifolium alpinum*. The pasture is mesophilic and acidophilic. The abandonment of the pasture is causing the formation of shrubs (*Calluna vulgaris*, *Rhododendron ferrugineum*, *Vaccinium myrtillus*, *Juniperus communis*, *Salix breviserrata*). The overgrazing determines a progressive increase in presence of *Nardus*, with loss of biodiversity and acidification of the soil. A presence of the 70% of *Nardus* is representative of a past pressure on the area. The increase in presence of *Nardus stricta* causes also a decrease of the fodder value of the pasture. Indeed, animals feed on *Nardus* only at the beginning of the flowering season, then they consume other species, contributing to the increase in presence of *Nardus* (Orsenigo, 2018). So it is necessary to maintain a good quality value of pasture with *Nardus* to manage its presence.

Other phytocoenosis are peat bog and xeric, and are difficult to colonize.

In Valtellina, pasture productivity ranges between 0.5 and 6.5 tha^{-1}y^{-1} (Gusmeroli et al., 2005).

The area of Orvieille is exposed to South–Southeast and is located around 1950–2230 m asl. The soil is acidophilic and 149 vegetal species are counted in the area: seven alpine endemic species, one sub-endemic and three species under total national protection. Different phytocoenosis could be identified for pasture and grassland.

For the classification of the pasture four diagnostic species are identified: *Geum montanum*, *Nardus stricta*, *Plantago alpine*, *Trifolium alpinum*. Pasture is principally present between 2000 and 2290 m asl. The overgrazing determines a progressive increase in presence of *Nardus*, with loss of biodiversity and acidification of the soil. The abandonment of pasture causes the advance of shrubs, like *Rhododendron ferrugineum*, *Vaccinium myrtillus* and *Rosa pendulina*.

Diagnostic species for the grassland are: *Bromopsis erecta*, *Thymus pulegioides* and *Festuca ovina*. Grasslands are present between 1900 and 2000 m asl.

An overgrazing here is causing an undermining of the grass with consequent erosion and runoff on the slope.

During the growth season of vegetation, the biomass increases but the energy content decreases. For this reason animals feed on grass at the beginning of the flowering stage, when the biomass is lower but the energy content is higher, then during the maturity season it is necessary to proceed to the cut of vegetation (Barcella & Gusmeroli, 2018). During the season it is necessary to proceed with a different number of cuts depending on the area and the pasture productivity, usually between 2 and 6-7 cuts are done during the growth season (Botter et al., 2021; Fatichi et al., 2014).

4   DATA

In this chapter all the data used for the study are presented. The process is the same for both the study areas but it was necessary to collect specific data for each study area.

Poli-Hydro is a semi-distributed cell-based hydrological model. It requires in input meteorological data and spatialized land cover information, while it needs discharge, snow depth and spatialized snow cover data for the calibration. The pasture module *Poli-Pasture* was calibrated with leaf area index maps, and local or distributed pasture biomass data.

4.1   Meteorological data

Poli-Hydro is driven by meteorological data, namely temperature *T*, total precipitation *P* and radiation *Rad*. Data from automatic weather stations AWS were collected, then spatialized for the entire study area through the application of Thiessen polygons. An altitudinal lapse rate is applied in each polygon, to consider the different elevation of each cell with respect to the AWS elevation. The altitudinal lapse rate is calculated at the monthly scale, using the weather data of AWS, and their elevation.

For what concerns temperature, daily minimum, maximum and average values were used.

Moreover, daily data of precipitation were split in solid and liquid precipitation, based on the average temperature of the day.

On ground snow depth data were used to calibrate the *Poli-Hydro* model, in particular the snow melt simulation.

AWS stations provide daily data of snow depth, as of precipitation and temperature.

4.1.1   Valtellina

Weather data are made available by ARPA Lombardia, the regional agency for environmental protection (Arpa Lombardia, 2020b). 13 ARPA stations were used for this study, and daily data for the period 2002-2019 were downloaded. Here, data of temperature *T* and precipitation *P* were used as input to the model.

Data of snow depth *Hs* of four AWS were used for the calibration of the snow dynamics simulated by the model, for the same period 2002-2019. A monthly average of the observed values in each station was calculated to be compared with the simulated value, as monthly average, in the corresponding cell of the AWS. In this way it is possible to compare the

behaviour of the observed and the simulated snow dynamics during the year, considering both the snow accumulation and melt. To transform the snow depth measured in cm, in m^3 of snow water equivalent *SWE*, and to compare it with the model simulation, a constant value of snow density of 115 kg/m^3 was used.

In Table 1 AWS are reported, with their coordinates and altitude.

The altitudinal lapse rates of temperature and precipitation, calculated in the Valtellina area, are reported in Table 2.

Table 1: Automatic Weather Stations of ARPA Lombardia considered for the model. *T* is temperature, *P* is precipitation and H_s is snow depth.

Station	Altitude [m asl]	Latitude [°]	Longitude [°]	Variables
Aprica	1950	46.13	10.15	*T, P, Hs*
Bema	930	46.11	9.57	*T, P*
Bormio	1172	46.45	10.37	*T, P*
Caiolo	274	46.15	9.79	*T, P*
Gerola Alta	2178	46.02	9.58	*T, P, Hs*
Lanzada Palù	988	46.27	9.88	*T, P*
Livigno La Vallaccia	2660	46.48	10.21	*T, P*
Morbegno	230	46.14	9.58	*T, P*
Samolaco	206	46.24	9.43	*T, P*
San Giacomo Filippo	2057	46.36	9.32	*T, P, Hs*
Sondrio	290	46.16	9.85	*T, P*
Val Masino	934	46.24	9.63	*T, P*
Valdisotto	1537	46.46	10.34	*T, P, Hs*

Table 2: Altitudinal lapse rate of temperature and precipitation in Valtellina.

Month	Thermal lapse rate		Precipitation lapse rate	
	Slope [°C/m]	Intercept [°C]	Slope [mm/m]	Intercept [mm]
January	-0.0030	1.59	0.0083	66.18
February	-0.0043	4.25	0.0118	58.14
March	-0.0054	9.33	0.0143	55.56
April	-0.0058	13.64	0.0066	98.36
May	-0.0059	17.17	0.0073	124.92
June	-0.0057	21.01	-0.0061	152.43
July	-0.0056	23.03	0.0003	133.00
August	-0.0053	21.83	-0.0040	139.07
September	-0.0051	17.80	-0.0009	125.98
October	-0.0041	12.52	0.0108	100.55
November	-0.0034	6.81	0.0183	124.83
December	-0.0024	1.82	0.0077	75.92

4.1.2   Gran Paradiso National Park

For the area of Gran Paradiso National Park, weather data are available from the Centro Funzionale (Centro Funzionale Regione Autonoma Valle d'Aosta, 2020) and the ARPA websites of Valle d'Aosta region (Arpa Valle d'Aosta, 2020).

Data were collected for a period of 15 years, from 2005 to 2019. Temperature data were available in 16 AWS, while precipitation data in 13 AWS of them.

Moreover, 10 AWS have data of snow depth. Here, to convert from cm of snow to m^3 of equivalent water, snow density was updated daily based on minimum temperature (Bocchiola & Rosso, 2007; Valt et al., 2014). In particular, the Martinec's method was used to calibrate the snowmelt module, accounting for snow compaction during days (Martinec & Rango, 1986).

In Table 3 AWS names and location, with available data, are reported, while in Table 4 thermal and precipitation lapse rates are reported.

Table 3: Automatic Weather Stations of the Gran Paradiso National Park area, considered for the model. *T* is temperature, *P* is precipitation and H_s is snow depth.

Station	Altitude [m asl]	Latitude [°]	Longitude [°]	Variables
Valsaverenche Pont	1951	45.53	7.20	*P, T, Hs*
Valsaverenche - Eaux Rousses	1651	45.57	7.21	*P, T*
Valsaverenche Orvieille	2170	45.58	7.19	*P, T, Hs*
Cogne Lillaz	1613	45.60	7.39	*P, T, Hs*
Cogne Grand Crot	2279	45.59	7.37	*P, T, Hs*
Cogne Valnontey	1682	45.59	7.34	*P, T*
Cogne – Crètaz	1470	45.61	7.34	*T*
Gressan Pila Leissé	2280	45.66	7.31	*P, T, Hs*
Fenis Clavalité	1531	45.69	7.50	*T*
Fenis Lavodilec	2250	45.64	7.49	*P, T, Hs*
Champorcher Rifugio Dondena	2181	45.61	7.55	*P, T, Hs*
Ayamvilles Vieyes	1139	45.65	7.25	*T*
Rhemes Notre Dame Chaudanne	1794	45.56	7.11	*P, T, Hs*
Rhemes Notre Dame Chavaney	1690	45.58	7.12	*P, T, Hs*
Rhemes Saint Georges Feleumaz	2325	45.60	7.12	*P, T, Hs*
Rhemes Saint Georges Capoluogo	1179	45.65	7.15	*P, T*

Table 4: Altitudinal lapse rate of temperature and precipitation in the Gran Paradiso National Park area.

Month	Thermal lapse rate		Precipitation lapse rate	
	Slope [°C/m]	Intercept [°C]	Slope [mm/m]	Intercept [mm]
January	-0.0024	0.59	0.0010	-0.16
February	-0.0032	1.94	0.0008	-0.21
March	-0.0042	7.23	0.0007	0.24
April	-0.0053	13.32	-0.0008	3.81
May	-0.0059	17.88	0.0012	1.52
June	-0.0057	21.63	0.0011	0.68
July	-0.0054	23.20	0.0009	0.68
August	-0.0046	20.85	0.0009	0.74
September	-0.0046	17.47	0.0006	0.81
October	-0.0033	11.03	0.0005	0.89
November	-0.0031	5.75	-0.0002	3.14
December	-0.0022	0.97	0.0008	0.27

4.2 Topographic data, land cover and soil properties

The hydrological model uses as input a Digital Elevation Model *DEM*, necessary to define, based on the chosen spatial resolution, the watershed and the flow accumulation. For Valtellina it was downloaded from the Nasa website (Earthdata, 2019) (Figure 2). It has an initial spatial resolution of 30 m ca., and it was developed during 2000-2013. While for Valle d'Aosta a *DEM* with spatial resolution of 100 m was used from the regional geoportal (Geoportale SCT, 2008), developed during 2005 and 2008 (Figure 5).

A land cover map is necessary to identify areas of pasture, and generally covered by vegetation, and to estimate the maximum soil water content *Smax*.

Indeed *Smax* was estimated with the SCS-CN method (Mishra & Singh, 2003).

$$S_{max} = 254(\frac{100}{CN} - 1)$$ Eq. 1

Based on the land cover, a CN value was associated to each cell, using the table developed by (Rosso, 2004). This table with the correspondence between the land cover and the CN value is reported in Table 5. CN assumes different values based on the soil type: for each land cover class a range is given, the first value was used for Valtellina, and the second one for Gran Paradiso National Park.

Land cover map was available from the Corine Land Cover (Copernicus Land Monitoring Service, 2012) experiment of the European Copernicus Programme. In particular the version of 2012 was used, to be in line with the period of availability of other data. The spatial resolution is 25 m.

In Figure 8 the maps of CN for Valtellina (a) and Valle d'Aosta (b) are reported.

From the same layer, the vegetation fraction map was also obtained. Indeed, the hydrological model calculates the evapotranspiration where vegetation is present, while the module on pasture is used only where pasture vegetation is present.

Table 5: CN value for each land cover class. CN assumes different value basing on soil type: for each land cover class a range is given, the first value was used for Valtellina, and the second one for Gran Paradiso National Park.

Land cover	CN
Forest	65 – 72
Sparsely vegetated area	67 – 82
Pasture and grassland	69 – 78
Agricultural area	75 – 83
Moorland	80
Bare rock	82 – 87
Urban area	85 – 88
Industrial and commercial area	92
Glacier	95 – 97
Water bodies	99

For the ice-covered area, maps from the Global Land Ice Measurements from Space (GLIMS) (National Snow and Ice Data Center, 2020) were used for Valtellina area (Raup et al., 2007), while data from the regional glacier cadastre, collected for the years 2005 and 2012 (Geoportale SCT, 2012), were used (Figure 2 and Figure 5).

The *Poli-Hydro* model requires as input the hydraulic properties of soil: wilting point θ_w, field capacity θ_l, saturation θ_s, and hydraulic conductivity K, dependent on soil texture (Saxton et al., 1986). For Valtellina area these parameters were made available in fulfilment of other studies, like (Aili et al., 2019; Bombelli et al., 2019; Soncini et al., 2017), while for Valle d'Aosta region they were estimated in the study of (Duratorre et al., 2020).

Also the depth of active soil layer was considered here constant for the entire area and for both study areas, and equal to 1 m.
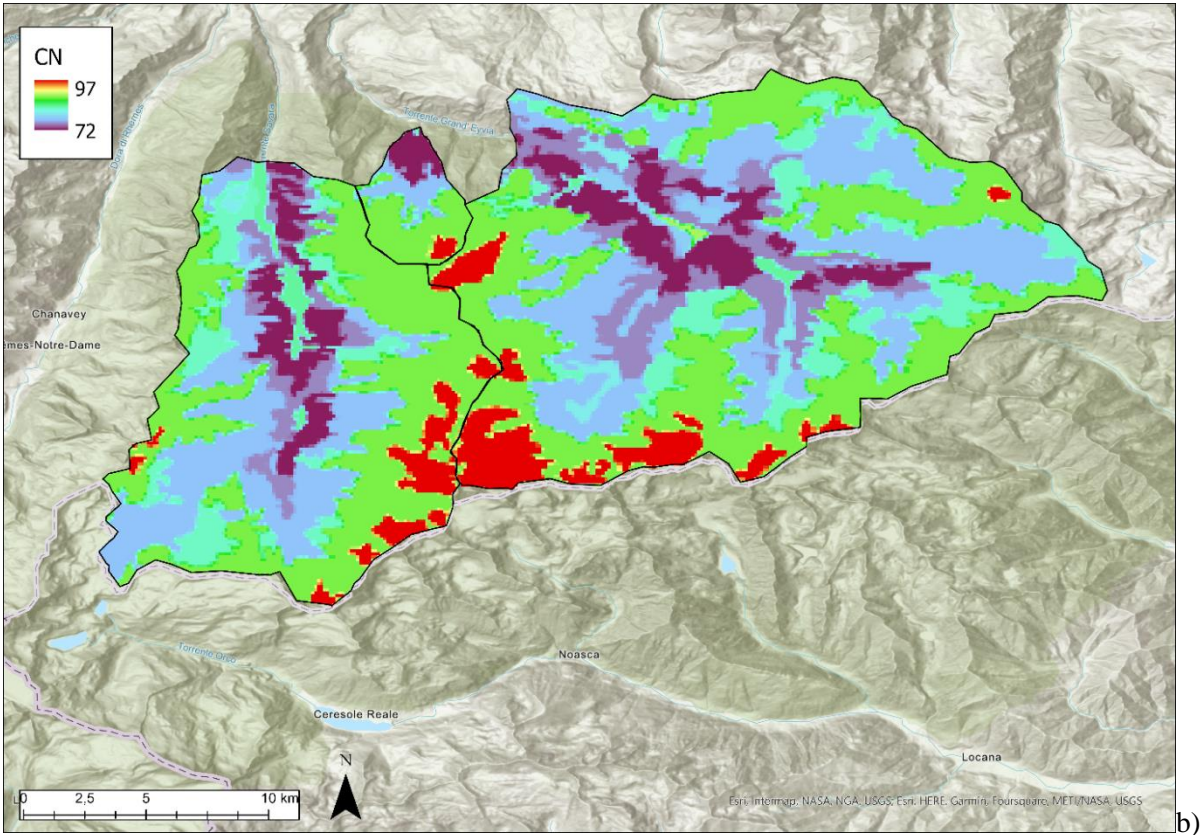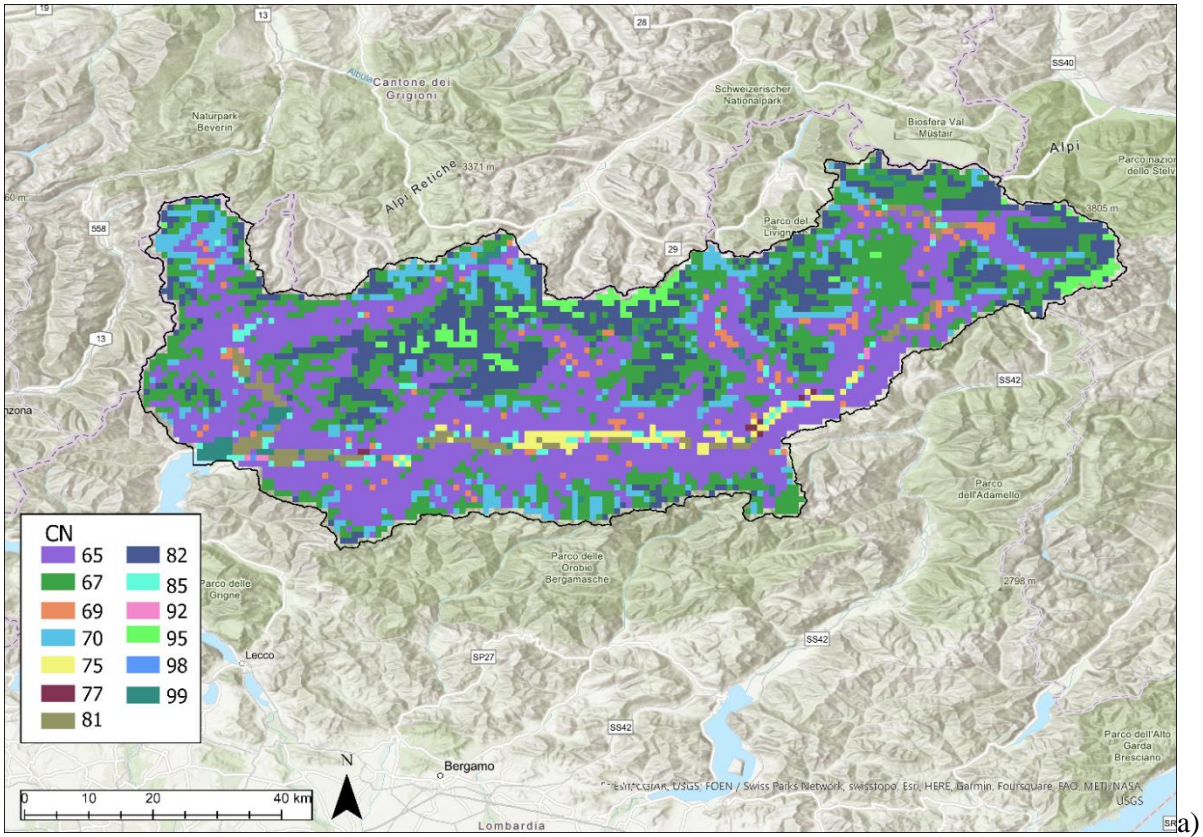
Figure 8: CN maps for Valtellina (a) and Valle d'Aosta (b) region.

4.3 Discharge data

For the calibration of *Poli-Hydro* model, one of the necessary data is discharge data in different closure sections. It is necessary to have daily data of discharge for a period comparable with available weather data.

4.3.1 Valtellina

For Valtellina and Valchiavenna valley data of two hydrometric stations were used. The first one is on the Adda river, before the confluence to the Lake Como. It is an ARPA station located in Fuentes (SO) and data are available for the period 2003-2018 (Arpa Lombardia, 2020a).The second one is on the Mera river, and it is a hydrometer of Consorzio dell'Adda (the consortium for water management of Adda river, (Consorzio dell'Adda, 2020)). It is located in Samolaco (SO) and data are available for the period 2009-2018.

4.3.2 Gran Paradiso National Park

For the area of Valle d'Aosta region, discharge data are available on the website of Centro Funzionale (Centro Funzionale Regione Autonoma Valle d'Aosta, 2020). Two stations are available for the period 2005-2018: Valsaverenche – Eaux Rousses and Cogne – Crètaz.

In Figure 9 automatic weather stations and hydrometric stations are reported in the map for Valtellina (a) and Valle d'Aosta (b).

In Table 6 coordinates of hydrometric stations for Valtellina and Valle d'Aosta are reported.

Table 6: Coordinates of hydrometric stations in Valtellina valley (SO) and Valle d'Aosta region (AO).

Station	Altitude [m asl]	Latitude [°]	Longitude [°]
Fuentes (SO)	198	46.14	9.41
Samolaco (SO)	203	46.24	9.41
Valsaverenche - Eaux Rousses (AO)	1651	45.57	7.21
Cogne - Crètaz (AO)	1470	45.61	7.34
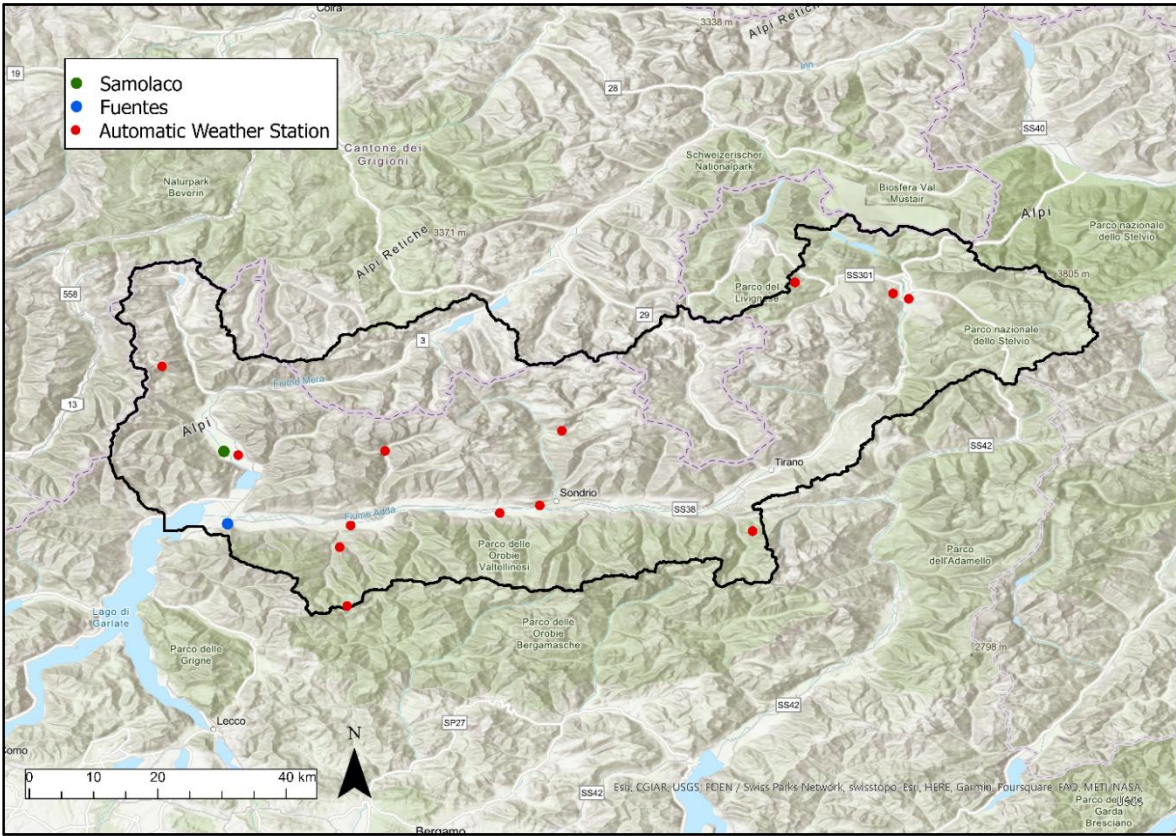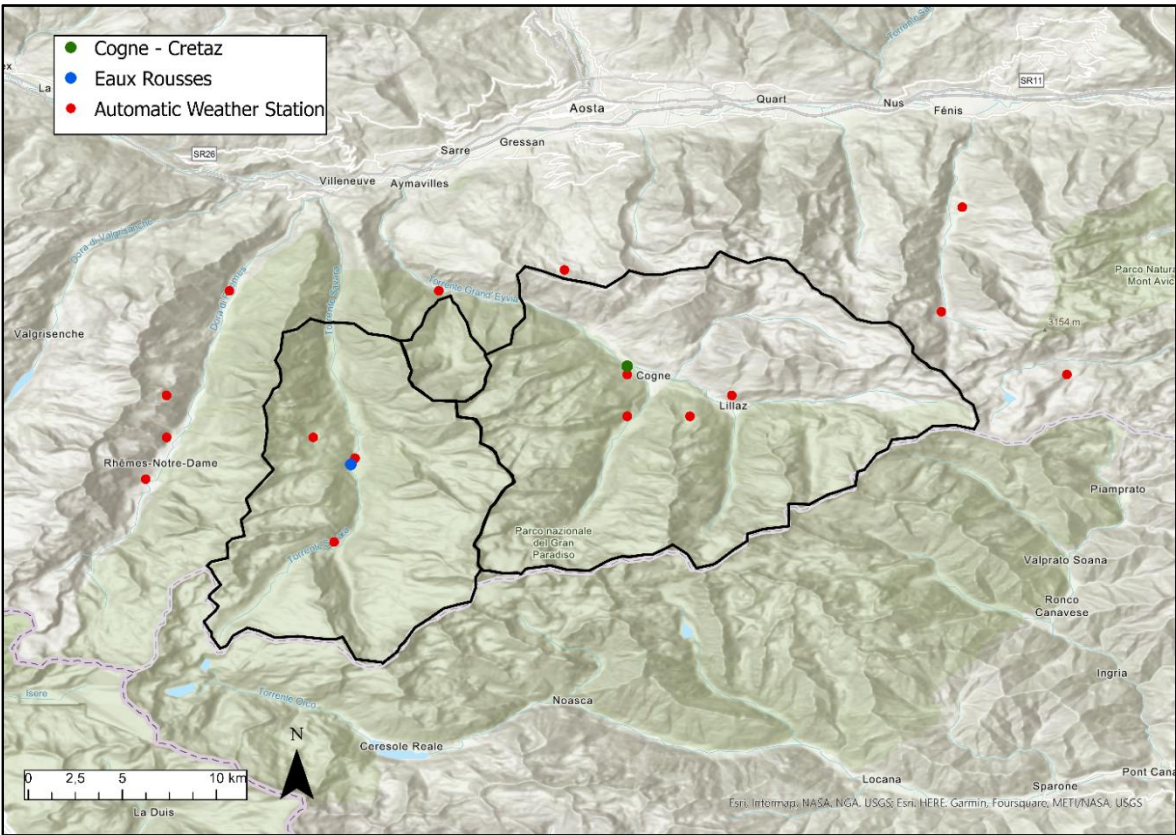
Figure 9: Automatic Weather Stations and hydrometric stations in Valtellina (a) and Valle d'Aosta (b).

4.4   Satellite data

The calibration and validation of models were also done using satellite data to have distributed information of variables and to improve the calibration considering specifically more variables. Images are downloaded at different spatial resolution. While the *DEM* was aggregated to have an acceptable resolution for the simulation, other maps were aggregated to have the same spatial resolution of *DEM*.

4.4.1   Snow Cover Area

For the case study of Valtellina valley, to calibrate the hydrological model, satellite data of snow cover area *SCA* were used. In this way the snow dynamics was calibrated considering the snow depth, using observed snow depth data, and the distribution, using satellite data. This guarantees a correct simulation of snow dynamics and distribution during the season, and a correct evaluation of the total volume of snow. It is important especially to estimate available water volume from snow melting. To calibrate the snow dynamics both the season of accumulation and the season of melt were considered.

For Valtellina valley gridded snow cover satellite maps were collected from the website of the Moderate Resolution Imaging Spectroradiometer on board the Terra satellite (MODIS, (National Snow and Ice Data Center, 2019)) (Bocchiola & Groppelli, 2010; Corbari et al., 2009; Parajka & Blöschl, 2008). In particular, 42 images were downloaded for calibration during 2005-2010, every 15 days from March 14th to July 18th, the seasonal snow melt period. For validation of the model 28 images were downloaded during 2015-2018, every 15 days. Spatial resolution is 500 m.

4.4.2   Leaf Area Index

The Leaf Area Index is a measure of the leaf area per unit of soil area [m^2/m^2] and it is a function of the vegetation biomass.

For the area of Gran Paradiso National Park, the *Poli-Pasture* module was calibrated using satellite data of Leaf Area Index *LAI*. Indeed, the model simulates the pasture biomass but also the daily *LAI* for each cell of the area. While pasture biomass information, is usually aggregated or collected locally, satellite maps permit to evaluate the simulation results in each cell. Moreover it was possible to verify the growth timing.

Here images with a resolution of 500 m were used. Images were available on the website of the Land Processes Distributed Active Archive Center LPDAAC of NASA (LP DAAC, 2020). Images were collected by the Moderate Resolution Imaging Spectroradiometer on board the Terra satellite. Images were available every 8 days since 2005 to 2019, for the period from May 25th to September 14th, namely the vegetation growing season. Here maps every two weeks were used in this period.

4.5   Pasture productivity

Conversely, for Valtellina area, the calibration of the model was done using pasture yield statistics, reported by ISTAT, the National Institute of Statistics (Istat, 2020), aggregated for each province of Italy. Valtellina and Valchiavenna cover the whole territory of Sondrio province. ISTAT reported the total annual production of pasture lands and data were available for the period 2006-2019. However, the pasture area changes during years, in particular the area of pasture and grassland decreases, as reported by ISTAT information. This is due to social and economic factors, such as land abandonment, generational changes or lack of public funding, and land use changes related to urbanization or other agricultural uses (Monteiro et al., 2011), which were not considered here in the model.

For this reason it was preferable to use specific pasture productivity to the area in [t/ha].

Information about pasture productivity in terms of biomass was found also in the literature. At high altitudes in the Alps, pasture biomass was estimated to be near to 3-4 t/ha, while below 1000 m asl biomass is higher, around 8 t/ha (Erfini, 2017; Gusmeroli et al., 2005).

4.6   Local pasture biomass

In fulfilment of the MOUPA project, data of pasture fresh biomass and relative species abundance were collected by the research group of the Università degli Studi di Milano in the Dosdè area (Valtellina) in three sites and in the Orvieille area (Gran Paradiso National Park) (Confalonieri R., personal communication). Sites are located at 2130 m asl in the Dosdè valley, and at 2300 m asl at Orvieille. These data were used for the validation of the model, comparing the observed fresh biomass data with the simulation of the model in the same cell.

In Table 7 a summary of collected information is reported.

Samples were collected during the summer of 2019. In the Gran Paradiso National Park area (Orvieille) the sample was collected on July 15th, only in one site. There were four species almost equally distributed (*Festuca, Alchemilla, Nardus* and *Ranunculus*), other species were

present in minor part. In the Dosdè valley three sites were chosen, of which the second one Dosdè 2 was a humid area. The samples were collected two times during the season, one July 25th and the other one August 29th, so it is possible also to evaluate eventual changes in the present species and their abundance. In Dosdè 1 in July two species were prevalent, and *Deschampsia* was more abundant than *Nardus* (86% vs 10%), but in August, the difference in abundance between the two was reduced (65% vs 34%), even though *Deschampsia* continued to be more abundant than *Nardus*.

Dosdè 2 is a particular site and it was not considered for this study, but the two most abundant species in July continued also in August, but their relative presence was inverted. In Dosdè 3, differently from Dosdè 1, *Nardus* was the most abundant species (84% of relative presence in July and 77% in August) during the entire season. Other three species were different from Dosdè 1 and was *Anthoxanthum*, *Mutellina* and *Poa*.

Other available in situ data were collected from literature. Specifically data were collected from samples in Alpe Boron, Valtellina, in the years 2003 and 2004 (Boschetti et al., 2007). Total observed biomass here in 2003 was 1.03 t/ha while in 2004 it was 1.36 t/ha.

Table 7: Fresh biomass and relative presence for each study site in Valtellina and Valle d'Aosta in different period of collecting samples.

Data	Site	Species	Fresh biomass [g in 0.5 m^2]	Relative presence [%]
15/07/2019	Orvieille (AO)	*Festuca nigricans*	39.12	22.80
		Alchemilla flabellata	34.67	20.20
		Nardus stricta	34.26	19.96
		Ranunculus acris	33.77	19.68
25/07/2019	Dosdè 1 (SO)	*Deschampsia cespitosa*	256.84	85.96
		Nardus stricta	30.62	10.25
		Anthoxanthum nipponicum	9.17	3.07
		Mutellina adonidifolia	2.17	0.73
25/07/2019	Dosdè 2 (SO)	*Trichophorum cespitosum*	50.39	87.30
		Eriophorum vaginatum	7.33	12.70
25/07/2019	Dosdè 3 (SO)	*Nardus stricta*	169.40	84.45
		Anthoxanthum nipponicum	16.75	8.35
		Mutellina adonidifolia	9.21	4.59
		Scorzoneroides helvetica	5.24	2.61
29/08/2019	Dosdè 1 (SO)	*Deschampsia cespitosa*	245.71	64.64
		Nardus stricta	131.02	34.47
		Mutellina adonidifolia	3.38	0.89
29/08/2019	Dosdè 2 (SO)	*Eriophorum angustifolium*	24.52	50.89
		Trichophorum cespitosum	12.64	26.23
		Eriophorum vaginatum	11.02	22.87
29/08/2019	Dosdè 3 (SO)	*Nardus stricta*	131.12	77.44
		Anthoxanthum nipponicum	19.42	11.47
		Mutellina adonidifolia	5.76	3.40
		Poa alpine	5.58	3.30

5   METHODS

For this thesis the hydrological model *Poli-Hydro* was used to simulate the hydrology of the two study areas, namely Valtellina valley (*Valt*) and Gran Paradiso National Park (Valle d'Aosta region) (*GPNP*). The hydrological model was completed with a module for the pasture dynamic simulation, *Poli-Pasture.* For the case study of Valtellina *Poli-Pasture* considered only an index pasture species for the entire area, while for the case study of Gran Paradiso National Park, *Poli-Pasture* was corrected to consider the inter-specific competition between different species. For this reason the *CoSMo* model (Confalonieri, 2014; Movedi et al., 2019) was adapted for *Poli-Pasture*. Here two different species were considered.

Moreover the pasture area was divided into two altitude belts, namely high altitude (*HighAlt*) and low altitude (*LowAlt*). In Valtellina the altitude threshold was 2000 m asl, while in the area of the Gran Paradiso National Park the altitude threshold was 1800 m asl. So, in *Valt* one pasture species was considered at *LowAlt, Trisetum flavescens* (Figure 10), and a different species was used at *HighAlt, Nardus stricta* (Figure 11). In *GPNP* two species was used at *LowAlt, Trifolium Alpinum* (Figure 12) and *Dactylis glomerata* (Figure 13), and two species at *HighAlt*, *Festuca rubra* (Figure 14) and *Nardus stricta.* These species were chosen between the most abundant species in the study areas, based on samples collected in fulfilment of MOUPA project and information from literature (Angus et al., 1980; D'ottavio & Ziliotto, 2003; Erfini, 2017; Gusmeroli et al., 2005; Haldemann & Fuhrer, 2005; Ziliotto et al., 2003). For this reason, these species were considered as representative of the pasture vegetation in the areas.

The hypothesis done for *Valt* study area was clearly a simplified one, also taken in other studies (Insua et al., 2019b; Liu & Basso, 2017; McCall & Bishop-Hurley, 2003; Ruelle et al., 2018). The case study of *Valt* was a preliminary assessing of potential impacts of climate upon pasture productivity in the area, while the case study of *GPNP* considered also the inter-specific competition for a more complete simulation, and to evaluate which species are more resilient to climate change.

Moreover, a different hypothesis in the two study areas was considered in terms of growth season (*GS*) of the pasture vegetation. In *Valt* the simulation was done considering both a fixed and a variable *GS*, while in *GPNP* the simulation was done only with a fixed *GS*. The fixed *GS* began April 1st in *LowAlt* and April 30th in *HighAlt*, while finished on September 30th in both altitude belts. The variable *GS* would start when the mean temperature would be higher than T_{base} of each species for 10 consecutive days, and it would stop when T would be lower than the average temperature of September 30th of the period 2006-2019 for 10 consecutive days.

This may account for yearly potential variations of the *GS* length, in response to climate conditions, so it was possible to improve the results of simulation and to evaluate the impact of future modified climate.

The *Poli-Hydro* model works on a gridded basis, so the *DEM* is the base layer for the simulation. From the original resolution, *DEM* was aggregated to a coarser resolution to guarantee a simulation of the model in more rapid interval times. In *Valt* the used spatial resolution was 1 km, while in *GPNP* it was 100 m.

Figure 10: *Trisetum flavescens*.

Figure 11: *Nardus stricta*.

Figure 12: *Trifolium alpinum*.

Figure 13: *Dactylis glomerata*.

Figure 14: *Festuca rubra*.

In the next figures (Figure 15 and Figure 16) schemes of the model under two settings are reported.

After the calibration and the validation of the model for the control run CR period, *Poli-Hydro+Poli-Pasture* was used for climate projections. In this way it was possible to evaluate potential variations in pasture productivity and dynamics with respect to present conditions, considering different climate scenarios.

For this thesis some agro-climatic indices were developed to summarise the potential effect of climate change on pasture dynamics. They are related to *GS* parameters, climate and water availability. Some of them could be calculated from the initial climate variables, while others use outputs of the model.
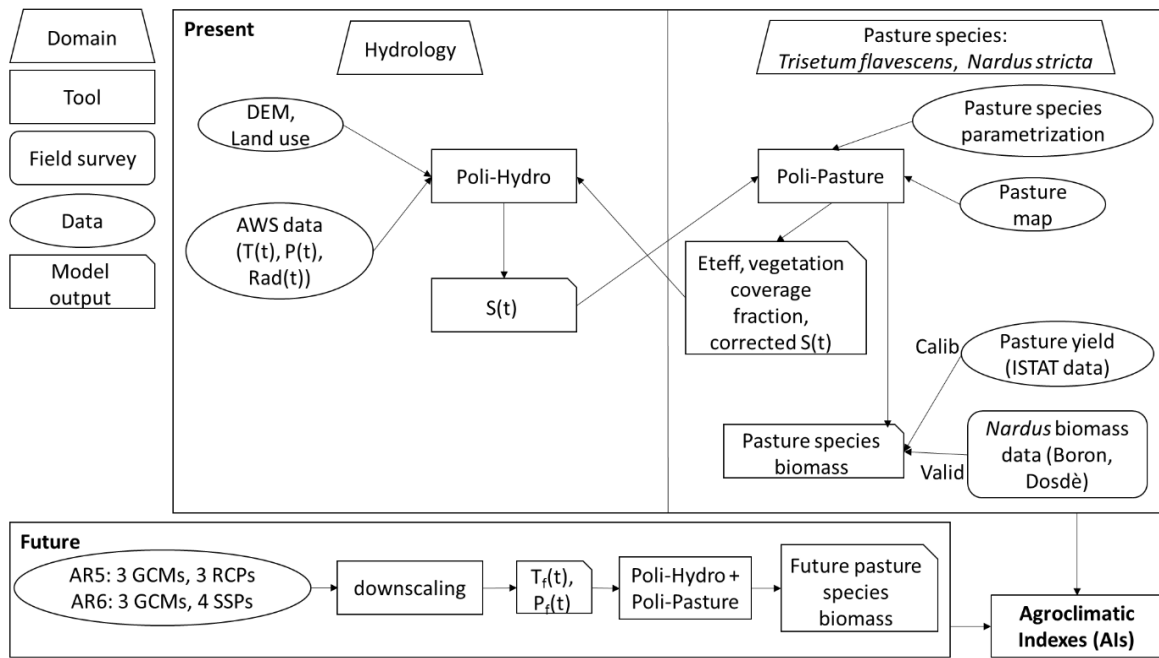
Figure 15: *Poli-Hydro* and *Poli-Pasture* scheme utilised for the case study of Valtellina.
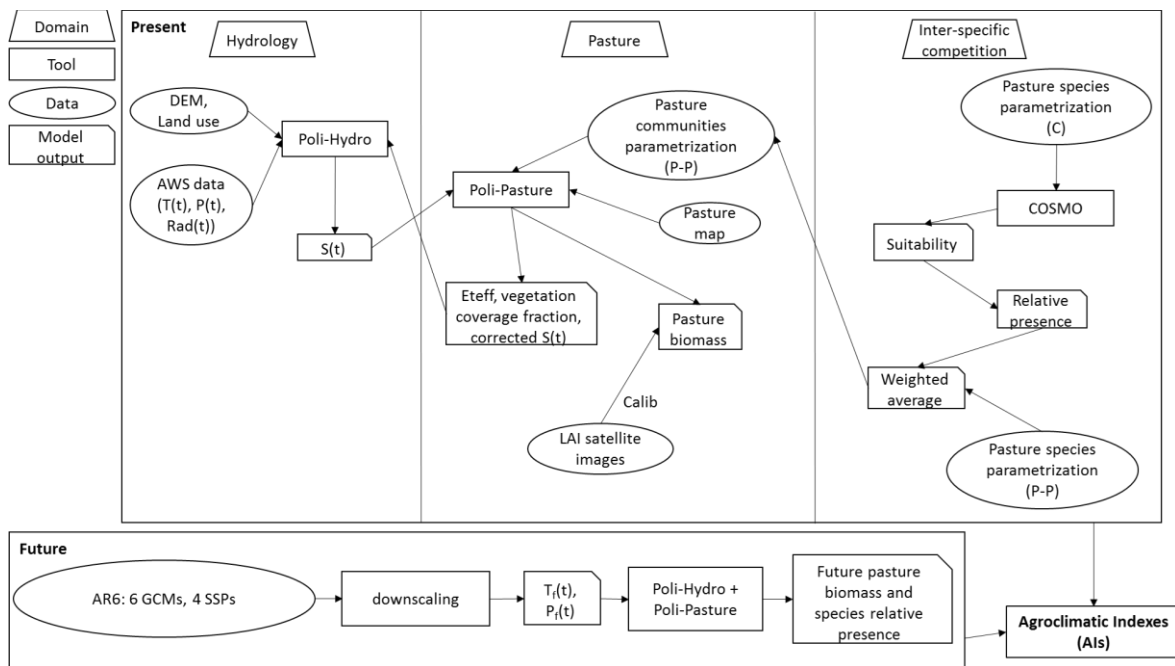
Figure 16: *Poli-Hydro* and *Poli-Pasture*, corrected with *CoSMo*, scheme utilised for the case study of Gran Paradiso National Park.

In practice, *Poli-Hydro* spatializes weather data and simulates the water balance in each cell of the study area and for each time step. *Poli-Pasture* uses weather information and soil water content results from *Poli-Hydro* to simulate the vegetation growth. This depends on the parametrization of pasture species characteristics. Then, *Poli-Pasture* gives as output the *LAI* value and the cumulated pasture biomass for each cell. Moreover, it calculates an updated value

of evapotranspiration and soil water content that provides again to *Poli-Hydro* (Figure 15). In the model scheme with the inter-specific competition, the *CoSMo* model, basing on suitability factors dependent on different variables, e.g. water availability, radiation, etc., calculates the relative presence of each species in each cell for each time step (Figure 16). The community parameters now are the weighted average of species parameters based on their relative presence in the specific cell for that day. In this way the community parametrisation is updated for each time step and is different in each cell of the study area.

5.1 Hydrological model: *Poli-Hydro*

Poli-Hydro is a spatially semi-distributed hydrological model based on the continuity equation applied to the soil water content. In practice a water balance is calculated in each cell of the study area for each time step, here 1 day (Equation 2).

For the water budget, *Poli-Hydro* considers dynamics of glaciers, the snow and ice melt, M_s and M_i respectively, and the actual evapotranspiration ET_{eff}, subsequently, based on two contributes to discharge, the superficial and groundwater flow, Q_s and Q_g, it provides routing flow at any river sections.

$$S(t + \Delta t) = S(t) + R(t) + M_s(t) + M_i(t) - ET(t) - Q_g - Q_s \qquad \text{Eq. 2}$$

Where S is soil water content, and R is the liquid share of precipitation. R is calculated from total precipitation using mean temperature for day t; when temperature T is below the threshold of 0°C, precipitation is solid and accumulates as snow, while when it is above the threshold, it is liquid, R, and it contributes to soil water content.

5.1.1 Cryosphere dynamic

Snow and ice melt are modelled by a T-index approach (Hock, 2003; Martinec, 1975; Ohmura, 2001; Singh et al., 2000), proportional to atmospheric temperature T through a degree-day factor DD.

$$M_s = DD_s(T_0 - T_t) \qquad \text{Eq. 3}$$
$$M_i = DD_i(T_0 - T_t) \qquad \text{Eq. 4}$$

Where DD_s is the degree day of snow and DD_i is the degree day of glaciers. T_t is temperature at time t and T_0 is temperature threshold for melting, here 0°C (Fuso et al., 2021). Ice ablation begins after complete melting of snow cover upon ice (Aili et al., 2019; Bocchiola et al., 2010, 2011; Hock, 2003).

Also ice dynamics is modelled, to update daily the volume and the area of glaciers. This is useful especially for climate projections. The model is based upon simplified gravity-driven ice flow (Aili et al., 2019; Bocchiola et al., 2018; Soncini et al., 2017), where ice flow velocity $v_{ice,i}$ is calculated as a function of the basal shear stress τ_b.

$$v_{ice,i} = K_d \, \tau_{b,i}^n \, h_{ice,i} + K_s \frac{\tau_{b,i}^n}{h_{ice,i}}$$
Eq. 5

With $h_{ice,i}$ ice thickness in cell i [m], K_s [1/m^3/y] and K_i [1/m/y] parameters of basal sliding and internal deformation respectively, and n exponent of Glen's flow law (Soncini et al., 2017).

Basal shear stress τ_b is calculated as:

$$\tau_{b,i}^n = \rho_{ice} g h_{ice,i} \sin\alpha_i$$
Eq. 6

with ρ_{ice} ice density [kg/m^3], g gravity acceleration [m/s^2] and α_i local slope. Ice flow is evaluated starting from an initial, spatially constant, value of ice thickness equal to 100 m (Aili et al., 2019; Soncini et al., 2017), from which the shear stress and the velocity are calculated. Then, the mass balance for each time step is performed and new ice thickness calculated as the difference between previous ice thickness and ice melt M_i.

$$h_{ice,i}(t + \Delta t) = h_{ice,i}(t) - M_i(t)$$
Eq. 7

The model also calculates the snow water equivalent SWE in each cell, and updates the value for each time step. SWE is calculated as:

$$SWE(t + \Delta t) = SWE(t) + P_{snow}(t) - M_s(t) - ET_{eff,snow}$$
Eq. 8

where P_{snow} is solid precipitation and $ET_{eff,snow}$ is the evapotranspiration from snow, equal to the 20% of potential evapotranspiration ET_{max}.

5.1.2 Evapotranspiration

Potential evapotranspiration ET_{max} is evaluated with the Hargreaves' formula:

$$ET_{max} = 0.0023 \, R_a (T + 17.8) \sqrt{\Delta T}$$
Eq. 9

where R_a is the extraterrestrial solar radiation, T is the mean temperature and ΔT is the daily thermal excursion, calculated as difference between minimum and maximum temperature T_{min} and T_{max}, spatialized for each cell from AWS observed data, like mean temperature T. For future climate projections monthly average values of ΔT are used, estimated from literature. These values are reported in Table 8.

Table 8: Monthly average of daily thermal excursion for Italian Alps, used for climate projections simulation.

Month	ΔT
January	6.44
February	7.67
March	9.33
April	9.89
May	10.22
June	10.56
July	11.00
August	10.56
September	9.56
October	8.56
November	7.00
December	6.22

Then actual evapotranspiration ET_{eff} is estimated as the sum of effective evaporation from bare soil E_{eff} and effective transpiration T_{eff}, both dependent on ET_{max}, soil humidity θ and vegetation coverage fraction fv.

$$E_{eff} = \alpha(\theta)ET_{max}(1 - f_v) \qquad \text{Eq. 10}$$

$$T_{eff} = \beta(\theta)ET_{max}f_v \qquad \text{Eq. 11}$$

where

$$\theta = \frac{S}{S_{max}}\theta_s \qquad \text{Eq. 12}$$

$$\alpha(\theta) = \theta \ \ if \ \theta > \theta_w \qquad \text{Eq. 13}$$

$$\beta(\theta) = \frac{\theta - \theta_w}{\theta_l - \theta_w} \ \ if \ \theta > \theta_w \qquad \text{Eq. 14}$$

with θ_w wilting point [-], θ_l field capacity [-] and θ_s saturation.

5.1.3   Runoff formation, groundwater discharge and flow routing

Based on the value of S with respect to S_{max} groundwater, discharge Q_g forms, while, only in condition of saturated soil, $S=S_{max}$, overland discharge Q_s originates. They could be calculated as follows:

$$Q_g = K\left(\frac{S}{S_{max}}\right)^k \qquad \text{Eq. 15}$$

$$Q_s = \begin{cases} S - S_{max} & if \ S > S_{max} \\ 0 & if \ S > S_{max} \end{cases} \qquad \text{Eq. 16}$$

where K [mm/d] is saturated permeability and k [-] is a power exponent.

Then, for the flow routing, two parallel systems are considered, one for superficial flow and one for groundwater flow. Two instantaneous unit hydrograms (IUH) are evaluated for each cell using the Nash approach (Rosso, 1984) for superficial and groundwater flow. In this way it is possible to have the superficial and the groundwater discharge contributions in all selected sections of the river. Indeed, the IUH of each cell is routed to the section based on two lag times, one for overland and one for groundwater. So, in each section for each time step the total superficial and groundwater discharge are the sum of all the contributions of all the contributing cells of that section (correspondent sub-basin) for that time step. Then the total discharge is calculated for each time step as the sum of groundwater and superficial discharge.

5.2   Pasture module: *Poli-Pasture*

Based on the pasture map given as input to the model, *Poli-Pasture* is applied only in cells covered by pasture. As reported before, pasture areas were divided in two altitude belts that run independently, based on characteristic parameters of the single species.

Poli-Pasture was developed starting from the *CropSyst* model (Addimando et al., 2015; Bocchiola et al., 2013; Nana et al., 2014; Stöckle et al., 1994).

Defined the start of *GS*, the model begins to simulate the pasture growth, until the end of *GS*.

The phenological stages of the pasture species (beginning of growth, flowering, maturity, end of growth) are reached by the accumulation of thermal time (degree-days [°C/d]) until a defined threshold for each stage (Stöckle et al., 1994). If the daily temperature is below a base temperature T_{base}, no thermal time is accumulated. The same if the daily temperature is larger than a cutoff temperature T_{cutoff}, so the growth is limited. Model tuning was attained by varying degree-day thresholds for each phenological stage.

In the two study areas vegetation is cut/harvested based on two different hypothesis. In Valtellina vegetation is harvested after flowering in *HighAlt* and cut before maturity in *LowAlt*. In *GPNP* vegetation is cut/harvested when biomass is larger than 1.5 t/ha, an average value between the necessity of animals and the correct number of animals per hectare of pasture, to guarantee the good maintenance of the area. After harvesting, the growth of vegetation in that cell begins again. Total annual production in a cell is the sum of peak biomass in each growth cycle.

For each time step, and based on the phenological stage, *Poli-Pasture* estimates daily production of fresh biomass for each species as the minimum value between water dependent growth G_{TR} [kg/m²/d] and solar radiation dependent growth G_R [kg/m²/d].

$$G_{TR} = \frac{T_{eff}\ BTR}{VPD} \qquad\qquad \text{Eq. 17}$$

$$G_R = LtBc\ PAR\ f_{PAR}\ T_{\lim} \qquad\qquad \text{Eq. 18}$$

With *VPD* [kPa] average vapour pressure deficit, *BTR* [kPa kg/m³] biomass transpiration coefficient, *LtBc* [kg/MJ] light-to-biomass conversion coefficient, *PAR* [MJ/m²/d] photosynthetically active radiation, f_{PAR} [-] fraction of incident *PAR* intercepted by canopy, and T_{lim} [-] temperature limitation factor. These variables are calculated for each time step from the calculated thermal time at that time step.

In the pasture areas, potential evapotranspiration is calculated with a different equation, the Priestley-Taylor's formula.

$$ET_{max} = 1.26\frac{\Delta}{\Delta+\gamma}\frac{R_n-G}{\lambda} \qquad\qquad \text{Eq. 19}$$

Where R_n is net radiation at ground [MJ/m²/d], Δ is the slope of pressure curve [kPa/°C], *G* is the heat flux from the soil [MJ/m²/d], γ is the psychrometric constant [kPa/°C] and λ is the vaporization latent heat [MJ/kg].

In this case the actual transpiration is calculated as:

$$T_{eff} = \frac{86,400\ C}{1,5\ (\Psi_s-\Psi_x)} \qquad\qquad \text{Eq. 20}$$

where *C* is root conductance [kg s /m⁴], Ψ_s is soil water potential [J/kg] depending on soil water content *S*, and Ψ_x is leaf water potential depending on plant roots development.

While the water dependent growth is influenced by evapotranspiration, the solar radiation dependent growth depends on the fraction of income radiation intercepted by vegetation. So f_{PAR} depends on leaf area index *LAI* in a specific cell:

$$f_{PAR} = 1 - \exp(-k\ LAI_{cum}) \qquad\qquad \text{Eq. 21}$$

LAI changes in each time step, LAI_{cum} is the cumulated value in the cell equal to the sum of the value of the previous time step and of the *LAI* variation. The variation of *LAI* in a time step is dependent on the biomass production of that time step.

$$LAI = \frac{SLA\ Bio}{(1+l_s\ Bio_{cum})^2} \qquad\qquad \text{Eq. 22}$$

Where *SLA* [m²/kg] is the specific leaf area, *Bio* the new daily biomass [t/ha], Bio_{cum} the total biomass present in that day [t/ha], and l_s the stem-leaf partition coefficient.

5.3   Interspecific competition: *CoSMo* module

The *Community Simulation Model*, *CoSMo*, simulates changes in pasture species composition during the *GS* (Confalonieri, 2014; Movedi et al., 2019; Piseddu et al., 2022; van Oijen et al., 2020)*. CoSMO* is a simplified model that simulates the overall community instead of the single species. Then, it is possible to evaluate parameters of a species, starting from the community parameters.

Here the *CoSMo* model was adapted to include the simulation of the interspecific competition between species in a distributed model, like *Poli-Pasture.* Indeed, in a previous study, the *CoSMo* model was used to simulate the competition between species in a site (Piseddu et al., 2022). In this work it was possible to analyse the distribution of pasture species in a large area like the *GPNP*, and to evaluate the effect of some variables on the presence of a species in a specific cell. Indeed variables that influence the presence of a species vary basing on climatic, hydrological and topographic conditions that are possible to evaluate using *Poli-Hydro* and *Poli-Pasture* models.

Moreover, the model *CoSMo* was simplified to adapt to the hypothesis of *Poli-Pasture*, different from that of the original *CropSyst*. This is helpful for the realization of the simulation for a long period and a large study area.

The model aims to find parameters for pasture community, based on the morphology and the physiology of the single species present in the community. Parameters are updated for each time step in each cell, based on the adaptation of the single species to the conditions of that day and that cell. The initial condition is that all the species are equivalently present; having here 2 species for each altitude belt, each of them occupies the 50% of the area in its altitude belt.

Basing on some information about soil, weather and pasture management, *CoSMo* model calculates for each species some suitability factors to each condition, than it calculates an overall suitability of the species, combining all the suitability factors, finally it calculates a suitability factor of the community. Based on the comparison between the suitability of the species and the suitability of the community, the relative presence of the species is evaluated.

In the end, based on relative presence, it is possible to calculate the parameters of the community, to use in the simulation of *Poli-Pasture.* Indeed, the community parameters are the weighted average of the species parameters, based on their relative presence.

This calculation is done in each cell and updated daily.

So it is possible to evaluate the dynamic and the presence of a species during the overall *GS*, in each point of the study area.

Suitability factors in practice consider the competition between species, based on their feature and phenological stage during *GS*, to different factors, like the liking by animals, average temperature, capacity to capture solar radiation, water availability.

Here these suitability factors were considered:

1) Pasture management: harvesting by animals. f_{liking} factor is calculated.

$$f_{liking} = (1 - L)\{1 + [2RP_{t-1} - 3)RP]\}$$ Eq. 23

L [0; 1] is the liking of an animal to eat that species. *L*=0 not liking, *L*=1 liking. Here we considered pasture of bovines. *RP* is the relative presence of the species.

2) Temperature. f_T factor is calculated.

$$f_T = \begin{cases} 0 & if\ T \leq T_{base} \\ \frac{T - T_{base}}{T_{opt} - T_{base}} & if\ T > T_{base}, T \leq T_{opt} \\ \frac{T_{cutoff} - T}{T_{cutoff} - T_{opt}} & if\ T > T_{opt}, T < T_{cutoff} \\ 0 & if\ T \geq T_{cutoff} \end{cases}$$ Eq. 24

T is the daily mean temperature, while T_{base}, T_{opt} and T_{cutoff} are respectively base, optimal and cutoff temperature, specific for the species.

3) Radiation. f_{Rad} factor is calculated.

$$f_{Rad} = 0.5 + 0.25 \left(\frac{LAI_{max} - LAI}{LAI_{max} + LAI} + \frac{H_{max} - H}{H_{max} + H} \right)$$ Eq. 25

here *LAI* and *H* are leaf area index and plant height at time step *t*, respectively, while LAI_{max} and H_{max} are maximum leaf area index and plant height.

4) Water. f_W factor is calculated.

$$f_W = \left(\frac{f_{PAW} + f_{root}}{2} \right)$$ Eq. 26

f_{PAW} is a factor that considers water availability in soil, while f_{root} is related to root depth.

f_{PAW} is calculated as:

$$f_{PAW} = \begin{cases} 0 & \theta < 1 - DT \\ \frac{DT - 1}{DT} + \frac{\theta}{DT} & elsewhere \end{cases}$$ Eq. 27

with θ volumetric soil water content and *DT* [0; 1] specific parameter of the species related to water stress tolerance. *DT*=0 sensible, *DT*=1 tolerant.

While f_{root} is calculated as:

$$f_{root} = \begin{cases} 1 - \frac{RD}{RD_{max}} & RD < RD_{max} \\ 0 & elsewhere \end{cases}$$ Eq. 28

with *RD* root depth at time *t* and RD_{max} maximum root depth.

For the calculation of total suitability, these factors are aggregated in a hierarchical way in other 4 factors.

$$HSf_1 = f_{liking}$$
$$HSf_2 = \sqrt{HSf_1}\, f_T$$
$$HSf_3 = \sqrt{HSf_2}\sqrt{f_T}\, f_{Rad}$$
$$HSf_4 = \sqrt{HSf_3}\sqrt{f_{Rad}}\, f_W$$

Eq. 29

$$Sf_s = \sum_{q=1}^{4} HSf_q$$

Eq. 30

The suitability factor of the community is calculated as:

$$CSf = \sum_{i=1}^{n} Sf_{s_i}$$

Eq. 31

where *n* is the number of species, here 2.

While *Poli-Pasture* simulates the new fresh biomass production for each time step, *CoSMo* updates the relative presence, as percentage of the total biomass, and re-calculates the new community parameters for the next time step.

The relative presence for each time step is calculated as:

$$RP_t = RP_{t-1} + \left(\frac{Sf_{s_i} - \frac{CSf}{n}}{4I} \right)$$

Eq. 32

Where 4 is related to the 4 suitability factors of the species and *I* [80; 120] is a parameters indicating the inertia of the system to change.

To calculate the community parameters y_{com} to use as input to *Poli-Pasture*, the weighted average is done from species parameters y_i:

$$y_{com} = \sum_{i=1}^{n} y_i\, RP_i$$

Eq. 33

5.4   Calibration of the model

The calibration of *Poli-Hydro* was done with discharge data, snow depth data at AWS, and *SCA* satellite images. For discharge an annual percentage *Bias*, the monthly and daily *NSE* were calculated in each section of the river with hydrometric station. For snow depth, a daily average value between stations was calculated and compared with the simulated value; here *Bias* and *NSE* or R^2 were calculated. The same was done with satellite images. In practice the *SCA*, simulated and observed, was calculated on the entire study area for each images and the *Bias* was calculated. A visual comparison between observed and simulated results was also done.

For *Poli-Pasture* different data were used in Valtellina and in Gran Paradiso National Park. In the first case the *Bias* was calculated between observed data of biomass and simulated

results, as average for the entire study area. In the area of Gran Paradiso National Park, the average value of *LAI* in each satellite images was calculated. The *Bias* and the *NSE* were calculated here comparing the observed results and the average simulated *LAI* in the same day.

For *Poli-Pasture* and *CoSMo* a validation was done using collected in-situ data. The biomass value and the relative presence is extracted for the specific cell and day of the samples. A *Bias* is calculated to compare simulation to the sample.

Bias is calculated as follow:

$$Bias = \frac{Sim - Obs}{Obs}$$
Eq. 34

where *Sim* is the average simulated value of the considered variable, and *Obs* is the average observed value.

NSE is calculated as:

$$NSE = 1 - \frac{(Sim - Obs)^2}{(Obs - Obs_{av})^2}$$
Eq. 35

where, in this case, Obs_{av} is the average value of observation for the entire period, and *Sim* and *Obs* are the daily/single/monthly value.

5.5 Climate projections and future scenarios

To simulate future projections of hydrology and pasture dynamics it was necessary to use climatic projections of precipitation *P* and temperature *T* from a several number of Global Circulation Models GCM. GCMs use a coarse spatial resolution, for this reason it was necessary to disaggregate this series of data to the same resolution of the hydrological model. In particular, a downscaling process was applied to have series of data of *P* and *T* in each AWS, then spatialized with Thiessen polygons. Future projections were done for the period 2020-2100. Here, analysis was done for two decades, the first at the middle of the XXI century, 2041-2050 (*P1*), and the second at the end of the century, 2091-2100 (*P2*).

For the case study of Valtellina three GCMs of the Coupled Model Intercomparison Project release 5 related to the Fifth Assessment Report AR5 of IPCC (the Intergovernmental Panel on Climate Change) (Stocker et al., 2013; Taylor et al., 2012) and three GCMs of the Coupled Model Intercomparison Project release 6 related to the Sixth Assessment Report AR6 (Eyring et al., 2015) were used, while for Gran Paradiso National Park six GCMs of the AR6 were used. The chosen models are able to acceptably describe the climate of Northern Italy, especially in terms of the seasonality of precipitation (Bombelli et al., 2019; Confortola et al., 2013; Fuso et al., 2021; Groppelli, Bocchiola, et al., 2011; Groppelli, Soncini, et al., 2011).

Three chosen GCMs of AR5 are ECHAM6.0 (European Centre Hamburg Model, version 6, of the Max Planck Institute for Meteorology) (Stevens et al., 2013), CCSM4 (Community Climate System Model, version 4, of the National Center for Atmospheric Research) (Gent et al., 2011), and EC-Earth2.3 (European Consortium Earth System Model, version 2.3) (Hazeleger et al., 2012). Three Representative Concentration Pathways RCPs were used for AR5: RCP 2.6, 4.5, 8.5.

For Valtellina valley three chosen GCMs of AR6 are EC-Earth3.0 (Döscher et al., 2022), ECHAM6.3 (Mauritsen et al., 2019) and CESM2 (Danabasoglu et al., 2020). For AR6 four Shared Socio-economic Pathways SSPs were used: SSP 1-2.6, 2-4.5, 3-7.0, 5-8.5. Combining GCMs with RCPs and SSPs, 21 future scenarios were used.

For Gran Paradiso National Park area these three GCMs of the AR6 were added to other three: HadGEM3 GC3.1 (Global Coupled Met Office Unified Model of the Headley Center, version 3.1) (García-Franco et al., 2020), MIROC6 (Model for the Interdisciplinary Research on Climate, version 6) (Kataoka et al., 2020) and CMCC-CM2 (Centro Euro-Mediterraneo sui Cambiamenti Climatici Climate Model, version 2) (Cherchi et al., 2019).

For these six GCMs four SSPs were used, for a total of 24 scenarios.

In Table 9 characteristics of the nine GCMs are reported.

Table 9: Characteristics of Global Circulation Models used in Valtellina and Gran Paradiso National Park areas.

	Model	Nationality	Cell dimension [km x km]
AR5	EC-Earth2.3	European Union	320x160
	ECHAM6.0	Germany	192x96
	CCSM4	USA	288x144
AR6	EC-Earth3.0	European Union	83x83
	ECHAM6.3	Germany	208x208
	CESM2	USA	139x100
	CMCC-CM2	CMCC	111x111
	HadGEM3-GC3.1	UK	28x28
	MIROC6	Japan	111x111

RCPs are characterised by an increase of radiative forcing in the atmosphere. So RCP 2.6 is characterised by a strong CO_{2eq} emission reduction, RCP 4.5 by a consistent emission reduction while the RCP 8.5 is the business as usual scenario.

The SSP 1-2.6 scenario is based on an optimistic and sustainable human development with strong CO_{2eq} emission reduction. SSP 2-4.5 is the scenario with future trend like the historical course with consistent CO_{2eq} emission reduction. SSP 3-7.0 is based on a pessimistic human development with regional security prioritization and no CO_{2eq} emission reduction. SSP 5-8.5 is based on an optimistic human development based on a fossil fuel economy without CO_{2eq} emission reduction.

5.5.1 Downscaling

Downscaling is necessary to have daily series of projections of precipitation and temperature for the period 2020-2100 in correspondence of AWS.

Here a static downscaling was applied, basing on the procedure developed by (Groppelli, Soncini, et al., 2011) for temperature and (Groppelli, Bocchiola, et al., 2011) for precipitation. A relationship between GCM cells data and AWS data for the present period was found and then applied to GCM projections to have information in AWS (Benestad et al., 2008). It is based on the hypothesis that the relationship of the past/present continues to be valid also for the future (Piani et al., 2010).

The static downscaling was done for precipitation through the stochastic space random cascades method, to reproduce the observed precipitation intermittence.

The control run CR period was defined to compare observed data with the historical series of GCMs. For Valtellina it was the period 2006-2017, while for Gran Paradiso National Park CR was the period 2005-2019.

R_{GAO} is the observed average daily precipitation in AWS, while R_{GCM} is the daily precipitation simulated by the GCM. The goal of downscaling is to adequate the value of R_{GCM} to the value of R_{GAO}, related to the precipitation tax and the intermittence.

$$Bias_{GAO} = \frac{R_{GAO}}{R_{GCM}} = B_{GAO}B_0W_0 \qquad \text{Eq. 36}$$

$$P(B_0 = p_0^{-1}) = P_0 \qquad \text{Eq. 37}$$

$$P(B_0 = 0) = 1 - p_0 \qquad \text{Eq. 38}$$

$$W_0 = \exp(w_0 - \frac{\sigma_{w_0}^2}{2}) \qquad \text{Eq. 39}$$

With:

$$E[B_0] = 1 \qquad\qquad \text{Eq. 40}$$

$$E[W_0] = 1 \qquad\qquad \text{Eq. 41}$$

$$w_0 \sim N(0, \sigma_{w_0}^2) \qquad\qquad \text{Eq. 42}$$

B_{GAO}, p_0 and σ^2_{w0} are parameters to calibrate based on data. B_{GAO} forces R_{GCM} to coincide with R_{GAO}. B_0 is a β model generator and represents the probability that R_{GAO} is null conditioned to a positive value of R_{GCM}. W_0 is a positive parameter that gives variability to precipitation.

For temperature an offset is calculated at the monthly scale between GCM and observed temperature.

$$T_d^{GCM,corr} = T_d^{GCM} - (T_i^{GCM} T_i^{obs}) \qquad\qquad \text{Eq. 43}$$

T_d^{GMC} is the temperature of day d given by GCM, T_i^{GCM} and T_i^{obs} are average monthly temperature of GCM and of observation. $T_d^{GCM,corr}$ is the corrected temperature of day d basing on the correction between monthly GCM and observed temperature.

5.6 Agroclimatic indices

Some agroclimatic indices AI are selected as indicators of climate change effects on pasture productivity. They are indicators of climate, pasture productivity and water availability and use, chosen in literature (Arnell & Freeman, 2021; Bocchiola, 2015; Briner et al., 2012, 2013; Dale & Polasky, 2007; Egarter Vigl et al., 2017; Life Pastoralp, 2019; Nana et al., 2014; Nobakht et al., 2019; Rivington et al., 2013). These eight indices are reported in Table 10 and concern different factors (average temperature of *GS*, extreme temperature, intermittence and quantity of precipitation, relationship between water demand and availability, etc.), giving a broad overview of the dynamics of pasture species.

Table 10: Agroclimatic indices.

AI	Agroclimatic indices	Symbol	Unit
AI1	Growth season length	GSL	[d]
AI2	Heat waves frequency (number of days with $T > T_{cutoff}$)	f_{HW}	[d]
AI3	Number of days in *GS* with precipitation >10 mm	d_{10}	[d]
AI4	Total precipitation in *GS*	P_{GS}	[mm]
AI5	Annual productivity	Y	[t]
AI6	*ET* efficiency in *GS*	$ET_{eff}/ET_{max,GS}$	[mm/mm]
AI7	*ET* relative in *GS*	ET_{eff}/P_{GS}	[mm/mm]
AI8	Specific (green) water footprint in *GS*	ET_{eff}/Y	[mm/t]

Index AI1 provides the length of the *GS* and it was calculated only for variable *GS* mode, in the case study of Valtellina. Index AI2 or frequency of heat waves and AI3, days with heavy

precipitation during *GS*, represent the variability of stress factors for species. Index AI4 indicates abundance or lack of rainfall for vegetation growth. Index AI5 provides an indication of pasture biomass in the area. AI6, the ratio of yearly actual-to-potential evapotranspiration during *GS* assesses the efficiency of species water use, in turn depending upon water availability and distribution in time (Bocchiola, 2015). If this ratio is close to 1, plants use most of the available water, with large evapotranspiration efficiency. AI7, relative evapotranspiration, is an indication of the necessary *ET* with respect to the available water (rainfall) in the *GS* period. This depends upon temperature, driving $ET_{max,GS}$, and available precipitation. Specific water footprint AI8 is an indication of how much water ET_{eff} is needed to be used for the production of a ton of biomass (Bocchiola et al., 2019).

AI values were calculated under present and future conditions for each RCP/GCM under AR5/AR6. The indices AI1-AI4 could be assessed using only climate data. Accordingly, climate data from the available stations were used for calculation under present conditions, while climate projections were used for future conditions. The indices AI5-AI8 explicitly depict the pasture species performance, and they were calculated using *Poli-Pasture* module's outputs under present and projected climate.

6   RESULTS AND DISCUSSION

6.1   Calibration and validation of *Poli-Hydro*

6.1.1   Valtellina

In Table 11 parameters of *Poli-Hydro* are reported, with the corresponding calibration method. The DD_S was calibrated both in terms of *SCA,* through the MODIS images, and snow water equivalent *SWE,* using nivometric data of snow depth. Lag times t_{lag}, saturated conductivity K and ground flow exponent k were calibrated using discharge data in different sections.

Table 11: Parameters of *Poli-Hydro* for Valtellina. Literature references: a (Bombelli et al., 2019), b (Soncini et al., 2017), c (Aili et al., 2019).

Parameter	Unit	Description	Value	Calibration method
DD_S	[mm/d/°C]	Degree day snow	3.4	Nivometer, MODIS
DD_I	[mm/d/°C]	Degree day ice	5	Literature (a)
t_g, t_s	[d]	Lag times, underground/surface, Fuentes/Samolaco	150, 140 / 120, 130	Hydrograph
n_g, n_s	[-]	Nash method, reservoirs number, underground/surface	3, 3	Literature (a, b, c)
K	[mm/d]	Saturated conductivity	3	Hydrograph
K	[-]	Ground flow exponent	1	Hydrograph
θ_w, θ_l, θ_s	[-]	Water content, wilting point, field capacity, saturation	0.15, 0.35, 0.45	Literature (a, b, c)
f_s	[1/m³/y]	Ice flow basal sliding coeff.	1.5×10^{-21}	Literature (b)
f_d	[1/m³/y]	Ice flow internal deformation coeff.	1.9×10^{-25}	Literature (b)

In Table 12 results of R^2 are reported for MODIS, for calibration and validation, and *Bias* and R^2 of snow depth, for calibration. For MODIS the calibration period was 2005-2010, while the validation period was 2015-2018. For *SWE* all snow depth data of the period 2002-2018 were used for calibration. In Table 13 *Bias* and *NSE* of discharge are reported for calibration. In Fuentes section data were available for the period 2003-2018, while in Samolaco section for the period 2009-2018.

The values of *Bias, NSE* and R^2 for both calibration and validation and for all the considered variables explain an acceptable result of calibration of *Poli-Hydro* model. In particular the values of R^2, calculated between average values of *SCA* for all images collected

every 15 days, and of H_s, calculated between average monthly values, are larger than 0.7, that correspond to a good calibration. The *Bias* of H_s is around 10%, corresponding to an acceptable simulation of the snow water equivalent *SWE* available at ground.

Table 12: Calibration and validation of *Poli-Hydro* in Valtellina for snow depth H_s and snow cover area *SCA*.

Variable	Period	*Bias* [%]	R^2 [-]
MODIS *SCA*	Calibration: 2005-2010	-	0.73
MODIS *SCA*	Validation: 2015-2018	-	0.78
Snow depth H_s	Calibration: 2002-2018	-12.11	0.89

Table 13: Calibration of *Poli-Hydro* in Valtellina for discharge *Q*.

	Fuentes (Adda river)	Samolaco (Mera river)
Area [km²]	2553	574
	Calibration: 2003-2018	**Calibration: 2009-2018**
Bias [%]	+-2.11	+8.54
NSE monthly [-]	0.69	0.80
NSE daily [-]	0.53	0.32

It is important to calibrate all the contributions to the water balance (Casale et al., 2021), because in this case study these variables are different conditions for the vegetation dynamics. Calibrating only the discharge at closure section is not a certainty of the good simulation of snow dynamics. In this way it is reliable that the model could simulate correctly the distribution of snow cover and the snow available volume in the watershed.

In Figure 17 the *SCA* is reported as percentage value on the total watershed area, for each MODIS images utilised for the calibration (Figure 17 a) and (Figure 17 b) validation of the model. The MODIS value and the simulated one are compared.

In Figure 18 the comparison of snow depth H_s between simulation and observation is reported. For observation the monthly average was calculated in 4 AWS of the study area and then averaged between the 4 AWS. For simulation the monthly average was calculated in 4 cells where AWS are, then these 4 values were averaged.

In Figure 19 the graph reports the comparison between the modelled monthly average discharge *Q* and the observed one at Fuentes (Figure 19 a) and Samolaco (Figure 19 b) river sections. The average was calculated for the respective period of calibration. In Figure 20 for each month the contribution to discharge is reported: snow and ice melt M_s and M_i, rain *R* and evapotranspiration *ET*. In Figure 21 the monthly discharge, observed and simulated, is reported for the period of calibration.
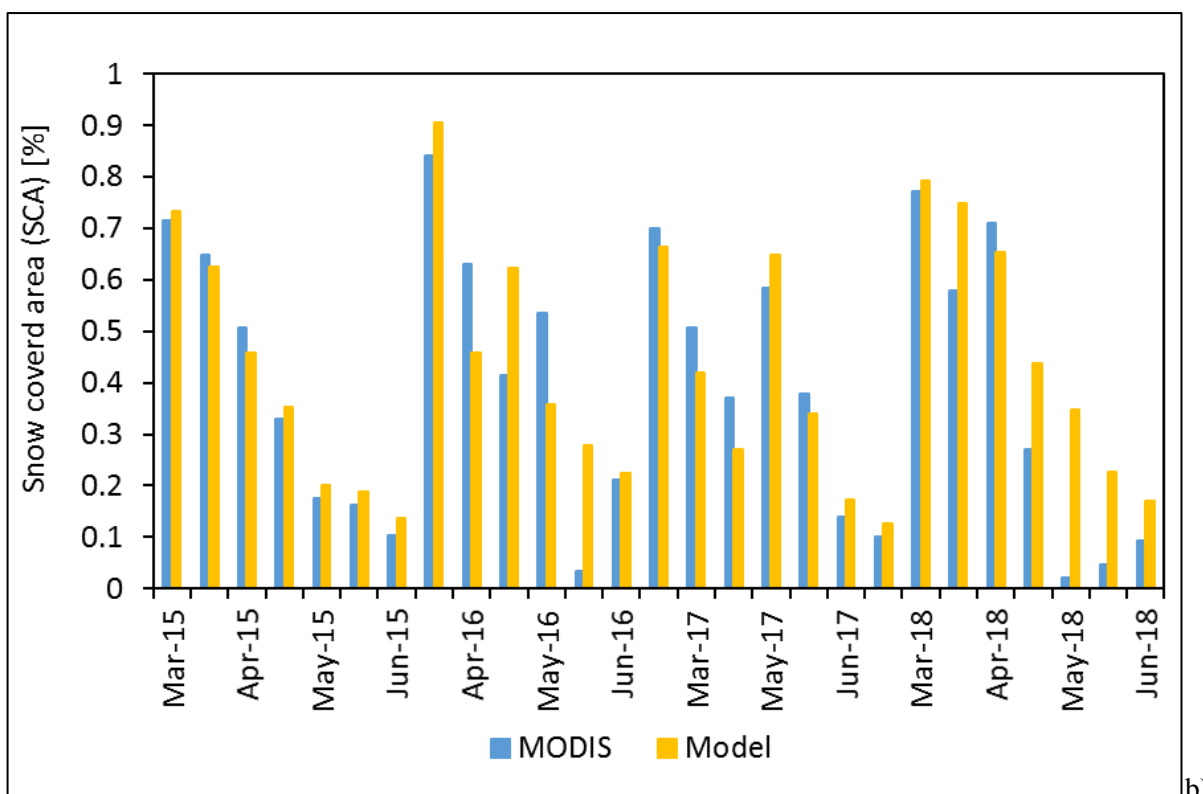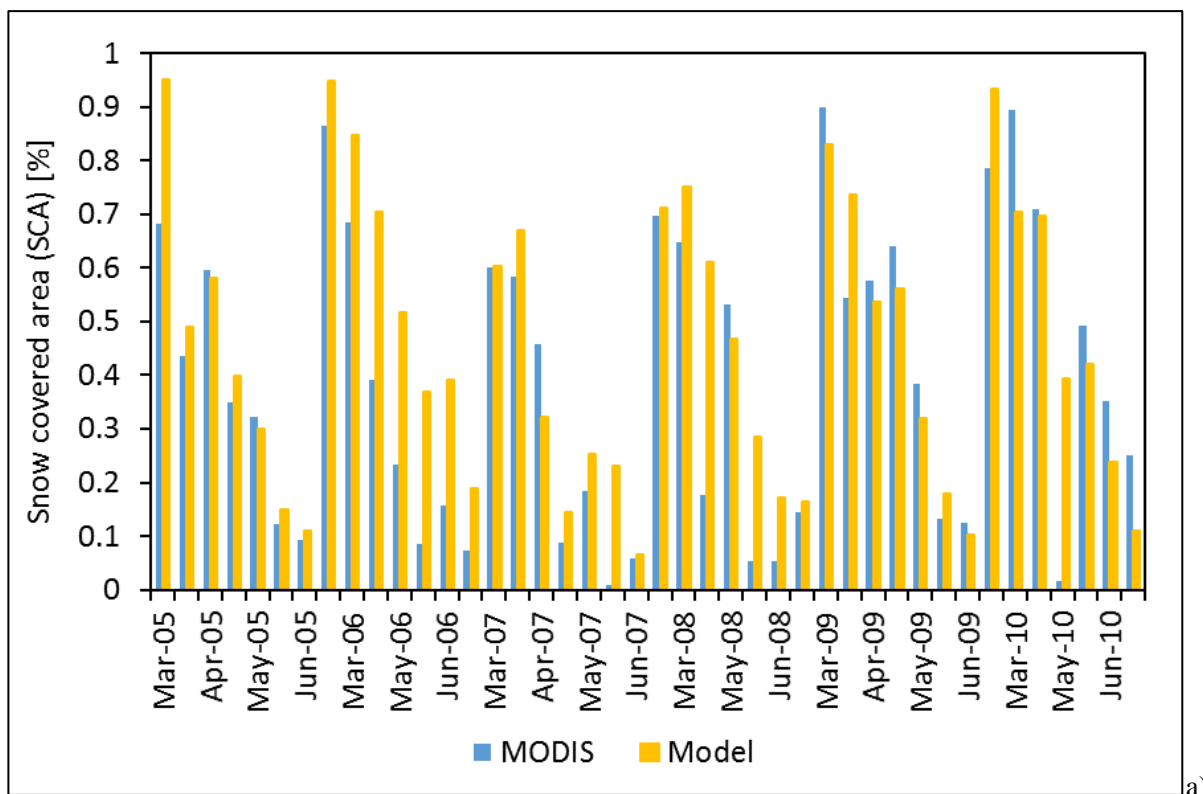
Figure 17: Comparison of snow cover area *SCA* in Valtellina between MODIS images and model simulation, for the calibration (a) and validation (b) period.
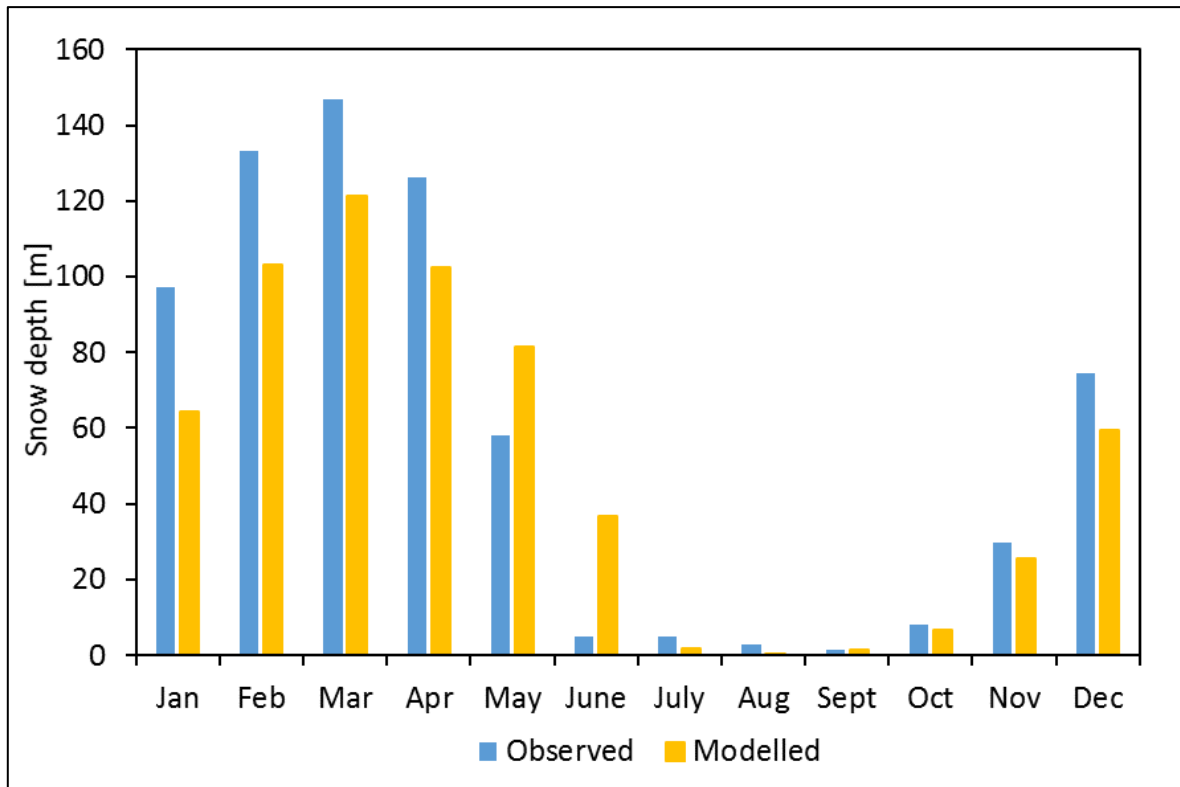
Figure 18: Comparison of snow depth H_s in Valtellina between observation at AWS and model simulation.

The average discharge simulated in Fuentes in the period 2003-2018 is 81.67 m³/s., while in Samolaco during 2009-2018 it is 28.04 m³/s. The peak is in June in both cases.

The contribution of snow melt to discharge is the 41% in Samolaco sub-basin, and the 45% in Fuentes sub-basin. Discharge related to snow melt is larger between April and June, but it is between January and April that snow melt contributes in larger percentage to discharge.

Ice melt in practice does not contribute to discharge, because of the small glaciers area in the watershed. But it contributes for a small percentage between July and September.
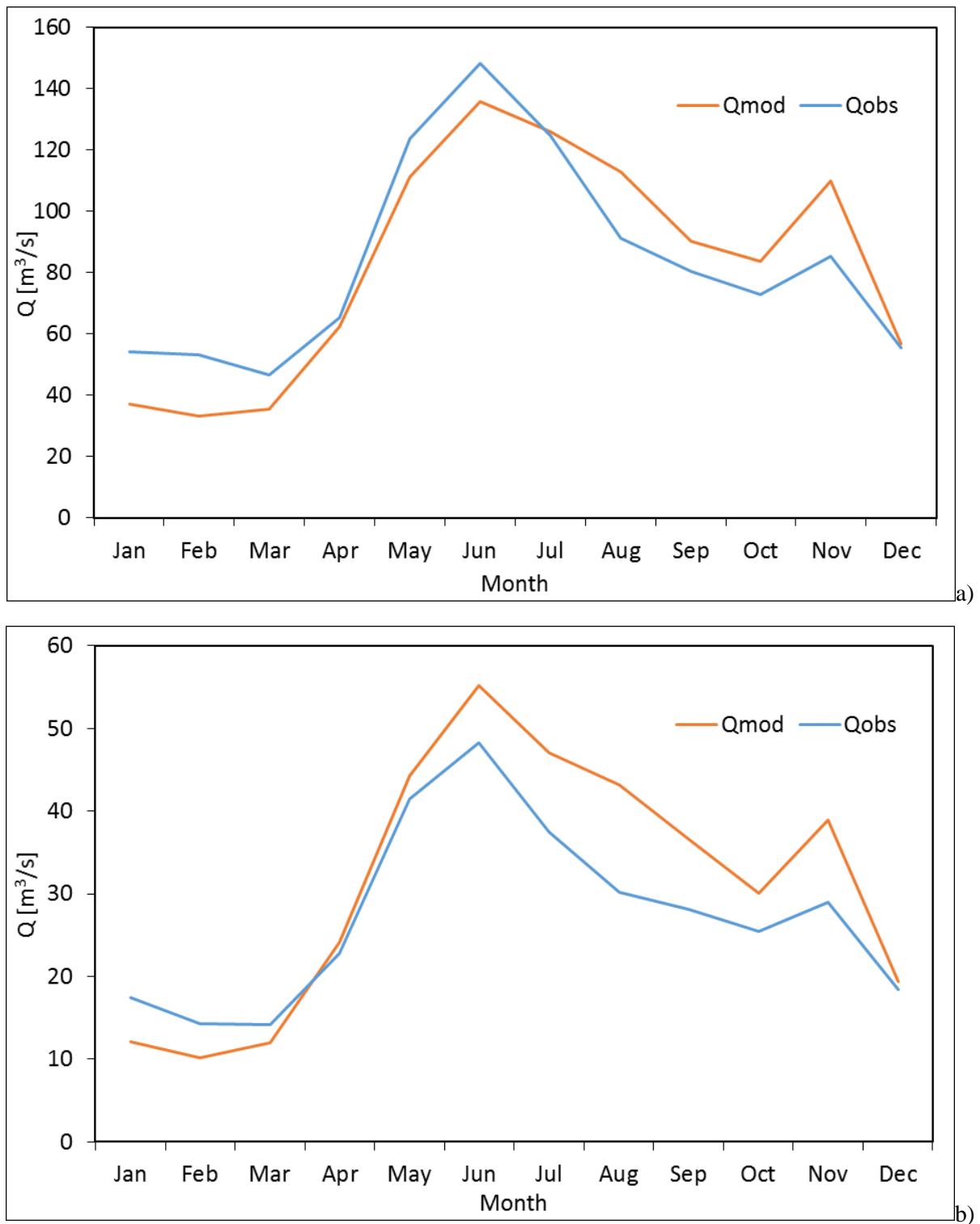
Figure 19: Average monthly discharge, comparison between simulation and observation. The average is calculated for 2003-2018 in Fuentes (a) and for 2009-2018 in Samolaco (b).
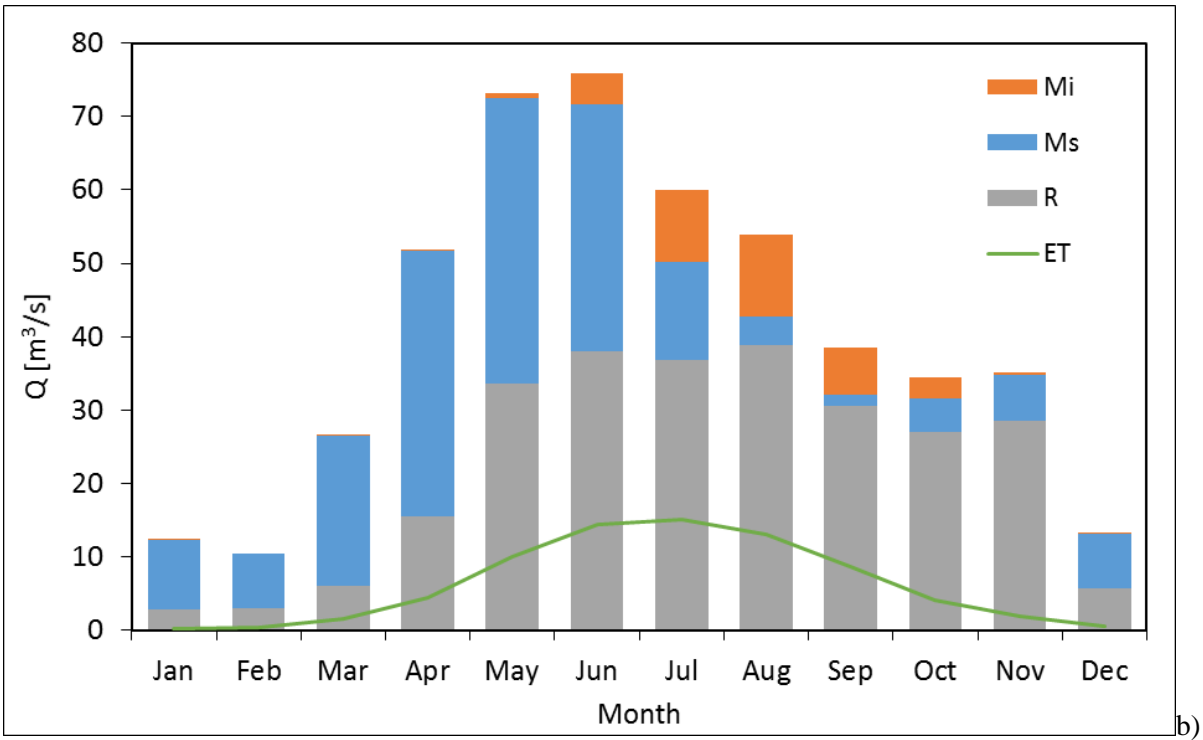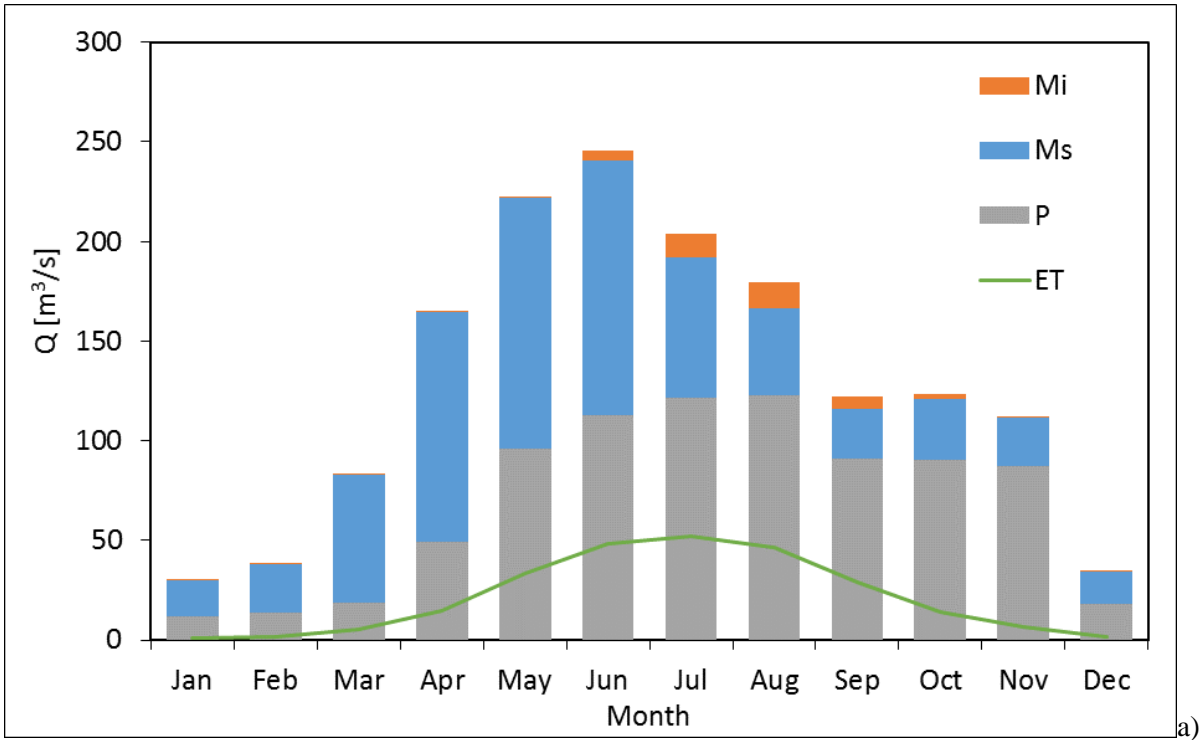
Figure 20: Contribution to discharge in Fuentes (a) and Samolaco (b). M_i is ice melt, M_s is snow melt, R is rain and ET is evapotranspiration.
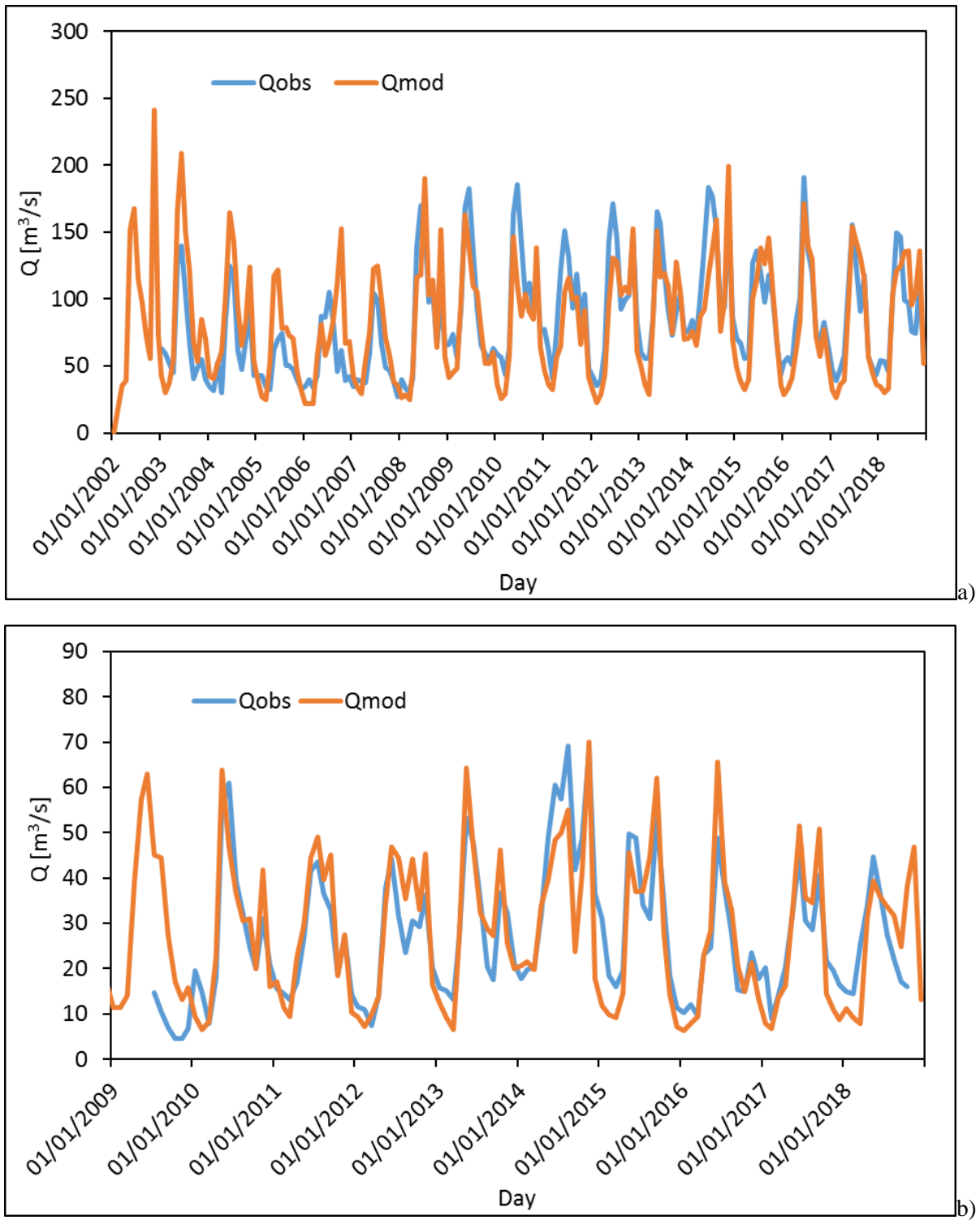
Figure 21: Comparison of observed and simulated monthly discharge, in Fuentes (a) and Samolaco (b), for the period of calibration.

6.1.2 Gran Paradiso National Park

In Table 14 parameters of *Poli-Hydro* for the area of Gran Paradiso National Park are reported.

Here in *GPNP* the calibration and validation is done for the periods 2005-2013 and 2014-2018 in the sections of Eaux Rousses and Cogne - Crètaz. The average discharge in these sections is 2.95 m^3/s and 7.24 m^3/s respectively. The peak is in June. As average in the year snow melt contributes with the 47.80% and the 45.08%, while ice melt contributes with the 0.94% and 1.80% respectively.

Snow melt peaks during April-June and ice melt peaks in July and August. As annual average snow melt generates a discharge of 1.19 m^3/s and 2.43 m^3/s respectively in Eaux Rousses and Cogne - Crètaz sub-basins, while ice melt contributes to discharge with an annual average of 0.02 m^3/s and 0.10 m^3/s.

In Figure 22 the monthly discharge is reported for Eaux Rousses (a) and Cogne - Crètaz (b) for the entire period 2005-2018. In Figure 23 the contribution to discharge of snow and ice melt and rain is reported for an average year of the period 2005-2018 for both the sub-basins, respectively in figure a and b, while in Figure 24 the monthly discharge, observed and simulated, for the entire period 2005-2018 is reported.

Table 14: Parameters of *Poli-Hydro* model for Gran Paradiso National Park case study.

Parameter	Unit	Description	Value
DD_S	[mm/d/°C]	Degree day snow	1.59
DD_I	[mm/d/°C]	Degree day ice	8
K	[mm/d]	Saturated conductivity	5.45
K	[-]	Ground flow exponent	3.4
$\theta_w, \theta_l, \theta_s$	[-]	Water content, wilting point, field capacity, saturation	0.15, 0.35, 0.45
f_s	[mm/y]	Ice flow basal sliding coeff.	1.5×10^{-21}
f_d	[mm/y]	Ice flow internal deformation coeff.	1.2×10^{-24}
$\alpha_{s,i}$	[-]	Albedo snow, ice	0.3, 0.7

In Figure 25 the comparison of simulation and observation of snow depth H_s is reported. The calibration of degree day of snow and of snow accumulation and melt was done here for *GPNP* through snow depth data. Data of four AWS are available for the period 2005-2018 at daily scale. For each AWS, data were compared with the simulation of *Poli-Hydro* in the same cell of AWS. Calibration was done calculating *Bias* and *NSE*. In Table 15 results of *Bias* and

NSE are reported for the entire period of simulation 2005-2018 for both snow depth and discharge.

a)

b)
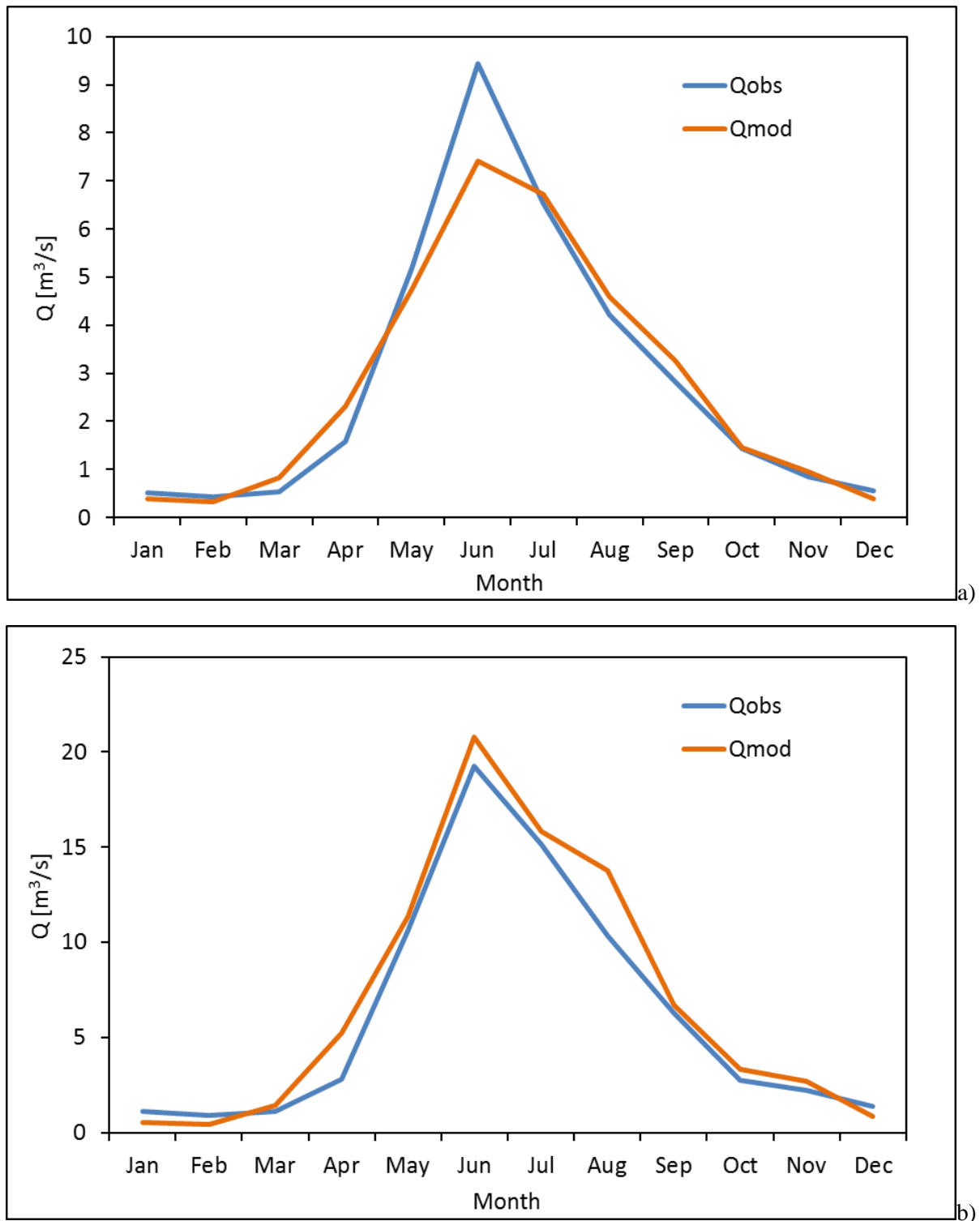
Figure 22: Average monthly discharge, observed and simulated, for the period 2005-2018, in Eaux Rousses river section (a) and in Cogne - Crètaz one (b).
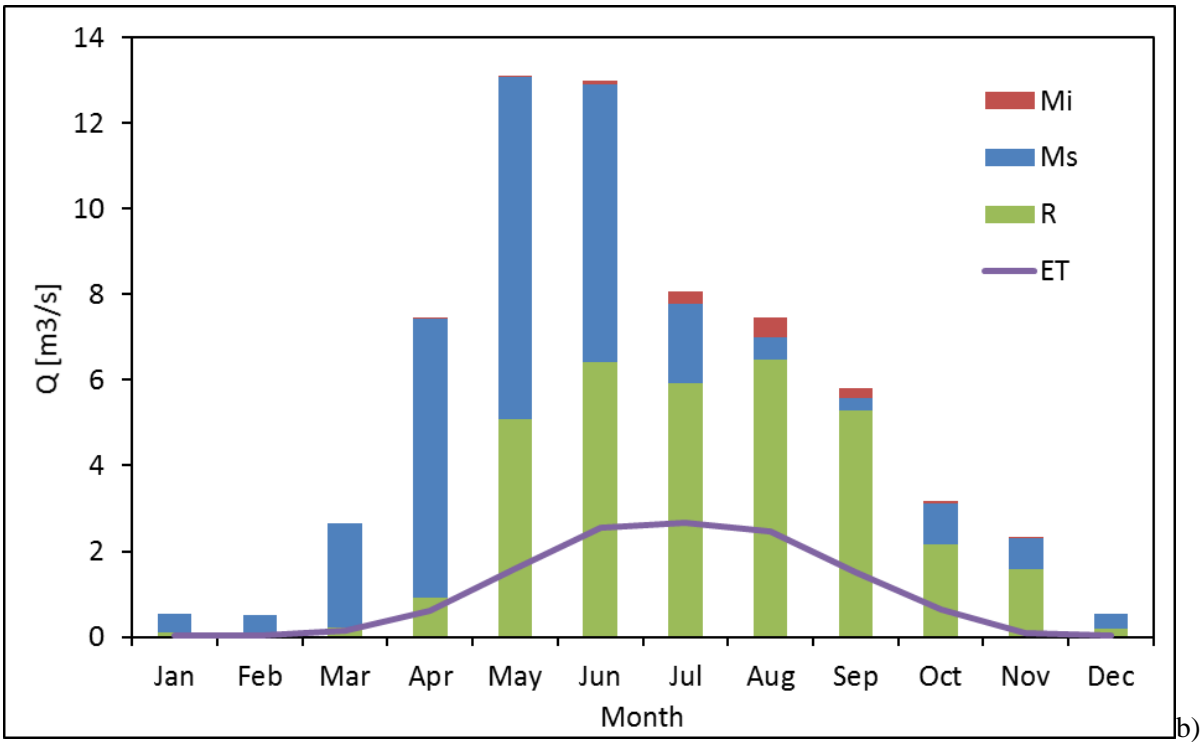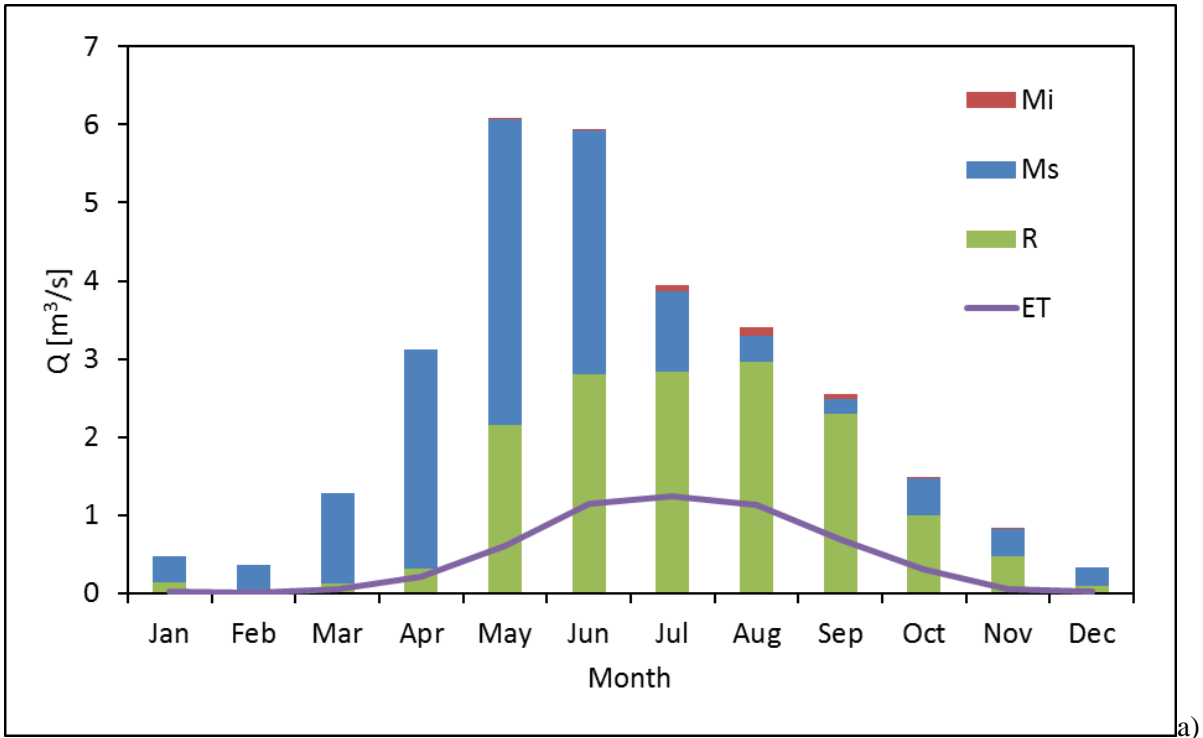
Figure 23: Contribution to discharge of snow and ice melt, M_s and M_i, of rain R, and of evapotranspiration ET for Eaux Rousses (a) and Cogne - Crètaz (b) sub-basins.
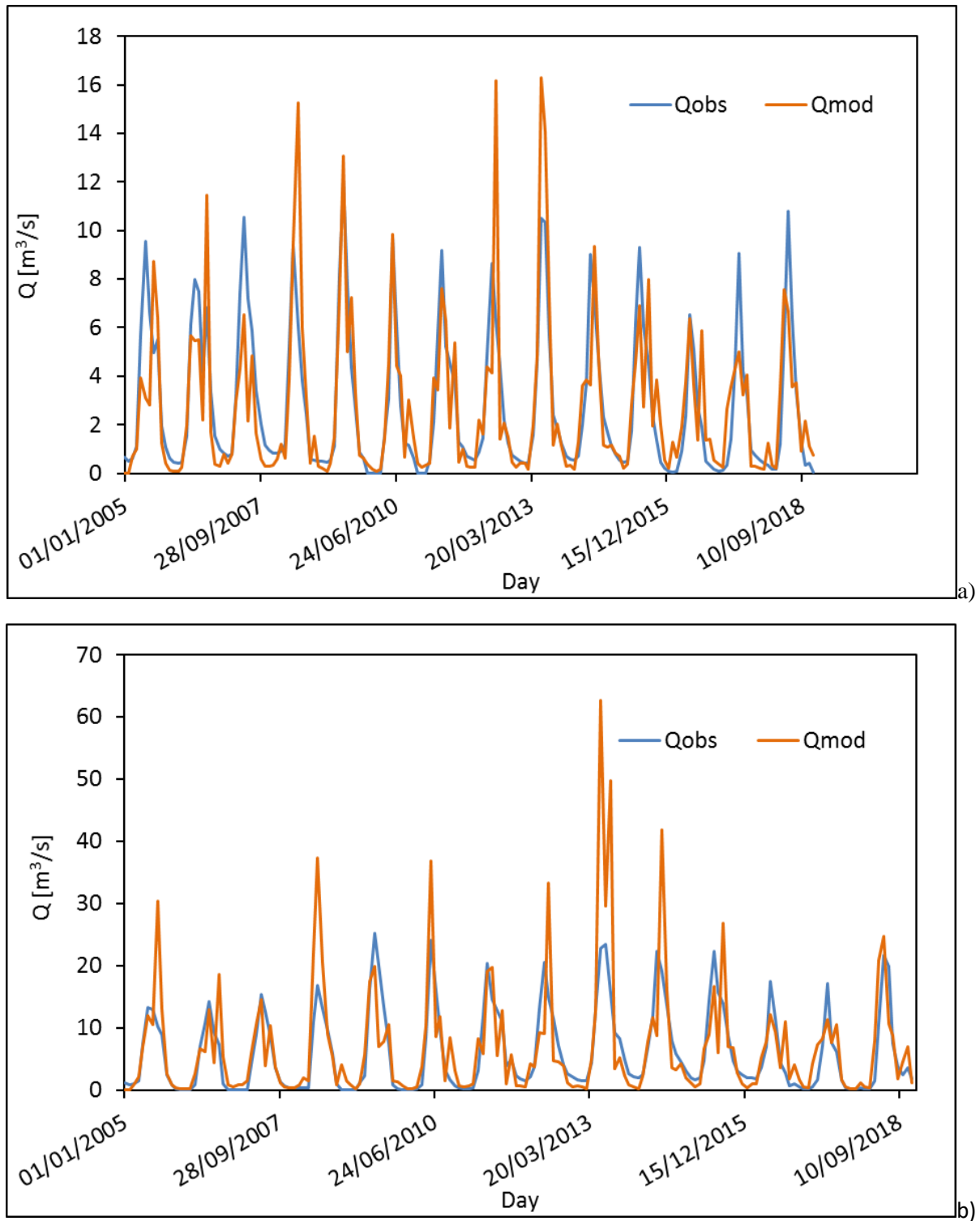
Figure 24: Monthly average discharge for the period 2005-2018, simulated and observe, for Eaux Rousses (a) and Cogne - Crètaz.

Table 15: *Bias* and *NSE* of snow depth H_s and discharge Q for Gran Paradiso National Park area for the entire period of simulation 2005-2018.

Period 2005-2018	Bias [%]	NSE monthly [-]
Q Eaux Rousses	-8.51	0.56
Q Cogne - Crètaz	+5.68	0.36
H_s	+16.63	0.48
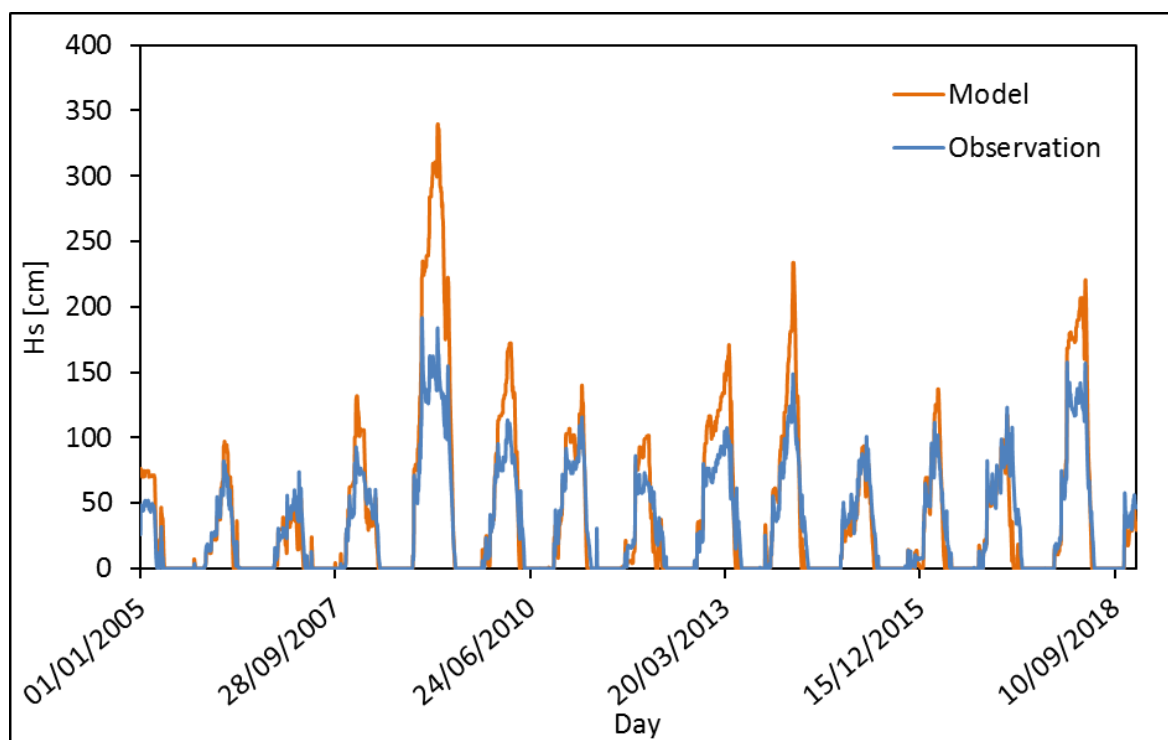
Figure 25: Daily snow depth H_s, as average of four AWS. Comparison between simulation and observation.

6.2 Calibration and validation of *Poli-Pasture*

6.2.1 Valtellina

Poli-Pasture here was calibrated for the conditions of fixed *GS*, then the same parametrization was used for the configuration with variable *GS*, only with the removal of the start and end date of *GS*. The calibration was pursued by iteratively changing the tuning parameters to mimic the observed values of specific annual production *Y* from ISTAT, in the period 2006-2017. Initial values of these parameters were obtained from literature. In Table 16 parameters of *Poli-Pasture* are reported, some of them were calibrated (in bold), while others were obtained from literature. Each species has different parameters values, namely *Nardus stricta* and *Trisetum flavescens*.

Goodness-of-fit statistics for Y for *Poli-Pasture* are reported in Table 17. Calibration was done considering the entire pasture area in Valtellina, while validation was done only for 3 sites in the high altitude belt, because of lack of data in the low altitude belt. It was not possible to calibrate separately *HighAlt* and *LowAlt* because ISTAT provides only aggregated data. The calculated percentage error *Bias* for the simulation with fixed *GS* was +10.82%, considering the production per hectare Y, and -4.90% considering the total production Y_{tot}. In the simulation with variable *GS, Bias* was -0.18% for Y and -9.93% for Y_y. This difference between Y and Y_y may depend on changes in the pasture areas during the study period in ISTAT data.

The model was then validated with in situ estimates of biomass of *Nardus stricta* in Alpe Boron (2003-2004) and Alpe Dosdè (2019). These estimates were compared with simulated biomass in the corresponding cell. Except for the year 2003, the model simulates acceptable values of biomass in Alpe Boron and Alpe Dosdè, according to observed data. In particular, in Alpe Boron *Poli-Pasture* simulates as average 0.81 t/ha of biomass more than the observation, considering a fixed *GS*, and 0.54 t/ha more considering a variable *GS*. An average between 2003 and 2004 was considered. In Alpe Dosdè it simulated -0.02 t/ha and -0.18 t/ha less than the observation, for fixed and variable *GS* respectively. Here an average between site 1 and 3 was considered for 2019.

In Figure 26 specific productivity per hectare is reported. Black squares are the ISTAT observations, red dots the simulations in fixed *GS* configuration, and blue dots the simulations in variable *GS* configuration for each year of calibration (2006-2017) and for last years 2018-2019. Void red and blue dots are the simulated values in Alpe Boron (2003 and 2004) and Alpe Dosdè (2019), with fixed and variable *GS* respectively. Green squares are the biomass observations in Alpe Boron for 2003 and 2004, and pink squares are the biomass observations in Alpe Dosdè for 2019 in sites 1 and 3.

Pasture productivity of ISTAT data is a sum of three classes of pasture, namely permanent grassland and pastures, poor pastures and other pastures. The estimates for 2006 and 2007 derive from a different methodology of the information collection campaign. Moreover, the class poor pastures compared only in 2013. Poor pastures have a lower specific productivity Y with respect to other classes, and contribute to the reduction of the total specific productivity after 2013. For this reason the growth rate was also compared between the simulation results and observation data. Considering only permanent grassland and other pastures for the period 2006-2017, the growth rate was of +0.11 t/ha/y, coherently with the result of the simulation where the rate was +0.07 t/ha/y in the configuration with fixed *GS* and +0.10 t/ha/y in the configuration with variable *GS* (Figure 27).

Table 16: Parameters of *Poli-Pasture* for Valtellina study area. In **bold**, calibrated parameters against yield data from ISTAT. Each species has different parameter values. Literature references: a (Moot et al., 2000), b (Monks et al., 2009), c (Nana et al., 2014), d (Addimando et al., 2015), e (Bocchiola & Soncini, 2017).

Variable	Symbol	Unit	*Nardus stricta*	*Trisetum flavescens*	Reference
Mean daily temperature optimal growth	T_{opt}	°C	12.00	17.00	a, b, d, e
Biomass-transpiration coefficient	BTR	kPa kg m^{-3}	5.00	6.50	d, e
Conversion light-biomass parameter	LtBC	g MJ^{-1}	1.30	2.50	d, e
Real/potential transpiration, end of leaf growth	AT/PT	-	0.50	0.50	C
Max daily water absorption	U_{max}	kg m^{-2} day^{-1}	13.00	15.00	d, e
Hydr. leaf potential, onset stomatal closure	psi_sc	J kg^{-1}	-2500.00	-2800.00	d, e
Hydraulic potential, leaf wilting	psi_w	J kg^{-1}	-2300.00	-2400.00	d, e
Morphology					
Max root depth	Rd_{max}	M	0.30	0.80	d, e
Maximum radical density	D_{max}	cm^{-2}	3.00	4.00	C
Initial Leaf Area Index	LAI_0		0.00	0.00	-
Specific Leaf Area	SLA	m^2 kg^{-1}	25.00	35.00	d, e
Partition stem/leaf	Ls	m^2 kg^{-1}	2.00	3.00	D
Degree-Day leaf	DD_{leaf}		500.00	600.00	D
Extinction coefficient of solar radiation	k_alfa	-	0.40	0.50	d, e
Coltural evapotranspiration coefficient	Kc_0	-	0.75	0.85	d, e
Phenology					
Degree-Day emergency	DD_{emerg}	°C d	50.00	50.00	a, d
Degree-Day flowering	$DD_{flowering}$	°C d	400.00	400.00	a, d
Degree-Day maturity	$DD_{maturity}$	°C d	800.00	800.00	D
Degree-Day for Rd_{max}	$DDrd_{max}$	°C d	300.00	300.00	-
Base temperature	T_{base}	°C	5.00	8.00	a, b, d
Cutoff temperature	T_{cutoff}	°C	18.00	21.00	a, b, d
Harvest					
Harvest Index	HI	-	0.70	0.70	E
Degree-Day harvest	DD_{har}	°C d	500.00	650.00	-

Table 17: Goodness-of-fit statistics for *Y* in Valtellina, with configuration of fixed *GS* and variable *GS*, *Bias*, *RMSE* (random mean square error), and percentage *RMSE%*. R^2 was not calculated due to constant values of *Y* in ISTAT data during years 2006-2007 and 2008-2012, for this reason variance of the observed sample is very low and R^2 makes little sense.

	Y fixed *GS*	Y variable *GS*
Bias [%]	+10.82	-0.18
RMSE [t/ha]	1.66	1.73
RMSE% [%]	37.81	39.48
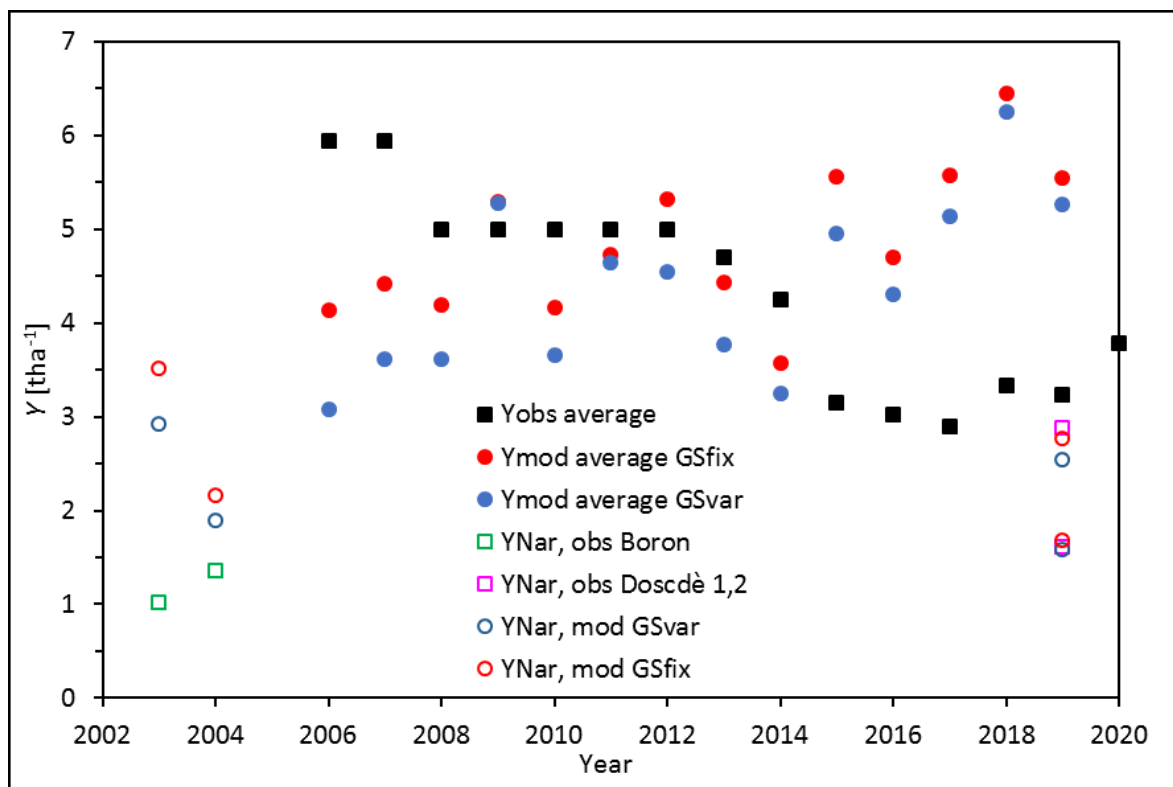
Figure 26: Calibration and validation of *Poli-Pasture* in Valtellina. Use of ISTAT data during the period 2006-2017 for calibration and in situ biomass data in 2003, 2004, and 2019 for validation.

Moreover, considering the total specific productivity of three classes (Figure 26), in the period 2015-2020 the growth trend was equal to +0.12 t/ha/y.

Concluding, the model performance is influenced by the paucity of data and the use of just bulk pasture yield data with additional in site estimates. Pasture yield estimates at the large scale of Sondrio, unfortunately, do not give information about the management of pasture areas and do not consider the large differences in altitude and climatic conditions within the study area (Bocchiola et al., 2019). For this reason it is not possible to verify the spatially distributed results of pasture productivity. Nevertheless it seems that the model simulation is acceptably representative of the pasture growth (Cho et al., 2007; Nana et al., 2014), and coherent with

other studies on pasture biomass in the same study area (Bocchiola & Soncini, 2017; Boschetti et al., 2007) and, generally, in Italy (Addimando et al., 2015).
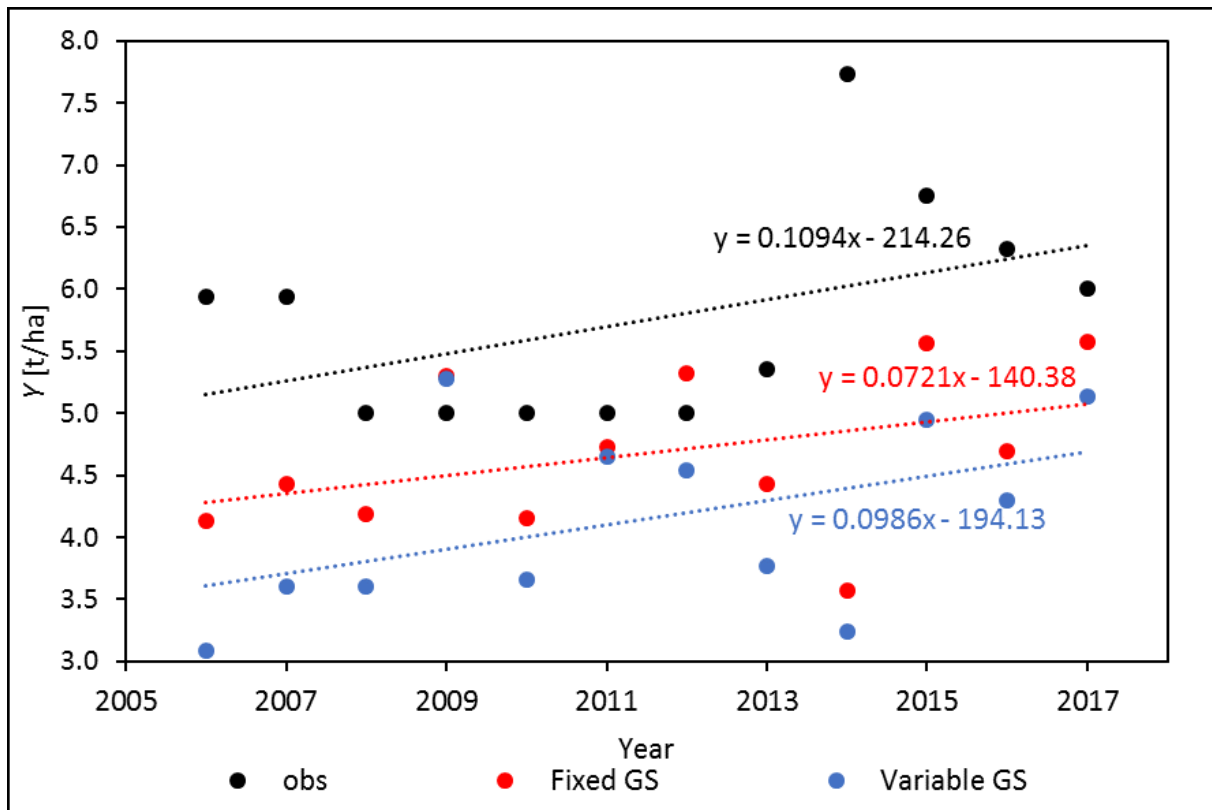
Figure 27: Growth rate in the period 2006-2017 for two classes of ISTAT data (permanent grassland and other pastures), in black, and for the model simulation with fixed and variable *GS*, in red and blue respectively.

6.2.2 Gran Paradiso National Park

In the area of *GPNP* the calibration is based on the *LAI* (Leaf Area Index) variable. The simulation of the model was compared with the observation from satellite images, from 2005 to 2019. Seven images were used for each year, collected every two weeks during the *GS* period (May 25th – September 14th). The single map and the average annual value were used both to analyse the model simulation. The *Bias* was calculated considering the overall average, while the *NSE* was useful to consider the comparison between each map. It was calculated an overall value of *Bias* and *NSE* for the entire pasture area, and values for the *HighAlt* and *LowAlt* pasture areas. Here the altitude threshold is 1800 m asl, so in *LowAlt* the area of pasture is around 0.77 km^2, while in *HighAlt* the area is 19.55 km^2. In Table 18 the results of *Bias* and *NSE* are reported for total area, *LowAlt* and *HighAlt*.

Table 18: Result of the calibration of *Poli-Pasture* in the Gran Paradiso National Park area.

	Bias [%]	*NSE* [-]
Total	3.56	0.02
HighAlt	4.05	-1.84
LowAlt	2.24	0.03

The results in terms of *Bias* are acceptable, they are always lower than the 5%, indicating a good capability of the model to simulate the average behaviour of the pasture *LAI* during the season. *NSE* has low values, in particular in *LowAlt*, this is due to the limited number of cells in this altitude belt, and to the consequent sensibility of the *NSE* indicator.

In Figure 28 the simulation is compared to the observation: the average value of *LAI* for each satellite image is calculated, as the average of simulated *LAI* in the correspondent day of the image. The *LowAlt* (Figure 28 a) is distinguished by *HighAlt* (Figure 28 b). The graphs show that the model (*Mod*) simulates the vegetation growing and, as a consequence, the increase of *LAI* in a correct timing, stabilizing the increase of *LAI* around the end of the season, when the satellite images show an initial decrease of it.

The scatter plot to compare the average value of *LAI* in the overall area for all the satellite images (all days for all years) is reported in Figure 29.

As average the *LAI* has a simulated value of 6.14 m^2/m^2 in *LowAlt*, against the 6.00 m^2/m^2 observed in satellite images, and a value of 4.58 m^2/m^2 in *HighAlt*, against the observed 4.78 m^2/m^2. Overall the simulated and observed values are 4.64 m^2/m^2 and 4.81 m^2/m^2.

Satellite maps of *LAI* were used in several studies for the calibration of model for pasture dynamics (Addimando et al., 2015; Bocchiola & Soncini, 2017; Zhu et al., 2013). Here, the use of satellite maps corrects for the *GPNP* study area the problem of a spatially distributed simulation and verifies that the model simulates correctly the pasture productivity in the overall area.

The results in terms of *LAI* were compared also with the in situ data in Orvieille area (2300 m asl), collected in fulfilment of the MOUPA project (Table 7), where the value of observed *LAI* for the 15th of July 2019 was 3.31 m^2/m^2. The simulated value of *LAI* for 12th of July 2019 is 3.55 m^2/m^2.
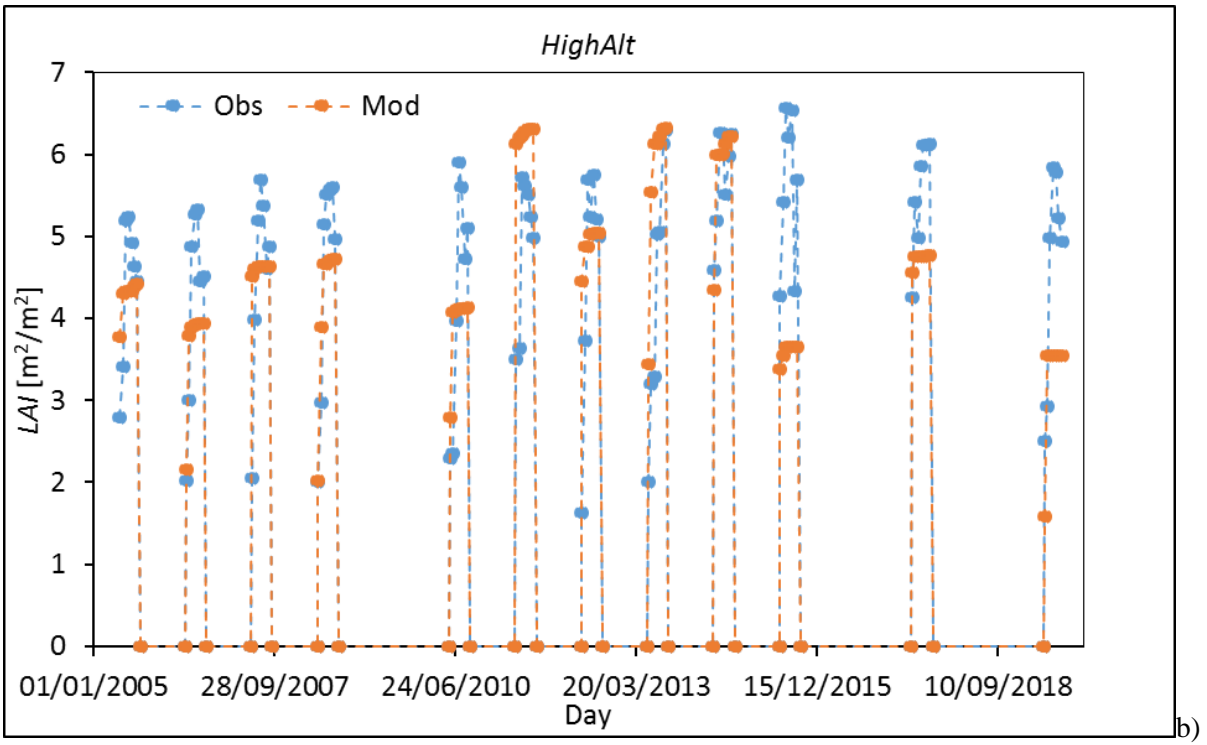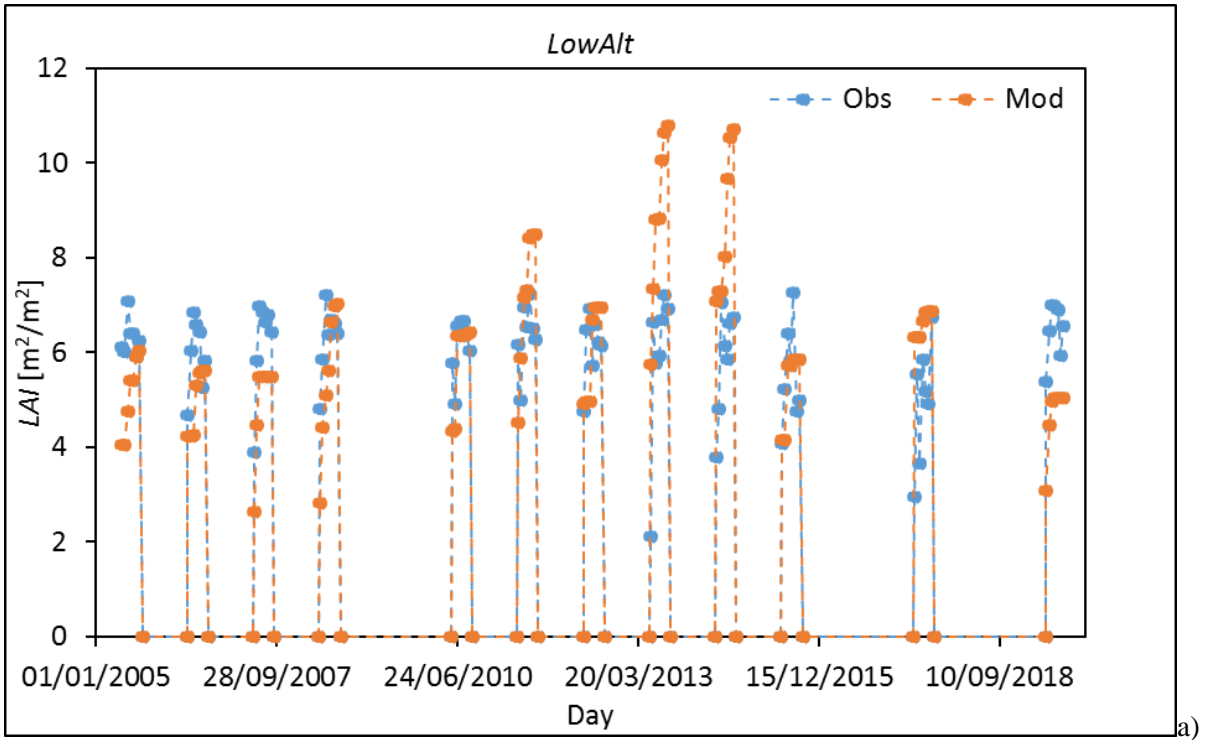
Figure 28: Comparison of average *LAI* in each satellite image with the simulation in the same day, for *LowAlt* (a) and *HighAlt* (b).
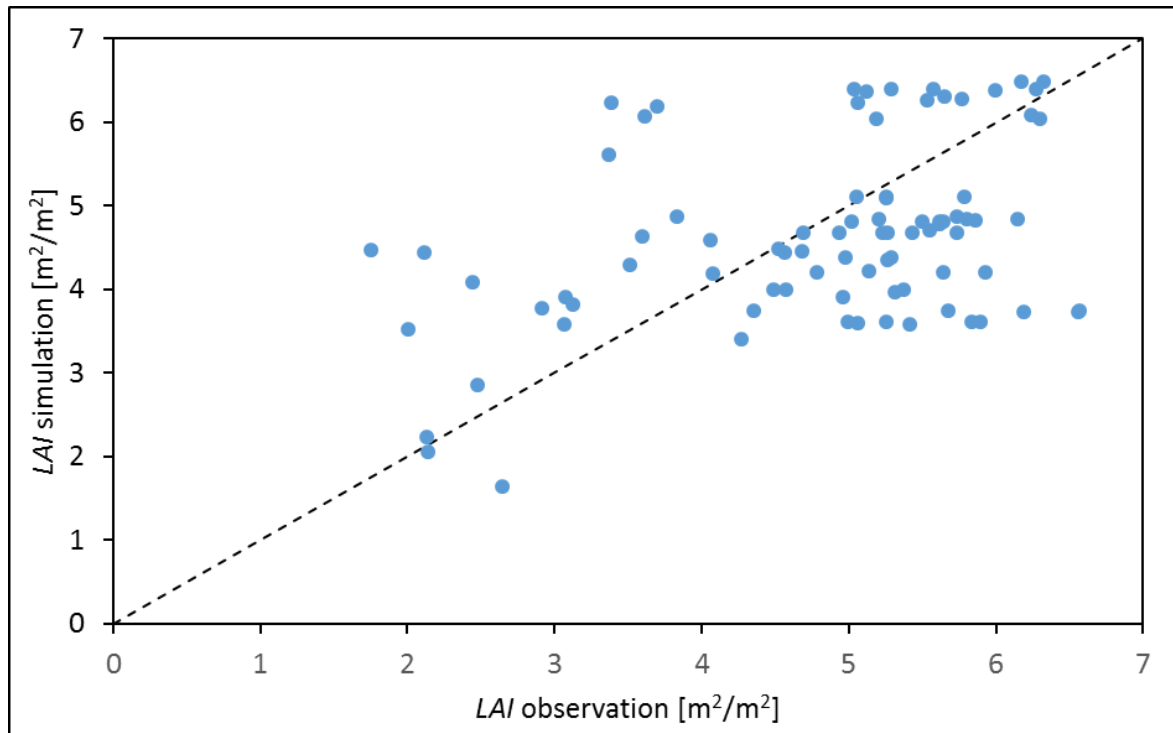
Figure 29: Scatter plot of average *LAI* in the overall pasture area, simulated and observed, for each satellite image during the period 2005-2019.

In Table 19 the calibrated parameters of *Poli-Pasture* are reported for the four pasture species in *LowAlt* (*Trifolium alpinum* and *Dactylis glomerata*) and *HighAlt* (*Festuca rubra* and *Nardus stricta*). The initial values of parameters are based on the results of Valtellina area and on the personal communication with the research group of Università Statale di Milano (Confalonieri R., Movedi E.). Additional parameters of *CoSMo* model, with respect to parameters used also for *Poli-Pasture*, are reported in Table 20, for the four pasture species.

Table 19: Parameters of *Poli-Pasture* for Gran Paradiso National Park study area. In bold, calibrated parameters against *LAI* satellite images. Each species has different parameter values.

Variable	Symbol	Unit	*Trifolium alpinum*	*Dactylis glomerata*	*Festuca rubra*	*Nardus stricta*
Mean daily temperature optimal growth	T_{opt}	°C	10.00	8.00	7.00	6.00
Biomass-transpiration coefficient	BTR	kPa kg m^{-3}	0.9	1.20	1.00	1.20
Conversion light-biomass parameter	$LtBC$	g MJ^{-1}	0.8	1.10	1.00	1.40
Real/potential transpiration, end of leaf growth	AT/PT	-	0.30	0.30	0.30	0.30
Max daily water absorption	U_{max}	kg m^{-2} day^{-1}	7.00	4.00	7.00	10.00
Hydr. leaf potential, onset stomatal closure	psi_sc	J kg^{-1}	-1200.00	-1200.00	-1200.00	-1200.00
Hydraulic potential, leaf wilting	psi_w	J kg^{-1}	-1500.00	-1500.00	-1500.00	-1500.00
Morphology						
Max root depth	Rd_{max}	M	1.00	1.40	1.45	1.50
Maximum radical density	D_{max}	cm^{-2}	4.00	4.00	4.00	4.00
Initial Leaf Area Index	LAI_0		0.45	0.45	0.42	0.42
Specific Leaf Area	SLA	m^2 kg^{-1}	38.00	35.00	35.00	38.00
Partition stem/leaf	Ls	m^2 kg^{-1}	0.80	1.00	1.20	1.30
Degree-Day leaf	DD_{leaf}		600.00	600.00	600.00	600.00
Extinction coefficient of solar radiation	k_alfa	-	0.50	0.60	0.47	0.50
Coltural evapotranspiration coefficient	Kc_0	-	1.00	1.00	1.00	1.00
Phenology						
Degree-Day emergency	DD_{emerg}	°C d	21.00	21.00	24.00	21.00
Degree-Day flowering	$DD_{flowering}$	°C d	400.00	650.00	500.00	400.00
Degree-Day maturity	$DD_{maturity}$	°C d	3000.00	4000.00	4000.00	3000.00
Degree-Day for Rd_{max}	$DDrd_{max}$	°C d	650.00	650.00	650.00	650.00
Base temperature	T_{base}	°C	3.00	5.00	5.00	2.00
Cutoff temperature	T_{cutoff}	°C	28.00	28.00	27.00	22.00
Harvest						
Harvest Index	HI	-	0.80	0.8	0.80	0.80

Table 20: *CoSMo* model parameters for Gran Paradiso National Park study area.

Variable	Symbol	Unit	*Trifolium alpinum*	*Dactylis glomerata*	*Festuca rubra*	*Nardus stricta*
Initial relative presence	RP_0	-	0.50	0.50	0.50	0.50
Liking bovines	L	-	0.70	0.80	0.80	0.30
Water stress tolerance	DT	-	0.70	0.70	0.80	0.70

6.3   *Poli-Pasture* results for the present period

In this chapter the results of *Poli-Pasture* in the present period are reported, in particular the total pasture productivity for altitude belts, and the specific productivity per hectare, in both the study areas. Here, for *GPNP*, the analysis of distribution of species is also reported. Present period in Valtellina goes from 2006 to 2019, in Gran Paradiso National Park area goes from 2005 to 2019.

6.3.1   Valtellina

In Valtellina, pasture area is distributed between 200 and 2600 m asl, 22,734 ha are present in *LowAlt* and 29,485 ha are present in *HighAlt*, for a total area of 52,219 ha.

Considering the fixed *GS* configuration, as average the *LowAlt* pastures have a larger productivity, equal to 12.56 t/ha, corresponding to a total of 29,303 t/y. *HighAlt* pastures have a lower productivity, equal to 1,85 t/ha, for a total of 30,638 t/y.

In Figure 30 the behaviour of pasture productivity in *LowAlt* and *HighAlt* areas during the period 2006-2019 is reported for fixed *GS* configuration. *HighAlt* pastures have a more variable behaviour with respect to *LowAlt* pastures. Generally, an increasing behaviour can be seen. Although average productivity is similar, considering the larger area at *HighAlt*, the specific productivity per hectare is clearly lower here with respect to *LowAlt*, but the behaviour in the period is similar between specific and total productivity, considering a constant area.

In Figure 31 8 altitude belts are considered with a range of 300 m. In blue altitude belts of *LowAlt* are reported, while in green altitude belts of *HighAlt*. The total productivity Y_{tot} is compared to the specific productivity Y, in the simulation with fixed *GS* configuration. As said before, specific productivity decreases with altitude, while total productivity depends on the area in each belt. Maxima values of Y_{tot} compare between 1400 and 2300 m asl.
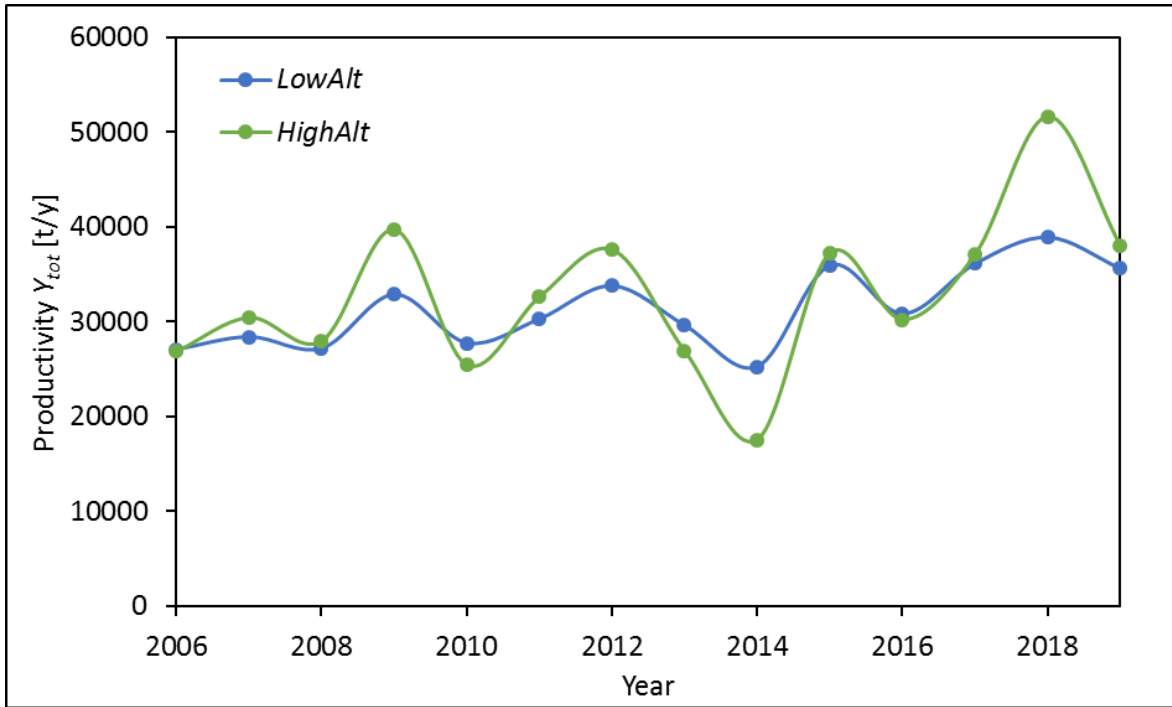
Figure 30: Total productivity Y_{tot} behaviour in the present period in Valtellina, at *LowAlt* and *HighAlt*, fixed *GS* configuration.
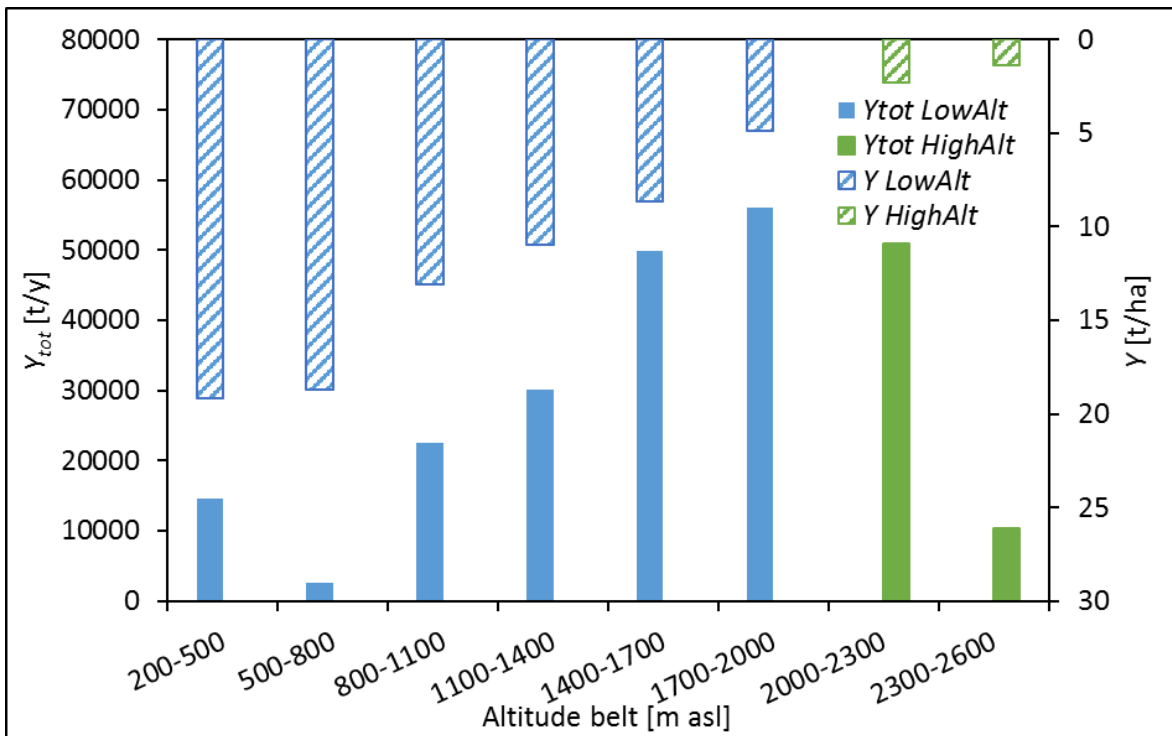
Figure 31: Total productivity Y_{tot} [t/y] (left axis) and specific productivity Y [t/ha] (right axis) for altitude belts of a range of 300 m, comparing *LowAlt* (in blue) and *HighAlt* (in green) in Valtellina study area. Fixed *GS* configuration.

Also Figure 32 and Figure 33 refer to the fixed *GS* configuration. In Figure 32 different classes of specific productivity *Y* were selected, and the number of cells with specific annual productivity corresponding to the *Y* ranges were calculated. The specific productivity of each cell is the average on the period 2006-2019. A lot of cells have a specific productivity below 0.5 t/ha, while the majority of cells have a specific productivity between 1.5 and 5 t/ha, in particular it is the class between 3,5 and 4 t/ha that has the largest number of cells.

In Figure 33 an example is reported for the year 2019 for 10 cells. The growth of biomass is reported in these cells during the year. It could be seen a regular growth with a maximum in correspondence of the harvesting, then a new cycle of growth begins.

In Figure 34 and Figure 35 similar graphs are reported referring to the variable *GS* configuration.

Figure 34 represents the total productivity in *LowAlt* and *HighAlt* during the simulation period 2006-2019. Figure 35 represents the total and specific productivity for altitude belts of 300 m.

Generally the behaviour is similar between two configurations, in spite of some differences. Indeed, in Table 21 differences in terms of specific productivity are reported for each altitude belt. In the configuration of variable *GS,* lower values of productivity resulted. As average, at *LowAlt* the specific productivity is 10.97 t/ha, for a total of 22,733.7 t/y, specifically 1.59 t/ha (11%) less than in the configuration of fixed *GS*. At *HighAlt* the difference is of 0.32 t/ha (15%), indeed specific productivity with variable *GS* is 1.53 t/ha, for a total productivity of 29,484.9 t/y.

The small difference between two configurations confirms that the variable *GS* simulates correctly the trend of *GS* beginning and end. It is possible to confirm that the variable *GS* configuration could be used for the simulation of the future, because it reflects correctly the *GS* defined by pasture managers.

Larger differences between two configurations are present below 800 m asl, but where area is low, so a small difference in total productivity is caused, and above 2000 m asl, in *HighAlt*, but where absolute value of specific productivity is small, like the absolute value of variation.

In Figure 36 a map of the average productivity *Y* during the period 2006-2019 is reported under the variable *GS* configuration.
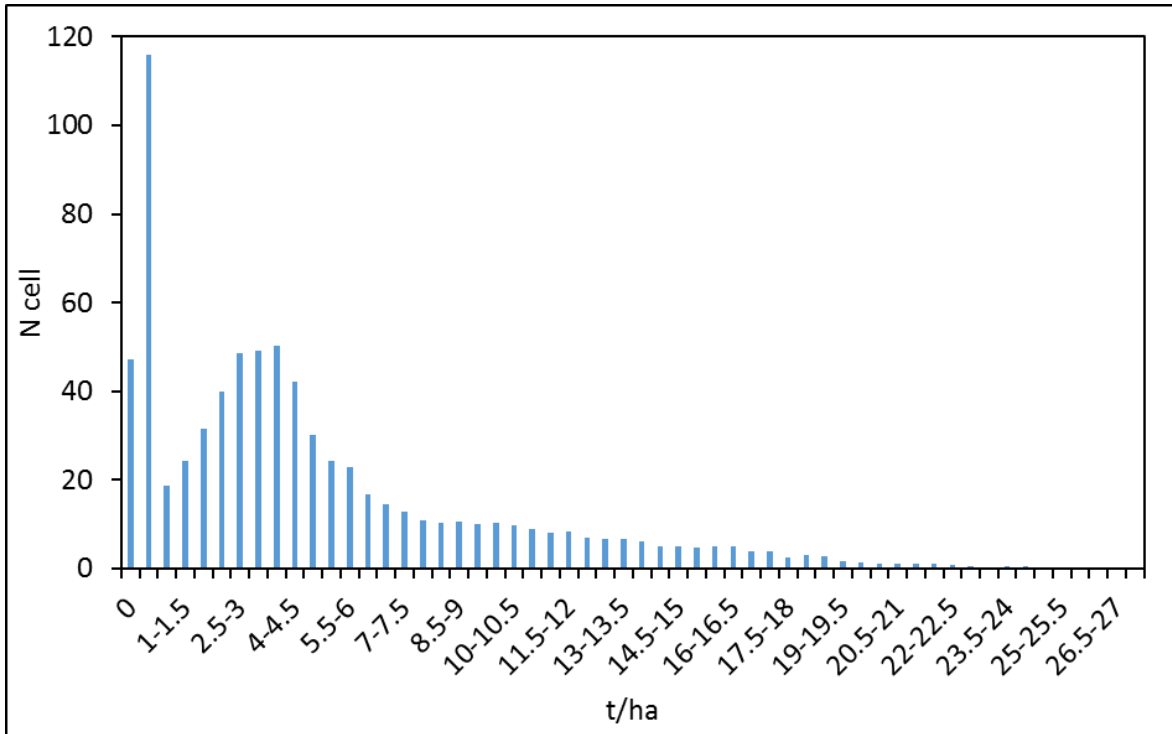
Figure 32: Number of cells in each class of specific productivity [t/ha] for an average year in the period 2006-2019, considering the fixed *GS* configuration in Valtellina study area.
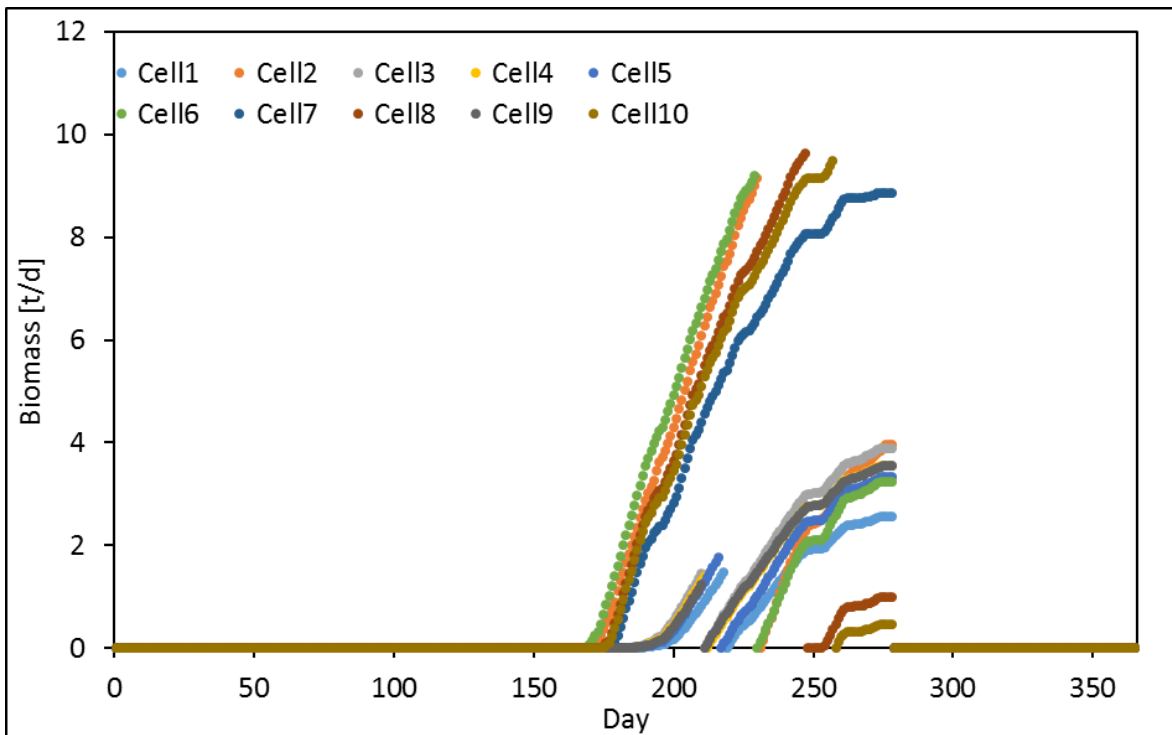
Figure 33: Example of biomass growth in 2019 for 10 cells in the fixed *GS* configuration in Valtellina study area.
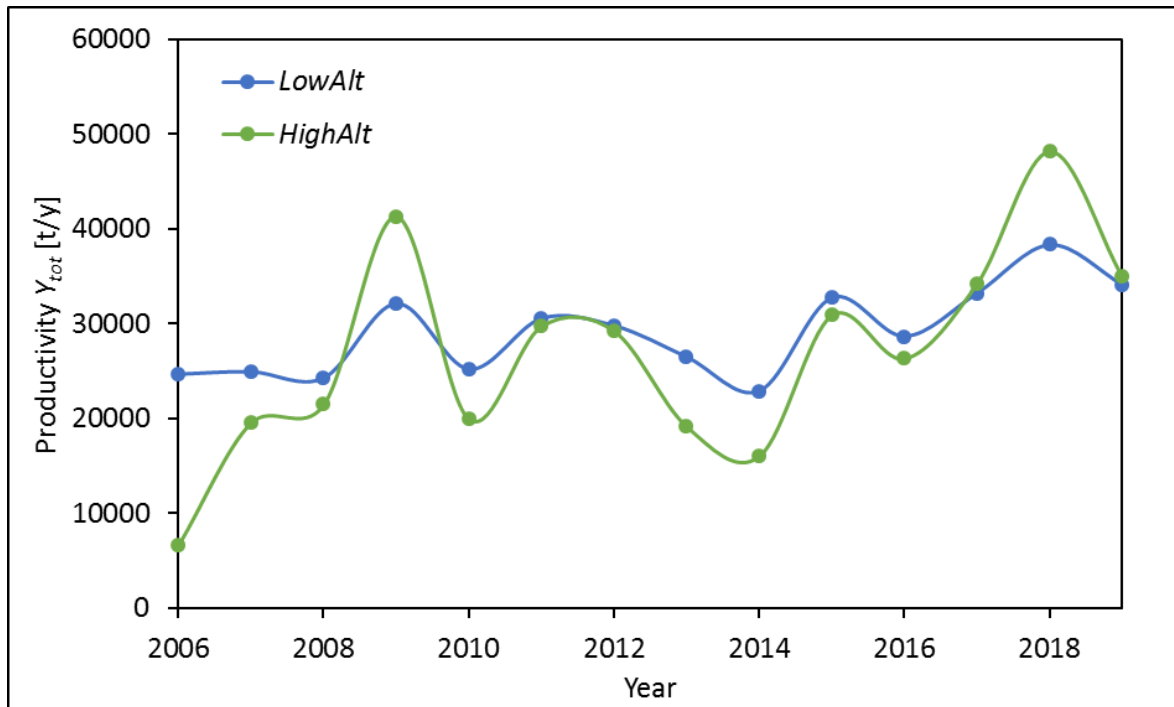
Figure 34: Total productivity Y_{tot} behaviour in the present period in Valtellina, at *LowAlt* and *HighAlt*, variable *GS* configuration.
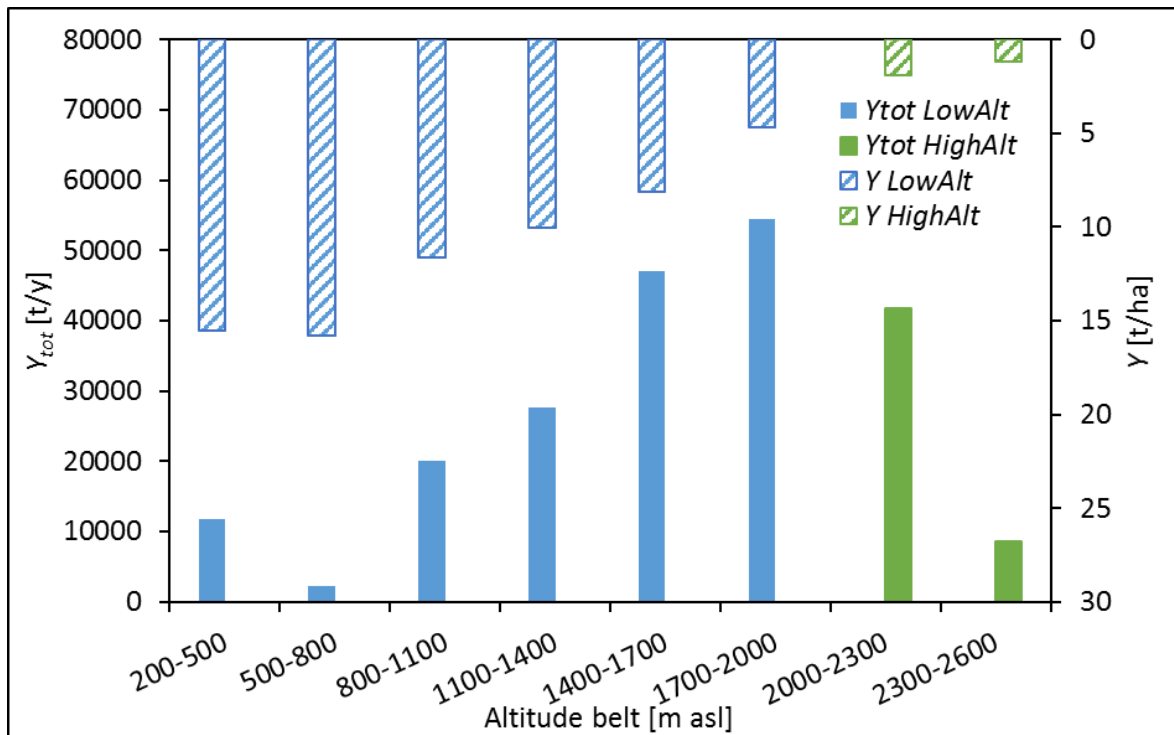
Figure 35: Total productivity Yt_{ot} [t/y] (left axis) and specific productivity Y [t/ha] (right axis) for altitude belts of a range of 300 m, comparing *LowAlt* (in blue) and *HighAlt* (in green) in Valtellina study area. Variable *GS* configuration.

Table 21: Comparing specific productivity *Y* [t/ha] for altitude belts in the fixed and variable *GS* configurations in Valtellina study area. Variation is the percentage difference between two absolute values.

Altitude belts	*Y* fixed *GS* [t/ha]	*Y* variable *GS* [t/ha]	Variation [%]
200-500	19.17	15.54	-23%
500-800	18.69	15.81	-18%
800-1100	13.10	11.62	-13%
1100-1400	10.96	10.01	-9%
1400-1700	8.62	8.14	-6%
1700-2000	4.85	4.71	-3%
2000-2300	2.32	1.90	-22%
2300-2600	1.38	1.15	-20%
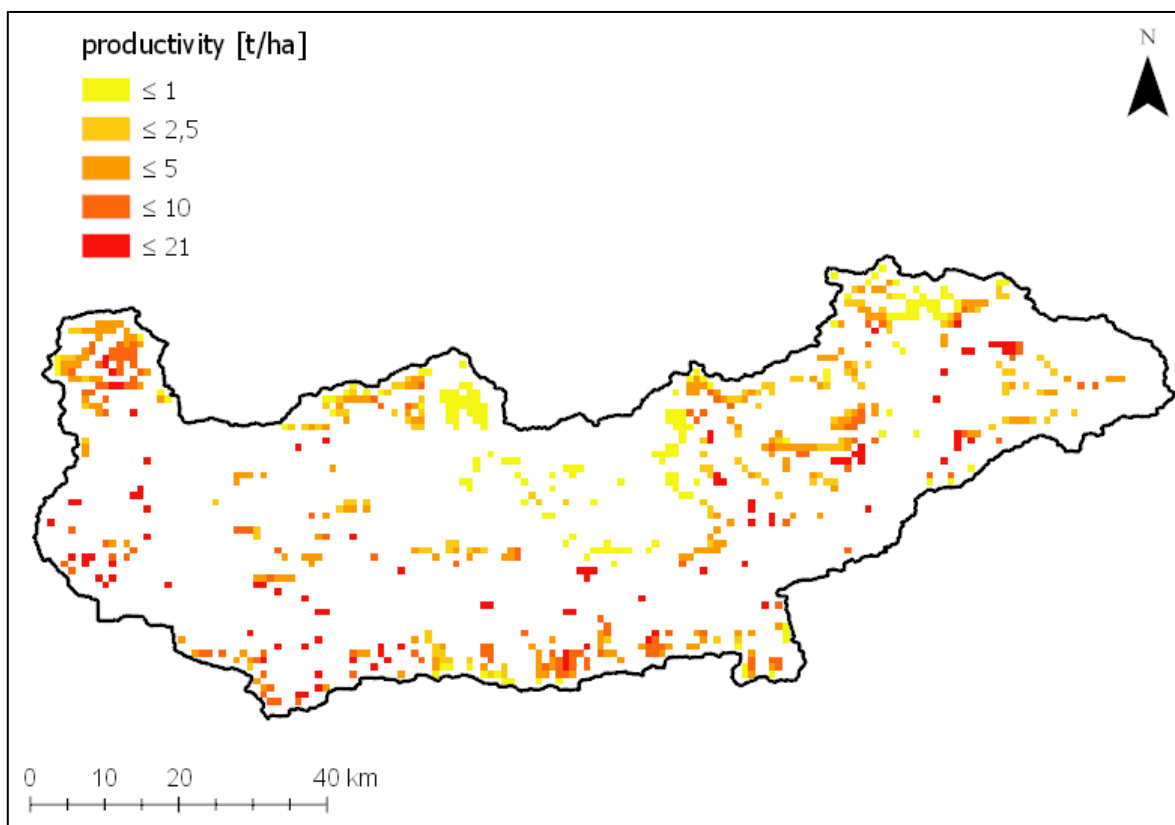
Figure 36: Map of the average productivity *Y* [t/ha] for the period 2006-2019 under the variable *GS* configuration, in the Valtellina valley area.

6.3.2 Gran Paradiso National Park

In *GPNP* study area the largest part of pasture land is in *HighAlt*, here over 1800 m asl. The area of pasture in *HighAlt* is 1955 ha, while the area in *LowAlt* is 77 ha. For this reason, differently from Valtellina area, the total productivity Y_{tot} in *HighAlt* is much larger than in *LowAlt*. In the CR period, 2005-2019, Y_{tot} is equal to 6901.94 t/y and 500.65 t/y respectively in *HighAlt* and *LowAlt*.

The specific productivity *Y* is reported for the CR period in Figure 37. In *LowAlt Y* is larger than in *HighAlt* and respectively equal to 6.50 t/ha and 3.53 t/ha. In *HighAlt* during years, the variability of *Y* is larger than in *LowAlt*. But it could not be seen a particular behaviour of the specific productivity during CR period.

In Figure 38 the total and specific productivity are shown for altitude belts of 300 m, from 1500 m asl to 3000 m asl. In Valtellina the largest total productivity are between 1700 and 2000 m asl, while here in *GPNP* area the largest Y_{tot} is between 2100 and 2400 m asl. This result shows that the pasture land occupies in Valle d'Aosta region area at higher altitude with respect to Valtellina valley. Another check is that here in *GPNP* altitude belts arrive at 3000 m asl, 400 m more than in Valtellina, even though in the last altitude belt (2700-3000 m asl) the productivity is very low, consequence of a small area occupied by pasture here.

As in Valtellina valley, the specific productivity decreases with altitude. It is larger in *LowAlt* (1500-1800 m asl), equal to 6.50 t/ha, and then decreases in the next four altitude belts, where it is respectively equal to 4.92 t/ha, 3.88 t/ha, 2.96 t/ha and 1.92 t/ha. These values are comparable to the results in Valtellina valley.

The value of specific productivity in *HighAlt* was confirmed also by the comparison with Orvieille sample data, where *Y* was 3.45 t/ha (15/7/2019), comparable to the value of 3.88 t/ha of the altitude belt 2100-2400 m asl.

In Figure 39 the specific productivity *Y* is divided for classes and the number of cells in each class is reported. Differently from Valtellina valley, here in *GPNP* area the number of cells with very low productivity <0.5 t/ha is negligible. The majority of cells, during the CR period, has an average productivity between 2.5 t/ha and 4 t/ha, a little bit lower than in Valtellina valley, but considering the average altitude of the cells the productivity is high. Differently from Valtellina valley, the specific productivity of cells does not exceed the 8 t/ha.

In Figure 40 the map of average productivity *Y* [t/ha] for the period 2005-2019 is reported for the study area of Gran Paradiso National Park.
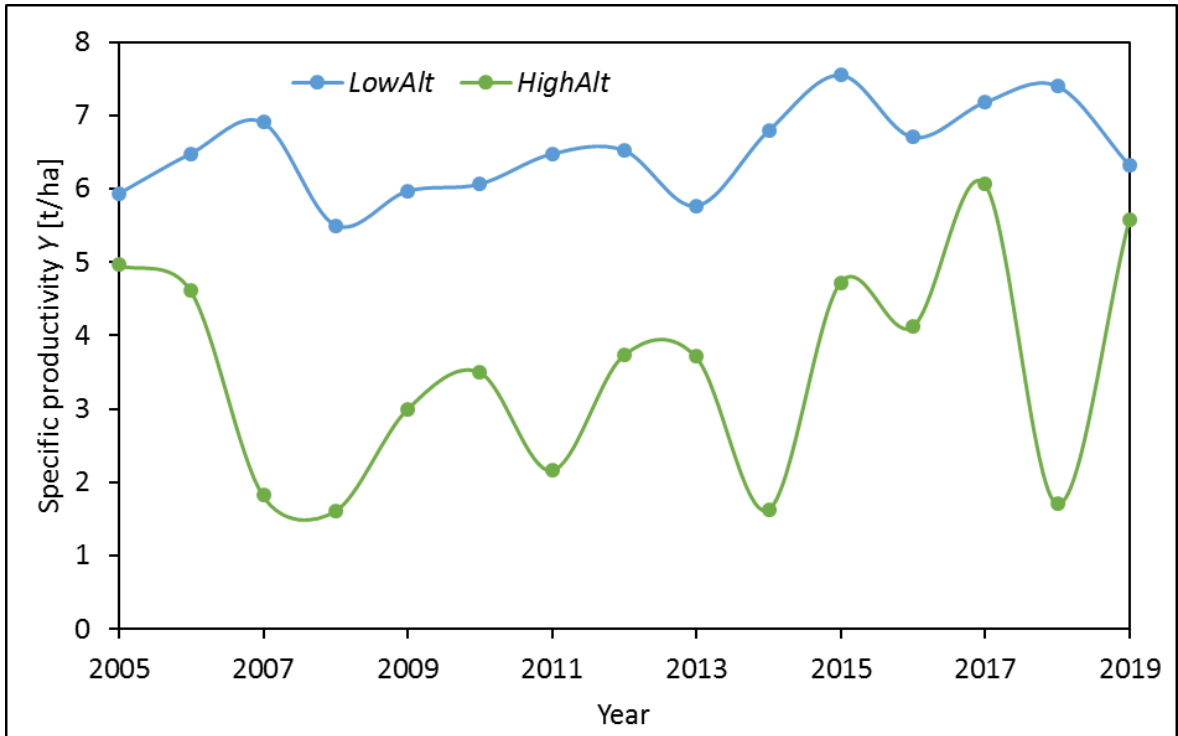
Figure 37: Specific productivity *Y* in Gran Paradiso National Park area during the CR period (2005-2019).
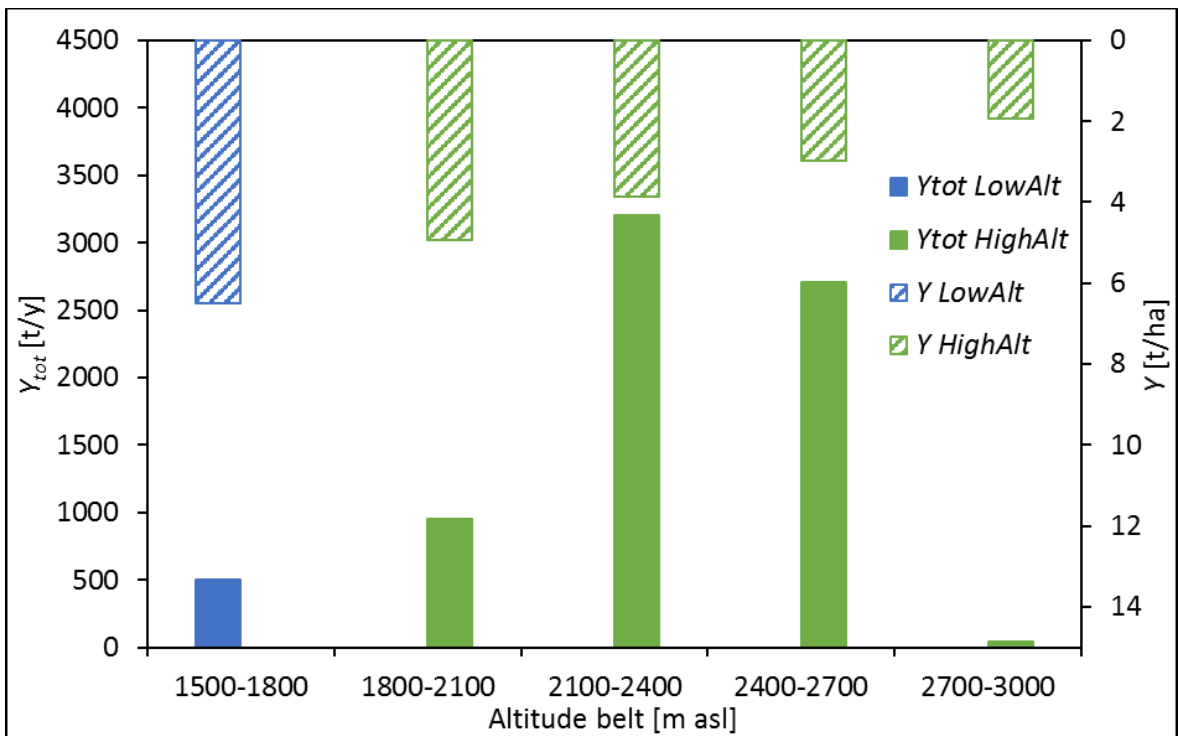
Figure 38: Total productivity Y_{tot} and specific productivity *Y* as average during the CR period (2005-2019), in Gran Paradiso National Park Area, divided for altitude belts of 300 m. In blue the area of *LowAlt* under 1800 m asl, in green the area of *HighAlt* above 1800 m asl.
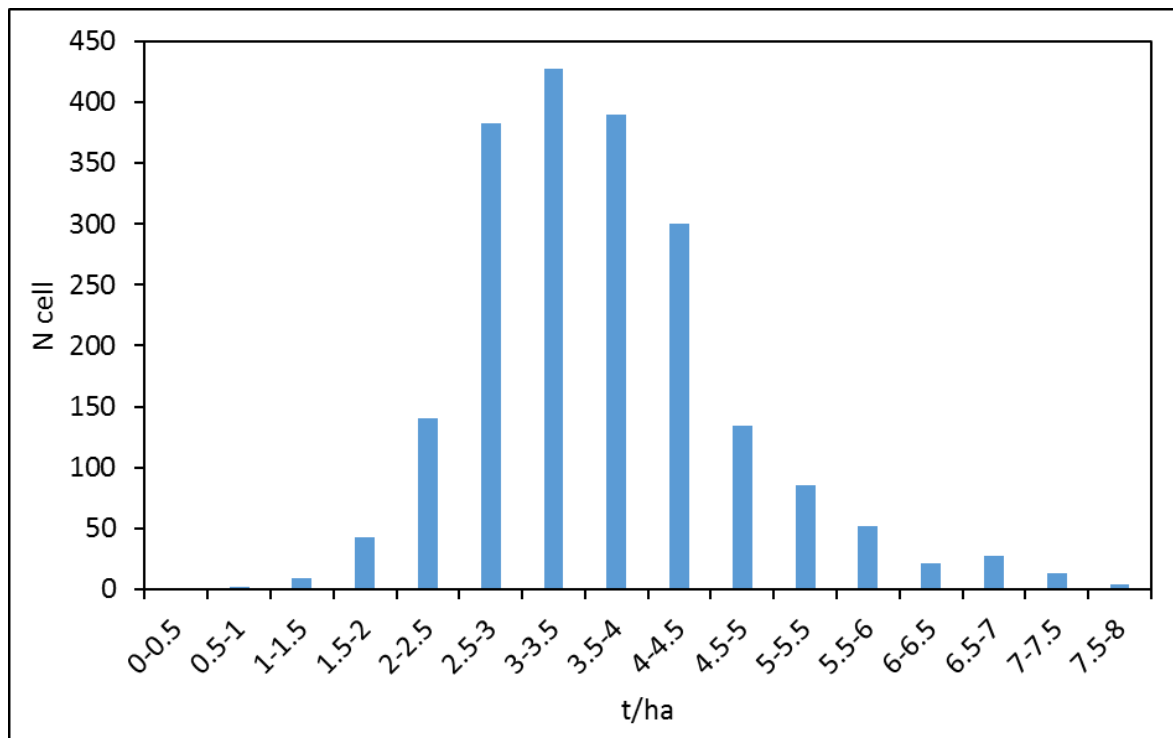
Figure 39: Number of cells for different classes of specific productivity *Y* in Gran Paradiso National Park study area.

In Figure 41 the relative presence of *Dactylis glomerata* and *Festuca rubra* is reported in the map of *GPNP*. Under 1800 m asl (*LowAlt*) the relative presence of *Dactylis glomerata* is shown, while above 1800 m asl (*HighAlt*) the relative presence of *Festuca rubra* is shown. The presence of two species is calculated as the average during *GS* for the CR period 2005-2019, but this value changes in each time step (day). The relative presence of *Trifolium alpinum* and *Nardus stricta* is complementary in *LowAlt* and *HighAlt*, respectively.

In Figure 42 the relative presence in each cell vs the altitude of the cell is reported, again for *Dactylis glomerata* in *LowAlt* and for *Festuca rubra* in *HighAlt*. The relative presence of both the species decreases with altitude. This is in line with the temperature gradient, so with the decrease of temperature with altitude. These two species decrease with altitude because they have higher values of optimal temperature with respect to the complementary species *Trifolium alpinum* and *Nardus stricta*. Looking at *Festuca rubra*, the decrease of the relative presence is of 2‰, while the decrease of temperature during the *GS* season (May-September) is between 4.6‰ and 5.9‰. Considering the influence of other parameters too, the *CoSMo* model can describe the influence of daily average temperature on the relative presence of species. It is difficult to analyse the decrease of relative presence of *Dactylis glomerata*, due to the small number of cells in *LowAlt*.
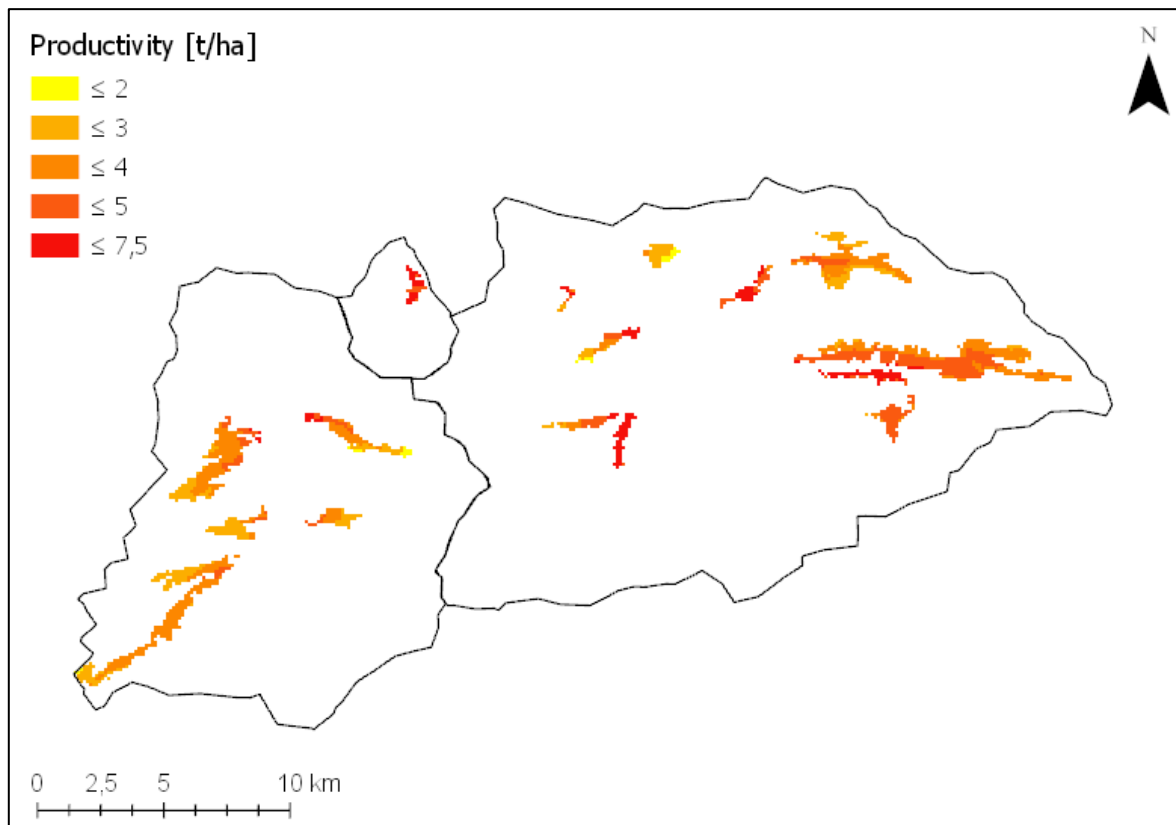
Figure 40: Map of average specific productivity *Y* [t/ha] for the period 2005-2019 in the area of Gran Paradiso National Park.

The presence of these species, as the most abundant, is confirmed in other studies, generally on alpine pasture (Bellini, Moriondo, Dibari, Bindi, et al., 2023; Movedi et al., 2019), and specifically on *GPNP* (Filippa et al., 2022; Stendardi et al., 2022). In particular (Stendardi et al., 2022) find, as more abundant species, *Dactylis glomerata* and *Festuca rubra* under 2000 m asl, and *Nardus stricta*, *Festuca rubra* and *Trifolium alpinum* between 2000 and 3000 m asl. Actually, in our simulation the presence of *Festuca rubra* decreases with altitude from 1800 m asl. In (Filippa et al., 2022) the correspondent productivity in these two altitude belts of the park is reported: between 2 t/ha and 3.25 t/ha under 2000 m asl, and between 0.83 t/ha and 0.37 t/ha above 2000 m asl. These values are slightly lower with respect to the results of the simulation with *Poli-Pasture*, but also with respect to collected samples.
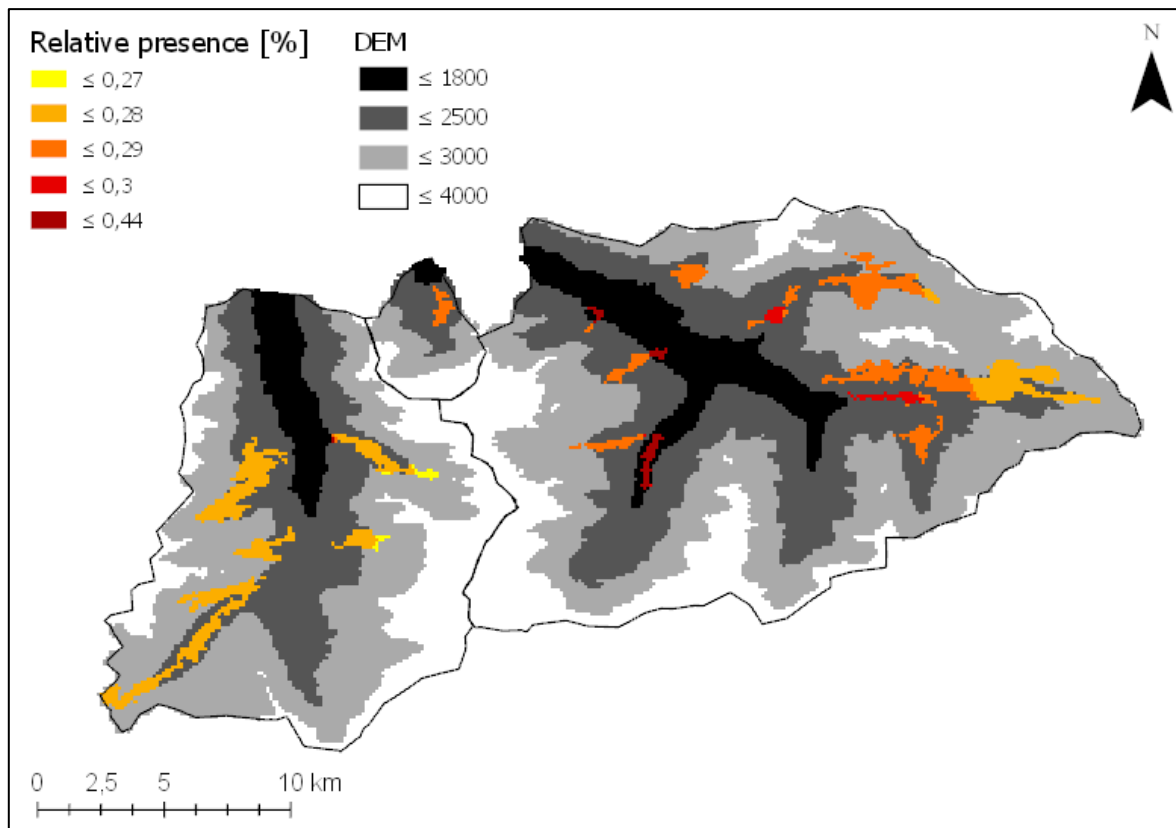
Figure 41: Relative presence of *Dactylis glomerata* (*LowAlt* <1800 m asl, black background) and *Festuca rubra* (*HighAlt*). The reported relative presence is the average during the *GS* for the entire period 2005-2019.
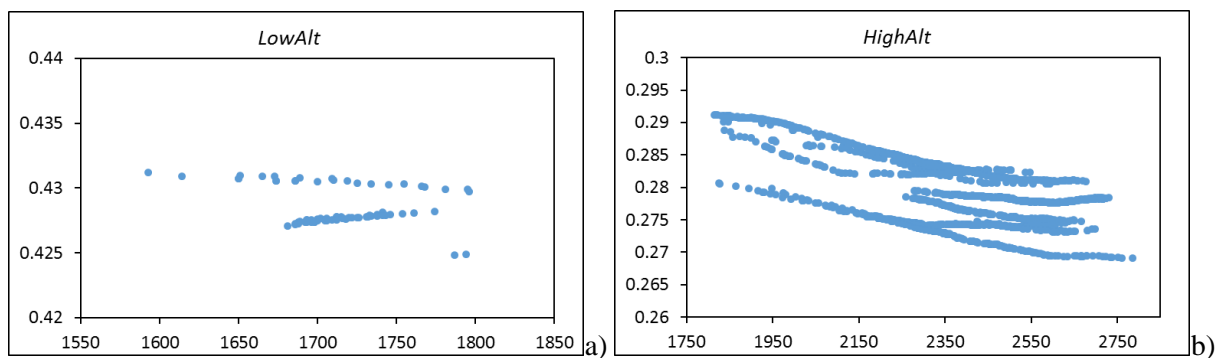
Figure 42: Relative presence of *Dactylis glomerata* (*LowAlt* <1800 m asl) (a) and *Festuca rubra* (*HighAlt*) (b). The relative presence is the average during the *GS* for the period 2005-2019.

6.4   Climate projections

6.4.1   Valtellina

Climate projections were analysed considering each scenario and each GCM, for IPCC AR5 and AR6.

For what concerns temperature (Figure 43), every models for all the scenarios show an increase, usually the increase is larger in *P2* (2091-2100) than in *P1* (2041-2050) and it is larger increasing the scenario since 2.6 to 8.5. Some exceptions are present, e.g. the CCSM model for AR5 shows a larger increase for 4.5 than for 8.5 scenario at the end of the century *P2*. The scenario 2.6, for AR6 for all the GCMs, and for AR5 only in the CCSM model, shows a larger increase at the middle of the century *P1* than at the end *P2*, coherently with the hypothesis at the basis of the scenario that the peak temperature is around the middle of the century, then temperature decreases stabilizing to a +1.5°C variation with respect to pre-industrial period. Looking at Table 22, it is possible to see that the increase of temperature is generally equally distributed during seasons, but for 4.5 and 8.5 scenarios of AR5 and for 7.0 and 8.5 scenarios of AR6 the largest increase is in summer.

The average annual increase goes between +0.83°C for the scenario 2.6 of AR6 in period *P2* to +5.56°C again in period *P2* for scenario 8.5 of AR6. In *P1* all variations are included between +1.36°C and +2°C.

For what concerns precipitation, a variable behaviour can be seen. Generally it is projected a potential decrease of total precipitation during the year, with exception for the GCM CCSM/CESM in the scenario 2.6 in *P1* and *P2*, in the scenario 4.5 in *P1*, for both AR5 and AR6, and in the scenario 8.5 in *P2* for AR6.

In *P1* average precipitation varies between -7.87% and +0.18%, for the scenarios 8.5 of AR6 and 2.6 of AR5, respectively. In *P2* it varies between -8.46% and +2.36% for the same scenarios. In *P1* for AR5 precipitation decreases principally in spring, while in AR6 a decrease can be seen in all seasons, with a large variation in summer. In *P2* for both AR5 and AR6 large decreases can be seen in spring and summer, even though accompanied by positive variations in winter and autumn. The average variation in a season could be different from the variation of annual cumulated precipitation in absolute value, based on the total precipitation of each season.
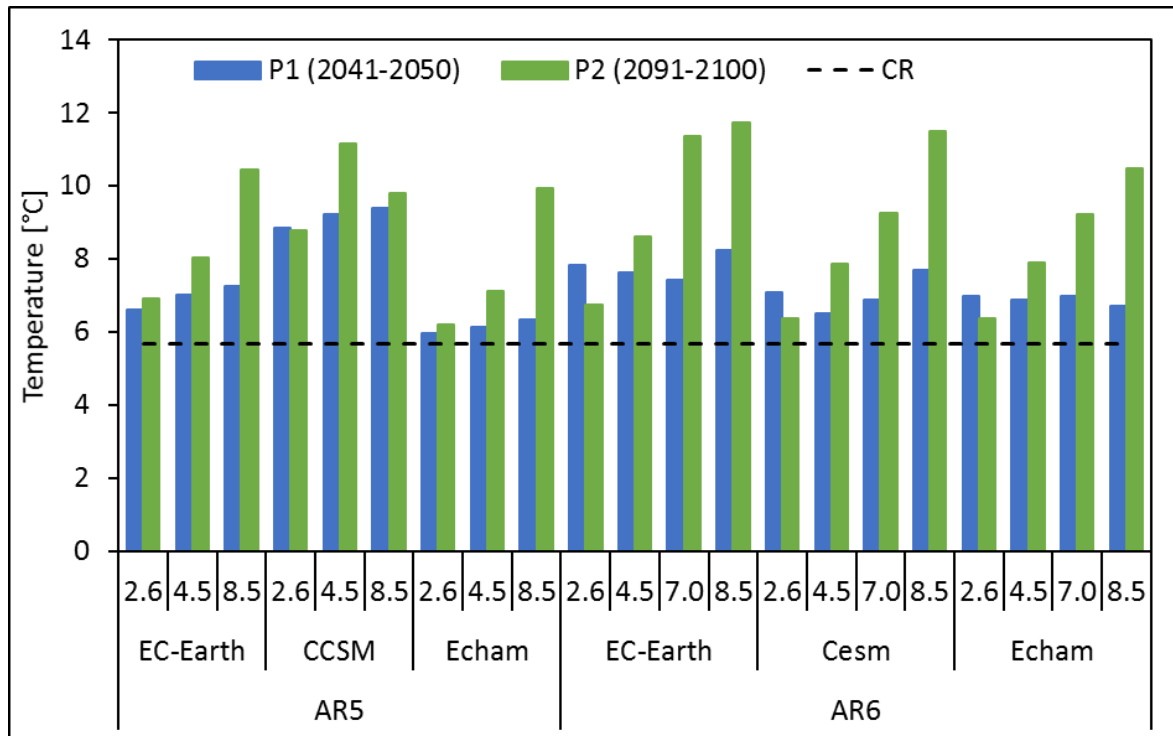
Figure 43: Annual average temperature T [°C] projections for three GCMs of IPCC AR5 and 3 GCMs of AR6, for two decades, one at the middle of the century, $P1$ (2041-2050) in blue, and one at the end of the century, $P2$ (2091-2100) in green. Black line is the present value of annual average temperature.

Table 22: Future seasonal variations of temperature T [°C] for two decades, $P1$ (2041-2050) and $P2$ (2091-2100), as average of scenarios for three GCMs of IPCC AR5 (2.6, 4.5, 8.5) and AR6 (2.6, 4.5, 7.0, 8.5).

Temperature ΔT [°C]		AR5			AR6			
		2.6	4.5	8.5	2.6	4.5	7.0	8.5
$P1$ (2041-2050)	Winter	+1.56	+1.45	+1.89	+2.02	+1.40	+1.48	+1.76
	Spring	+1.47	+1.54	+1.90	+2.07	+1.53	+1.46	+1.80
	Summer	+1.33	+2.34	+2.16	+1.55	+1.34	+1.75	+2.28
	Autumn	+1.53	+1.85	+2.07	+0.94	+1.15	+1.01	+1.69
	Average	+1.47	+1.80	+2.00	+1.65	+1.36	+1.43	+1.88
$P2$ (2091-2100)	Winter	+1.86	+3.18	+4.05	+0.77	+2.54	+4.05	+5.15
	Spring	+1.74	+2.95	+4.06	+1.00	+2.39	+3.89	+5.11
	Summer	+1.25	+3.43	+5.38	+1.04	+2.98	+5.38	+7.16
	Autumn	+1.72	+2.89	+4.04	+0.52	+1.92	+3.80	+4.83
	Average	+1.64	+3.11	+4.37	+0.83	+2.46	+4.28	+5.56
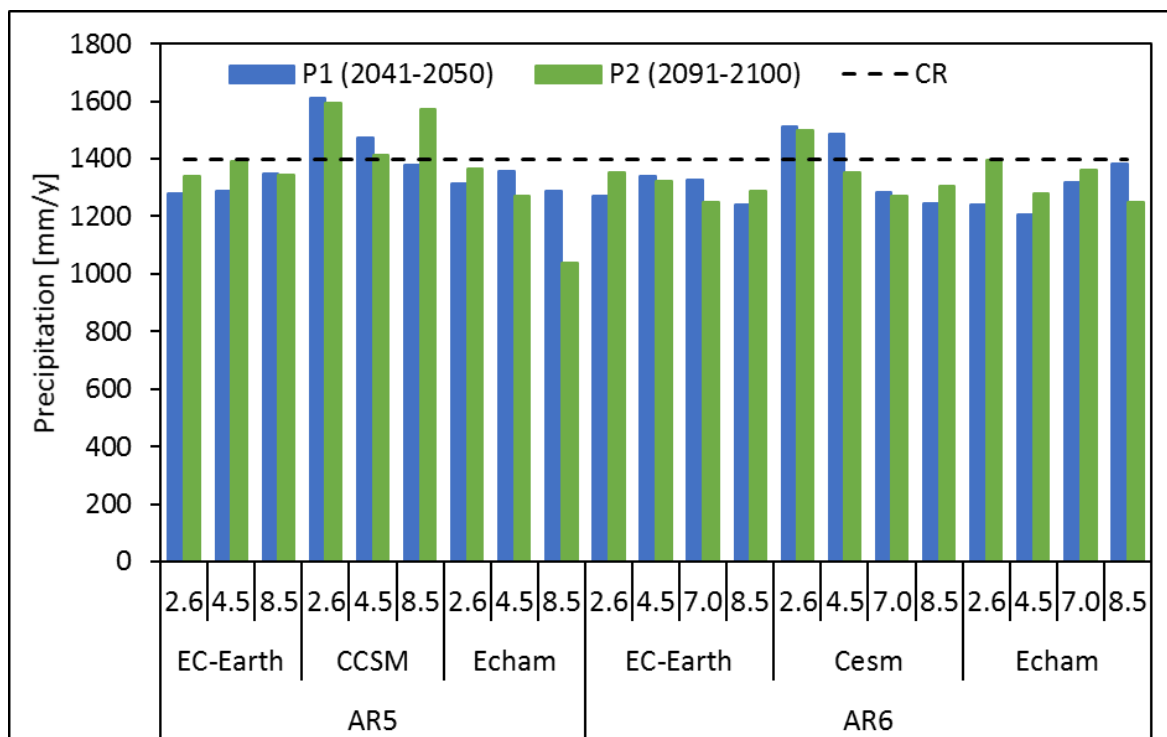
Figure 44: Annual total precipitation *P* [mm/y] projections in Valtellina study area for three GCMs of IPCC AR5 and 3 GCMs of AR6, for two decades, one at the middle of the century, *P1* (2041-2050) in blue, and one at the end of the century, *P2* (2091-2100) in green. Black line is the present value of annual total precipitation.

Table 23: Future seasonal percentage variations of precipitation *P* [%] in Valtellina study area for two decades, *P1* (2041-2050) and *P2* (2091-2100), as average of scenarios for three GCMs of IPCC AR5 (2.6, 4.5, 8.5) and AR6 (2.6, 4.5, 7.0, 8.5).

Precipitation *ΔP* [%]		AR5			AR6			
		2.6	4.5	8.5	2.6	4.5	7.0	8.5
P1 (2041-2050)	Winter	+9%	-7%	+6%	-4%	0%	-13%	-2%
	Spring	-14%	-11%	-14%	-7%	-5%	-6%	-10%
	Summer	+4%	+5%	-9%	-7%	-14%	-6%	-15%
	Autumn	+8%	+5%	+8%	+3%	+6%	-3%	-1%
	Average	+0.18	-1.86	-4.30	-4.19	-3.95	-6.39	-7.87
P2 (2091-2100)	Winter	+9%	+3%	+4%	+2%	+10%	+21%	+13%
	Spring	-1%	-11%	-16%	+1%	-6%	-21%	-15%
	Summer	-2%	-7%	-10%	-5%	-17%	-28%	-30%
	Autumn	+9%	+9%	+6%	+9%	-2%	+17%	+14%
	Average	+2.36	-2.89	-5.89	+1.17	-5.76	-7.58	-8.46

6.4.2   Gran Paradiso National Park

In Figure 45 the variation of average temperature is reported for the two decades *P1* and *P2*, for all the six GCMs and each SSP scenario. Temperature increases for all the GCMs and all the SSPs, and it is larger in *P2* than in *P1*, with the exceptions of EC-Earth and ECHAM models where the increase in *P2* for SSP 2.6 is lower than during *P1*. As reported in Table 24 the increase of temperature is between +1.14°C and +1.64°C during *P1*, respectively for SSPs 2.6 and 8.5, and between +1.25°C and +5.27°C during *P2*, respectively again for SSPs 2.6 and 8.5. The increase of temperature is always larger in summer than in other seasons, followed by winter, with some exceptions during *P2* for SSPs 7.0 and 8.5. The increase is limited here in *GPNP* with respect to Valtellina valley. This could be explained hypothesizing that at low altitudes, in valleys, the increase of temperature is larger than at higher altitudes.
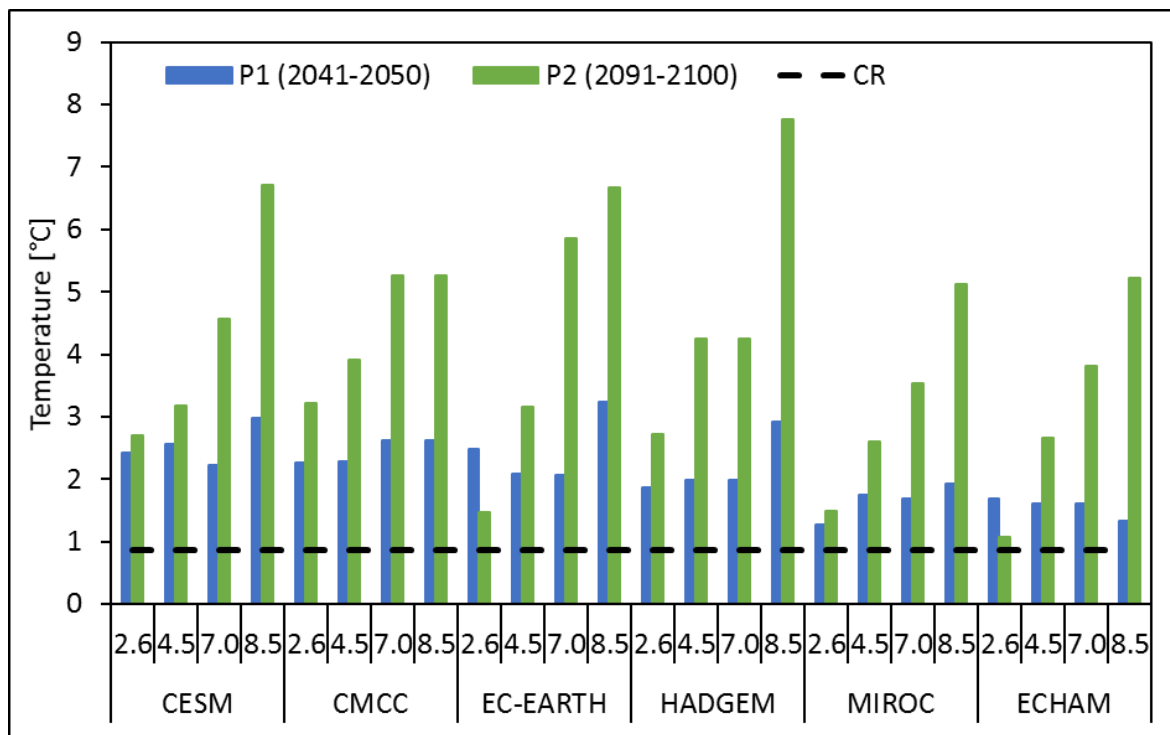
Figure 45: Projections of temperature in Gran Paradiso National Park area for six GCMs of AR6 and four SSPs, and comparison with average value during CR period (2005.2019). In blue *P1*, the decade between 2041 and 2050, and in green *P2*, the decade between 2091-2100.

In Figure 46 projections of annual precipitation are reported for all GCMs and all SSPs, considering two periods *P1* and *P2*. The behaviour is different for each model and each scenario, and the variation is usually small. Generally EC-Earth and CMCC models show an increase of total precipitations, while HadGEM, MIROC and ECHAM models show a decrease.

As average between GCMs, as reported in Table 25, small variations can be seen for *P1*, between -1.55% for SSP 8.5 and +0.51% for SSP 7.0, and larger, but again small, variations for *P2*, between -8.70% for SSP 8.5 and +4.19% for SSP 2.6. But usually projections show an increase in fall and winter and a decrease in spring and summer. The decrease in summer is between -5.66% and -16.45% for SSPs 7.0 and 8.5 during *P1*, and between -9.73% and -32.15% for SSPs 2.6 and 8.5 during *P2*. The increase of temperature and precipitation in winter will cause a large increase of liquid precipitation at the expense of snow accumulation. For this reason and for the decrease of precipitation in summer, a reduction of water availability during vegetation *GS* is expected. In some cases this behaviour is different from projections in Valtellina valley.
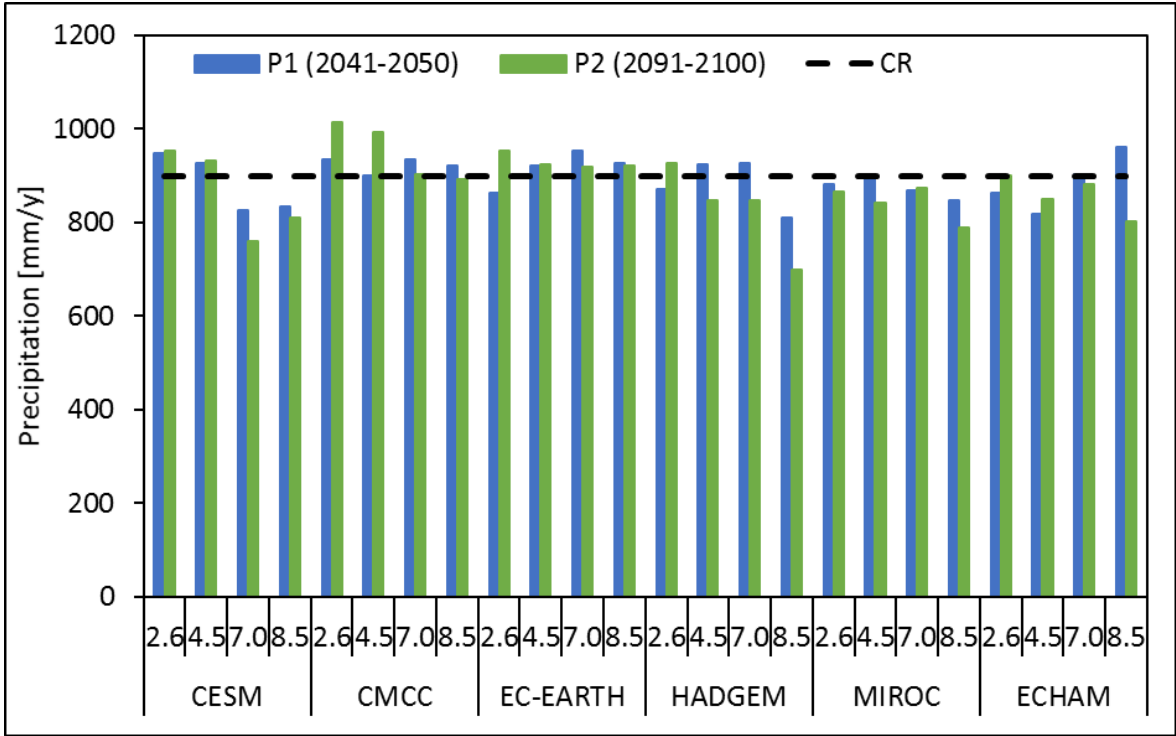
Figure 46: Projections of annual total precipitation in Gran Paradiso National Park area, for six GCMs of AR6 for four SSPs, and comparison with value during CR period (2005-2019). In blue *P1*, the period 2041-2050, and in green *P2*, the period 2091-2100.

Table 24: Variation of temperature in Gran Paradiso National Park area for two decades, *P1* (2041-2050) and *P2* (2091-2100). The average variation of all the GCMs for four SSPs of AR6 is reported for each season and as average of the year.

Temperature ΔT [°C]		2.6	4.5	7.0	8.5
P1 (2041-2050)	Winter	+1.07	+1.31	+1.12	+1.53
	Spring	+1.02	+1.00	+0.95	+1.36
	Summer	+1.67	+1.44	+1.62	+2.14
	Autumn	+0.81	+0.98	+0.99	+1.53
	Average	+1.14	+1.19	+1.17	+1.64
P2 (2091-2100)	Winter	+1.14	+2.37	+3.18	+4.45
	Spring	+1.03	+2.13	+3.39	+4.99
	Summer	+1.60	+3.16	+4.84	+7.00
	Autumn	+1.24	+2.06	+3.34	+4.63
	Average	+1.25	+2.43	+3.69	+5.27

Table 25: Variation of precipitation in Gran Paradiso National Park area for two decades, *P1* (2041-2050) and *P2* (2091-2100). The average variation of all the GCMs for four SSPs of AR6 is reported for each season and as average of the year.

Precipitation ΔP [%]		2.6	4.5	7.0	8.5
P1 (2041-2050)	Winter	+0.31	+3.50	+6.41	+6.59
	Spring	+2.45	+1.41	-0.26	+1.95
	Summer	-13.84	-8.20	-5.66	-16.45
	Autumn	+13.42	+6.33	+5.47	+7.24
	Average	-0.43	-0.02	+0.51	-1.55
P2 (2091-2100)	Winter	+15.64	+21.98	+20.77	+12.99
	Spring	+8.74	+0.76	-10.06	-9.60
	Summer	-9.73	-18.57	-26.20	-32.15
	Autumn	+7.15	+6.74	+17.37	+7.64
	Average	+4.19	+0.03	-3.72	-8.70

6.5 Future projections of pasture productivity

Climate projections of temperature and precipitation, after the downscaling, were used as input for *Poli-Hydro* and *Poli-Pasture*. In this paragraph results of *Poli-Pasture* under future projections are reported.

An increase of productivity is expected, related to the increase of temperature, reaching more suitable temperature for growth. This means that degree-day accumulation increases, reaching in less time the phenological stages, and guaranteeing more cycles during the *GS*. Moreover, increasing *T*, potential evapotranspiration increases, and if enough water is available, also ET_{eff} increases. For this reason biomass growth related to evapotranspiration increases (Eq. 17).

On the contrary, the lack of water or too excessive increase of temperature will cause a limitation of growth. Indeed, the water scarcity reduces ET_{eff} and the related growth, while an average temperature higher than T_{cutoff} limits the degree-day accumulation.

6.5.1 Valtellina

Here, for Valtellina, a variable *GS* is considered for future projections.

Generally, 8.5 scenario shows a larger increase of productivity *ΔY* with respect to 2.6 scenario, and the AR6 GCMs projects larger increase with respect to AR5 GCMs.

In Figure 47 and Figure 48 specific productivity variation *ΔY* is reported for each GCM and each scenario for AR5 and AR6 respectively. Variation of the total area, in *HighAlt* and in *LowAlt* can be distinguished. On left axis results for *P1* (2041-2050) are reported, while on the right axis results are reported for *P2* (2091-2100).

In Table 26 the average variation of specific productivity for AR5 and AR6 is reported for each scenario. Percentage variation in *HighAlt* is larger than in *LowAlt*, but in *HighAlt* specific productivity is low, so absolute variation is not significative. In the total area of Valtellina variation goes between +37.68% for *P1* for the 2.6 scenario of AR5 and +210.32% for *P2* for the 8.5 scenario of AR6. *LowAlt* has a variation for *P1* between +31.53% (scenario 2.6, AR5) and +81.00% (scenario 8.5, AR6), and a variation for *P2* between +34.04% and +163.19% for the same scenarios. *HighAlt* variation goes between +59.24% and +175.61% for *P1* for 2.6, AR5 and 8.5, AR6 scenarios respectively, and between +75.40% and +375.54% for *P2* in the same scenarios.

In Figure 49 and Figure 50 the graphs represent the percentage variation of specific productivity for altitude belts of 300 m, as reported above in paragraph 6.3.1. On the right axis

the absolute value of specific productivity is reported as reference. Figure 49 is for AR5 and Figure 50 for AR6. Dotted lines represent the range of variation, in particular the maximum and minimum variation values. Period *P1* is reported in blue, while *P2* is in green.

Under 1100 m asl, in particular altitude belts 200-500 and 800-1100 m asl, the variation is negative, for both middle and end of the century decades. For AR5 the variation is -14% and -18% in the two altitude belts in *P1*, and -2% and +2% in *P2*. For AR6 in these two altitude belts the variation is respectively of -4% and -2% in *P1*, while in *P2* it is positive. But the minimum value of the variation reaches the -31% in *P1* for AR5 in altitude belt 800-1100 m asl, and the -27% in the same altitude belt for *P2* for AR6.

These values of variation correspond to small variation in terms of absolute values [t/ha]. In AR5 projections, in *LowAlt*, the 2.6 scenario does not give differences with respect to the CR period, both at the middle and at the end of the century. The 4.5 scenario returns an increase of +1 t/ha at the middle of the century and of +2.4 t/ha as average at the end of the century. Only the scenario 8.5 gives a large increase at the end of the century, equal to +8.3 t/ha, but an increase of only +2.5 t/ha at the middle of the century. In *HighAlt*, the variation is of +0.9 t/ha and +1.2 t/ha for 2.6 scenario respectively in *P1* and *P2*, +1.5 and +2 t/ha for 4.5 scenario, and +1.8 t/ha and +4.7 t/ha for 8.5 scenario.

In AR6 the absolute variation is larger, between +0.8 t/ha (scenario 2.6, *P2*) and +8.2 t/ha (scenario 8.5, *P2*) in *LowAlt* and between +1.3 t/ha (scenario 2.6, *P2*) and +5.2 t/ha (scenario 8.5, *P2*) in *HighAlt*.

These results are reported in Table 27 as variation in terms of absolute values [t/ha], and in Table 28 as average specific productivity in future projections. For AR5 and AR6 for each scenario the average between GCMs was done.
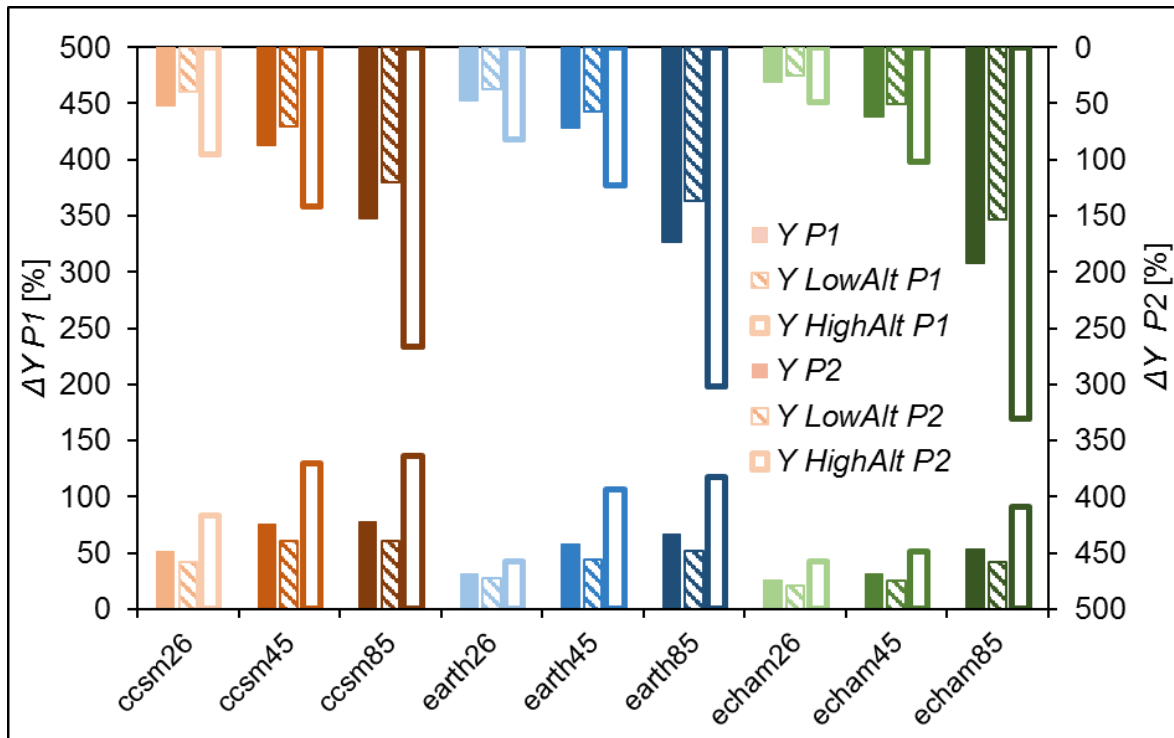
Figure 47: Specific productivity percentage variation *ΔY* in Valtellina, for the entire area, in *LowAlt* and in *HighAlt*. The middle *P1* and the end *P2* of the century are distinguished. Variations are reported for each GCM and each scenario of AR5.
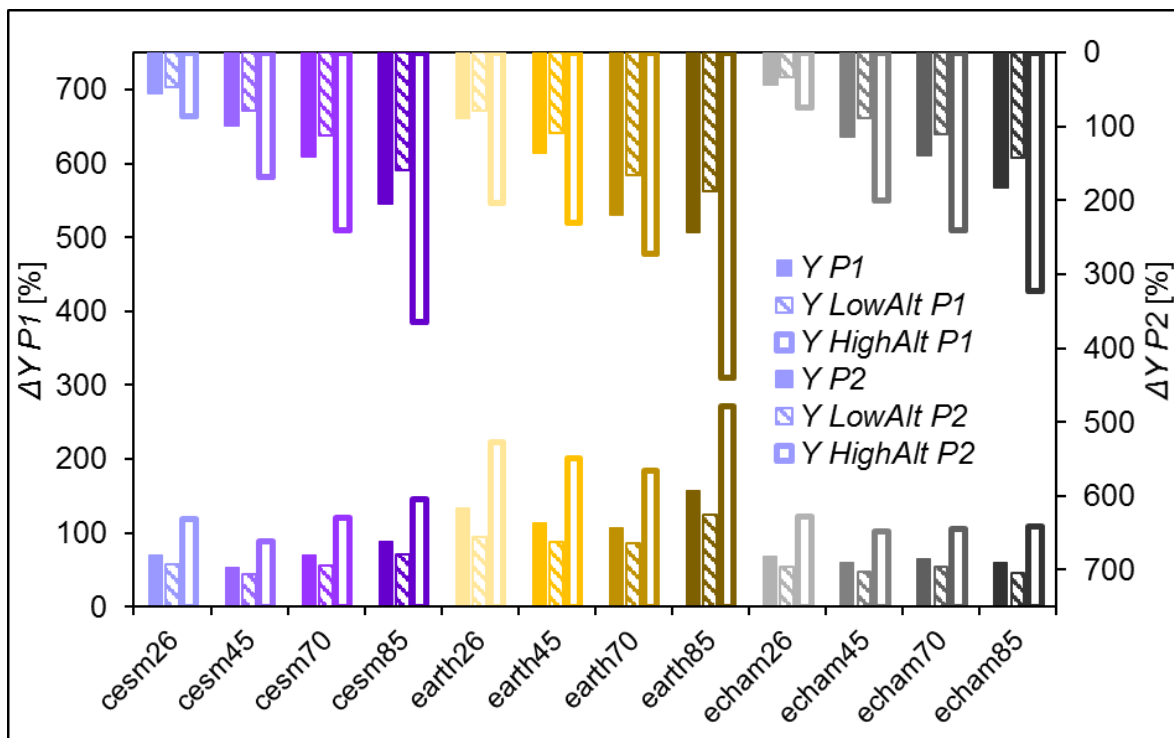
Figure 48: Specific productivity percentage variation *ΔY* in Valtellina, for the entire area, in *LowAlt* and in *HighAlt*. The middle *P1* and the end *P2* of the century are distinguished. Variations are reported for each GCM and each scenario of AR6.

Table 26: Average specific productivity variation [%] for each scenario of AR5 and AR6. *P1* and *P2*, total area of Valtellina, *LowAlt* and *HighAlt* are reported.

ΔY [%]		P1 (2041-2050)			P2 (2091-2100)		
		Tot	LowAlt	HighAlt	Tot	LowAlt	HighAlt
AR5	2.6	+37.68	+31.53	+59.24	+43.22	+34.04	+75.40
	4.5	+62.26	+48.91	+109.06	+73.33	+59.38	+122.20
	8.5	+72.28	+56.63	+127.13	+172.90	+136.76	+299.57
AR6	2.6	+90.95	+68.49	+154.64	+62.43	+53.01	+121.45
	4.5	+75.66	+59.94	+130.78	+116.13	+92.25	+199.82
	7.0	+80.91	+65.11	+136.28	+166.66	+129.54	+250.84
	8.5	+102.00	+81.00	+175.61	+210.32	+163.19	+375.54

Table 27: Average variation in terms of specific productivity [t/ha] for each scenario of AR5 and AR6 in *LowAlt* and *HighAlt* in *P1* and *P2* in Valtellina study area.

ΔY [t/ha]		P1 (2041-2050)		P2 (2091-2100)	
		LowAlt	HighAlt	LowAlt	HighAlt
AR5	2.6	+0.1	+0.9	+0.4	+1.2
	4.5	+1.1	+1.5	+2.4	+2.0
	8.5	+2.5	+1.8	+8.3	+4.7
AR6	2.6	+4.9	+3.5	+0.8	+1.3
	4.5	+2.6	+2.1	+4.9	+3.2
	7.0	+5.5	+3.7	+4.7	+3.0
	8.5	+3.9	+2.7	+8.2	+5.2

Table 28: Average specific productivity for each scenario of AR5 and AR6 in *LowAlt* and *HighAlt* in *P1* and *P2* in Valtellina study area.

Y [t/ha]		P1 (2041-2050)		P2 (2091-2100)	
		LowAlt	HighAlt	LowAlt	HighAlt
AR5	2.6	11.6	2.3	11.9	2.6
	4.5	12.6	2.9	13.9	3.4
	8.5	14.0	3.2	19.8	6.1
AR6	2.6	16.4	4.9	12.3	2.7
	4.5	14.1	3.5	16.4	4.6
	7.0	17.0	5.1	16.2	4.5
	8.5	15.4	4.1	19.7	6.6
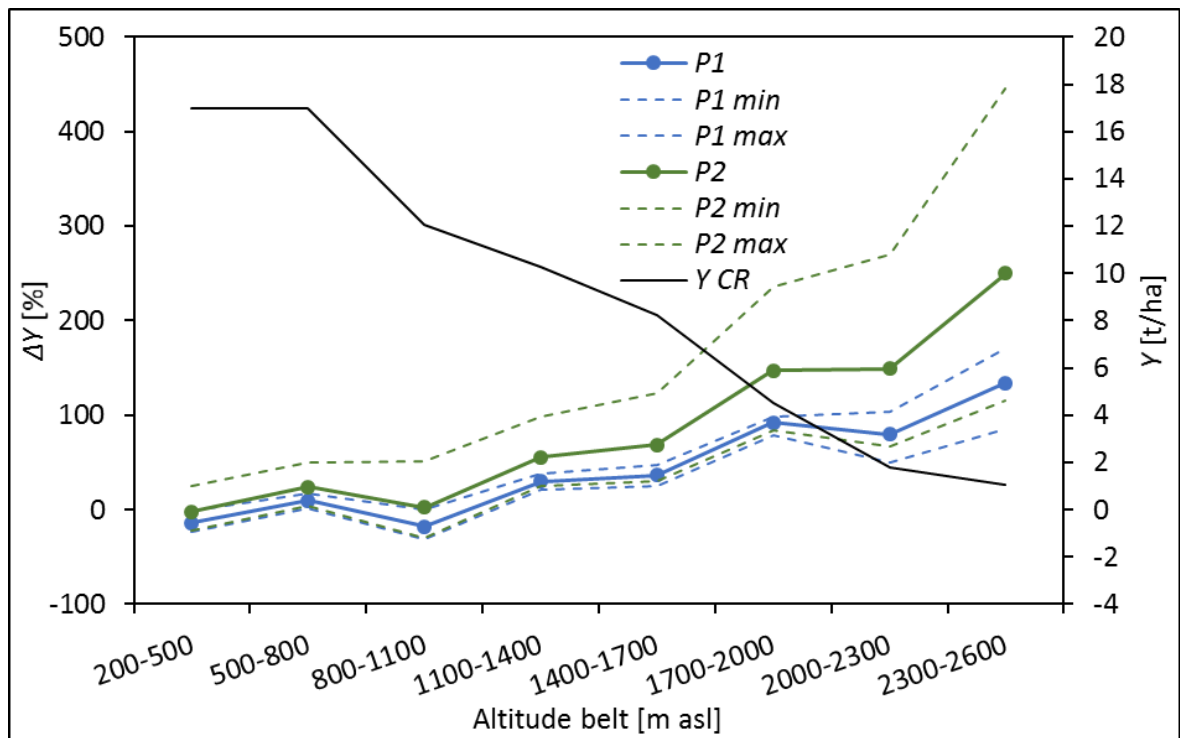
Figure 49: Percentage variation of specific productivity (left axis) and absolute value of *Y* in the CR period, for altitude belts of 300 m, for projections of AR5 in Valtellina study area. In blue results of *P1* are reported and in green results of *P2*. Dotted lines represent the range of variation.
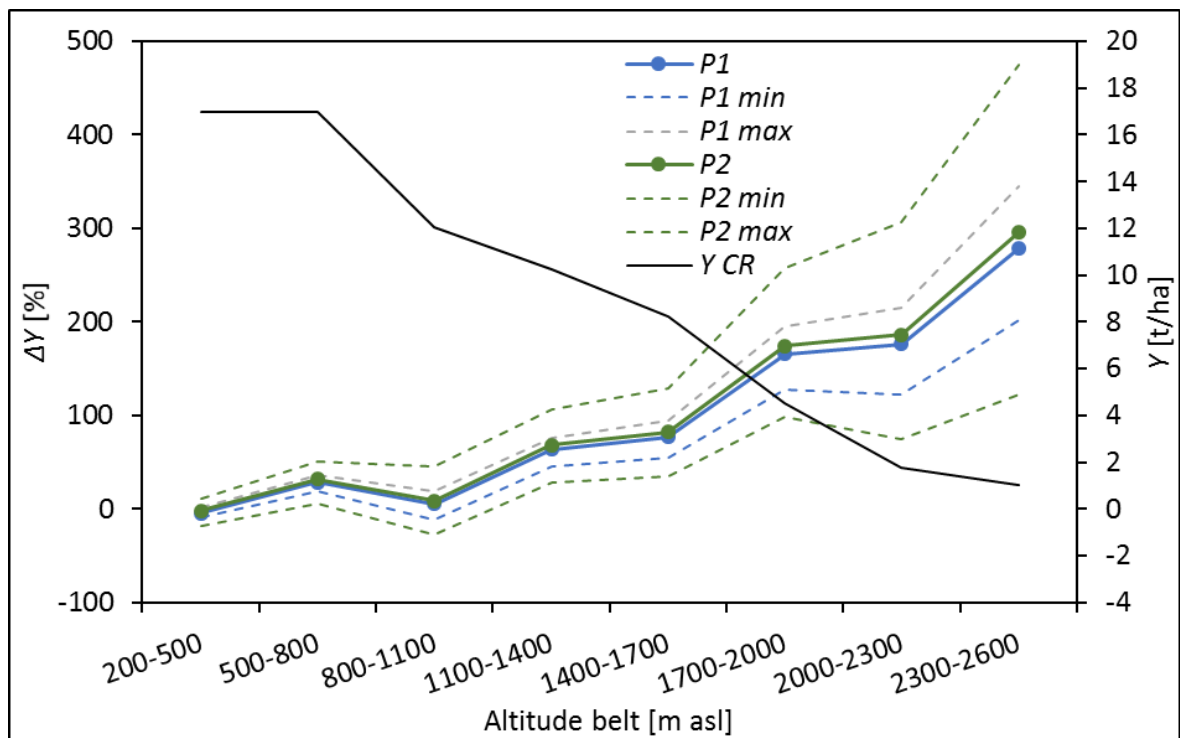
Figure 50: Percentage variation of specific productivity (left axis) and absolute value of *Y* in the CR period, for altitude belts of 300 m, for projections of AR6 in Valtellina study area. In blue results of *P1* are reported and in green results of *P2*. Dotted lines represent the range of variation.

6.5.2   Gran Paradiso National Park

Here the projections in terms of productivity are reported for *GPNP* study area. In Figure 51 the percentage variation of specific productivity *Y* is represented for each GCM of the AR6 and each SSP scenario. The variation is reported for the middle of the century *P1* (2041-2050) and the end of the century *P2* (2091-2100). In *HighAlt* the variation is significant, while in *LowAlt* it is contained. Considering the total area (*Tot*) the variation is high because the largest part of pasture area is in *HighAlt*.

Looking at *P1*, the models HadGEM, MIROC and ECHAM show a lower increase of productivity with respect to other models for all the scenarios. Another difference between models is that CMCC, EC-Earth and HadGEM present a lower increase for intermediate scenarios, like SSPs 4.5 and 7.0, than "extreme" scenarios, e.g. SSPs 2.6 and 8.5. Other models, like MIROC, present an increasing variation with SSPs.

In *P2*, all the models show larger increases for SSP 8.5, than SSP 7.0, as 4.5 and 2.6.

The GCM ECHAM for the SSP 2.6 projects a decrease of -0.63% in *LowAlt* for *P2*.

Differently from Valtellina case study the decrease of productivity is limited because of the high average altitude of *LowAlt*.

In Table 29 the percentage and in absolute value variations are reported, as the resulting average productivity. These values are averaged between GCMs for each SSP scenario.

The productivity in *LowAlt* increases between +10.87% and +12.95% for SSPs 7.0 and 2.6 respectively in *P1*, and between +13.48% and +17.46% for SSPs 2.6 and 4.5 in *P2*. In *HighAlt* it increases between +86.43% and +96.66% in *P1* for SSPs 7.0 and 8.5, and between +90.03% and +123.38% in *P2* for SSPs 2.6 and 8.5. These are similar conditions to Valtellina case study for AR6. While in *P1* the increase is differently distributed in SSPs, in *P2* the increase is larger for SSP 8.5 than SSP 2.6. Moreover the increase between *P1* and *P2* is larger for intermediate scenarios, like SSPs 4.5 and 7.0, in *LowAlt*, and for worse scenarios, like SSPs 7.0 and 8.5, in *HighAlt*. So for scenario 2.6 the increase is larger between CR and *P1* than between *P1* and *P2*, where the temperature variation remains constant in practice, while for scenario 8.5 the continuous increase of temperature causes an increase of productivity also between *P1* and *P2*.

The increase in *LowAlt*, as absolute value, is contained here with respect to the case of Valtellina valley. Here the increase is around +0.80 t/ha (between +0.71 t/ha and +0.84 t/ha for SSPs 7.0 and 2.6) for *P1* and +0.98 t/ha (between +0.88 t/ha and +1.14 t/ha for SSPs 2.6 and 4.5) for *P2*. On the contrary the increase in *HighAlt* is similar to Valtellina valley. The increase

is between +3.05 t/ha and +3.41 t/ha in *P1* for SSPs 7.0 and 2.6 (same scenarios of *LowAlt*), and between +3.18 t/ha and +4.36 t/ha for SSPs 2.6 and 8.5 in *P2*.

The final average productivity is similar between *LowAlt* and *HighAlt*. In particular for *P1* the specific productivity is between 7.21 t/ha and 7.34 t/ha (SSPs 7.0 and 2.6) in *LowAlt* and between 6.58 t/ha and 6.94 t/ha (SSPs 7.0 and 2.6) in *HighAlt*. While for *P2* it is between 7.38 t/ha and 7.64 t/ha (SSPs 2.6 and 4.5) in *LowAlt* and between 6.71 t/ha and 7.89 t/ha (SSPs 2.6 and 8.5) in *HighAlt*.

In *LowAlt* and in *HighAlt* for *P1* the variation does not have a specific behaviour because of the differences in projections of each GCM. The average between GCMs could not highlight these differences. On the contrary in *HighAlt* for *P2* the increase has a significant behaviour, increasing with SSP, because all GCMs have the same trend in projections.

It is important to say that the projections in specific productivity *Y* depends on different variables, and in particular on projections in *P* and *T*, that are different for each SSP and each GCM. For this reason it is useful to analyse agroclimatic indices to identify the reason of a specific variation of a projection.
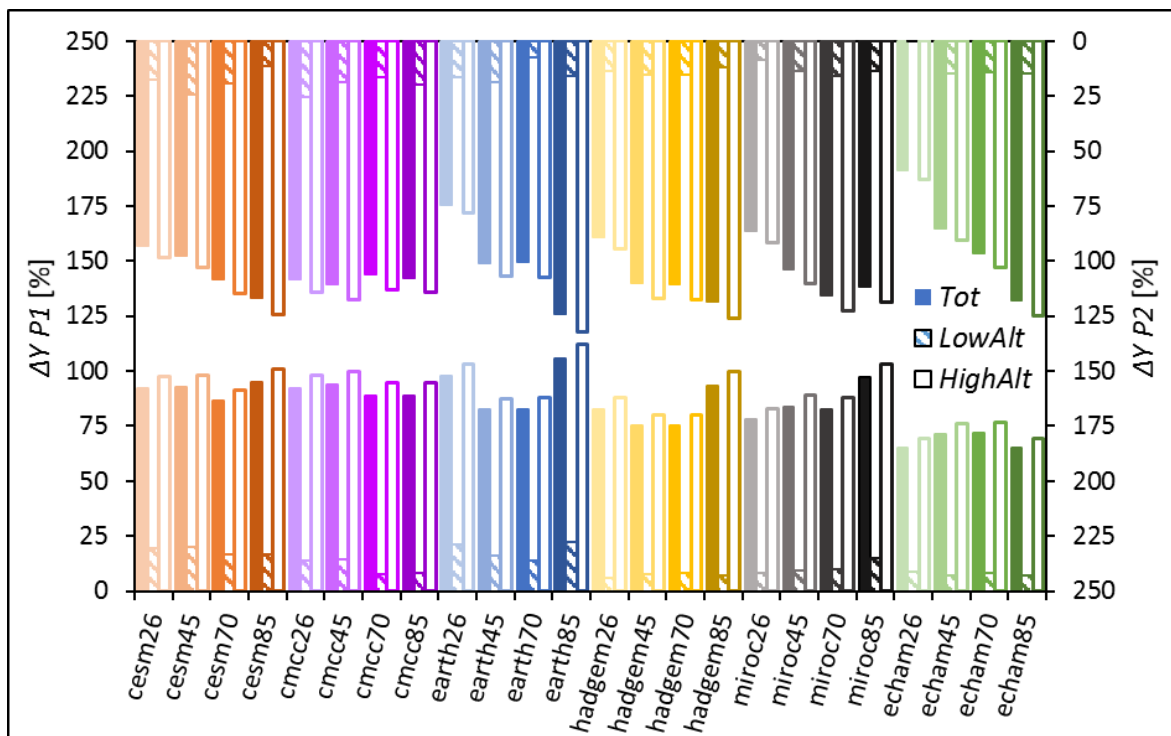
Figure 51: Percentage variation of specific productivity *Y* in *LowAlt* (<1800 m asl), *HighAlt* (>1800 m asl) and in the overall area of pasture, for each GCM and SSP of AR6 in Gran Paradiso National Park study area, in *P1* (2041-2050), left axes, and in *P2* (2091-2100), right axes.

Table 29: Percentage variation and in absolute value of specific productivity, and the average specific productivity *Y* in *LowAlt* (<1800 m asl) and *HighAlt* (>1800 m asl), in *P1* (2041-2050) and *P2* (2091-2100), for the study area of Gran Paradiso National Park. Values are averaged for SSPs between GCMs.

	SSP	P1 (2041-2050)		P2 (2091-2100)	
		LowAlt	*HighAlt*	*LowAlt*	*HighAlt*
ΔY [%]	2.6	+12.95	+89.86	+13.48	+90.03
	4.5	+12.39	+88.37	+17.46	+107.39
	7.0	+10.87	+86.43	+14.77	+112.91
	8.5	+12.70	+96.66	+14.63	+123.38
ΔY [t/ha]	2.6	+0.84	+3.17	+0.88	+3.18
	4.5	+0.81	+3.12	+1.14	+3.79
	7.0	+0.71	+3.05	+0.96	+3.99
	8.5	+0.83	+3.41	+0.95	+4.36
Y [t/ha]	2.6	7.34	6.70	7.38	6.71
	4.5	7.31	6.65	7.64	7.32
	7.0	7.21	6.58	7.46	7.52
	8.5	7.33	6.94	7.45	7.89

6.5.3 Projections of species relative presence in Gran Paradiso National Park

The relative presence of *Dactylis glomerata* (Figure 52) is projected to reduce for all the scenarios and for both *P1* and *P2*, on the contrary the presence of *Trifolium alpinum* is projected to increase (not shown). The presence of *Dactylis glomerata* was between 0.425 and 0.435 during the present period (Figure 42 a), while in future projections it is between 0.41 and 0.42. The variation is small because of the inter-specific competition model is driven principally by the bovines liking, but the increase of temperature in future period influences the relative presence of species and a decrease here could be seen. Moreover, in *LowAlt*, differently than in *HighAlt*, the bovines liking is similar for the two species (0.70 and 0.80 for *Trifolium alpinum* and *Dactylis glomerata*, respectively, Table 20) and the different distribution of species is here more influenced by temperature, radiation and water availability conditions. The reduction of *Dactylis glomerata* in climate projections is confirmed in other studies (see e.g. (Dibari et al., 2021)), precisely due to the increase of temperature.

The reduction in *LowAlt* of *Dactylis glomerata* is more considerable in *P2* with respect to *P1* for scenarios 7.0 and 8.5, while the difference in variation for SSPs 2.6 and 4.5 is smaller between the two periods. In *LowAlt* it is possible to find two different values of *Dactylis glomerata* relative presence at the same altitude. While in SSP 2.6 the higher value reduces

more than the lower value, in SSP 4.5 the higher values increases and the lower value decreases. On the contrary, as said before, for SSPs 7.0 and 8.5 the reduction is significant for all the cells.

For *HighAlt* (Figure 53) the relative presence of *Festuca rubra* is reported for all the scenarios as average of the GCMs. With respect to the present period (Figure 42 b) the relative presence of *Festuca rubra* is projected to decrease. During CR it was between 0.265 and 0.295, while for projections the value varies between 0.25 and 0.29. The major reduction can be seen for SSP 4.5 during *P1*, while in *P2* the value is higher for all the scenarios. For SSP 7.0 and 8.5 the altitudinal lapse rate is levelled during *P2*.

The reduction of *Festuca rubra* in the future is reported also in (Dibari et al., 2013).
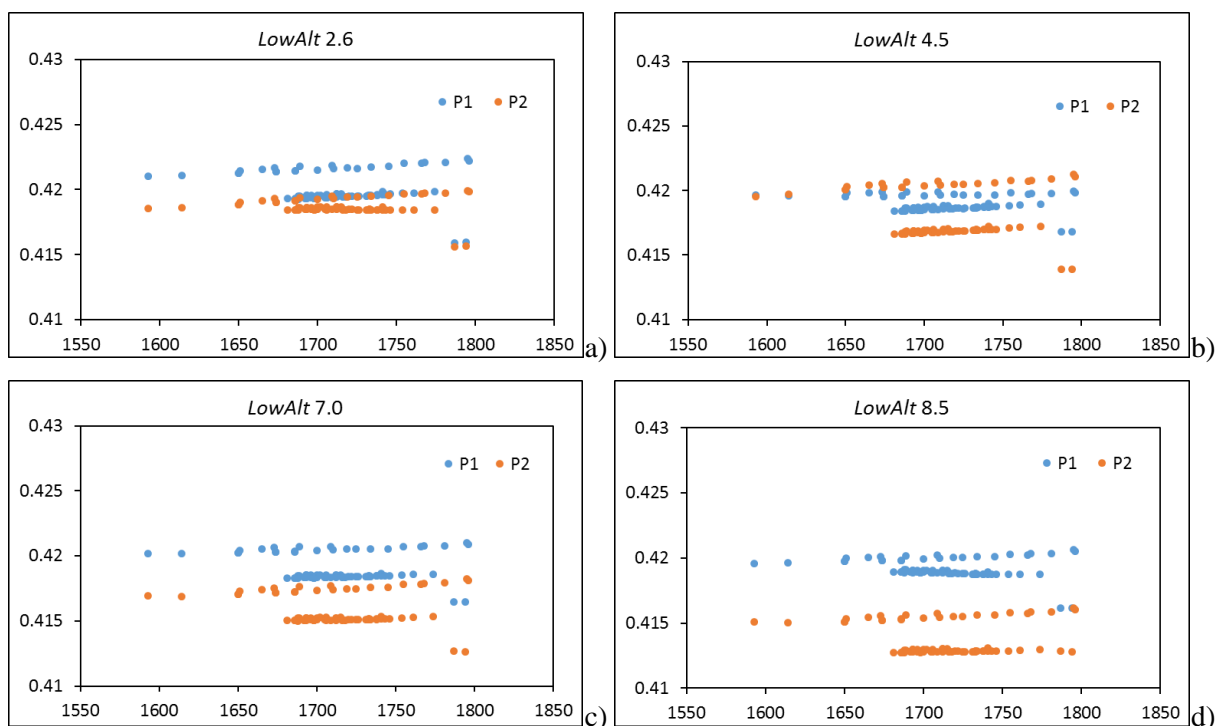
Figure 52: Relative presence of *Dactylis glomerata* in *LowAlt* for SSPs 2.6 (a), 4.5 (b), 7.0 (c), 8.5 (d), for *P1* (blue dots) and *P2* (orange dots). The values of relative presence are reported basing on the cells altitude and they are the average for each scenario for all the GCMs.
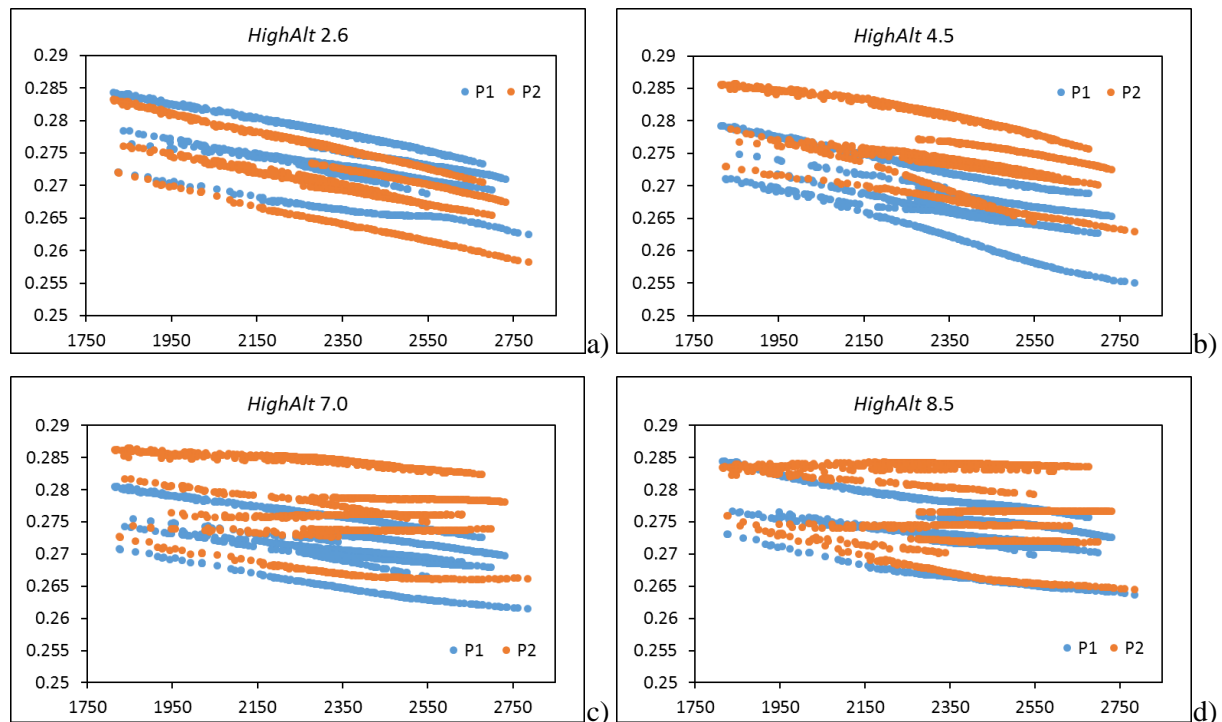
Figure 53: Relative presence of *Festuca rubra* in *HighAlt* for SSPs 2.6 (a), 4.5 (b), 7.0 (c), 8.5 (d), for *P1* (blue dots) and *P2* (orange dots). The values of relative presence are reported basing on the cells altitude and they are the average for each scenario for all the GCMs.

6.6 Agroclimatic indices (AIs)

Agroclimatic indices AIs were estimated in the CR period and for each scenario and GCM in *LowAlt* and *HighAlt*, in *P1* and *P2*. In next paragraphs the AIs are reported as average values among all GCMs for each scenario.

6.6.1 Valtellina

In Figure 54 results of AIs are reported for Valtellina. In all the cases the growth season length, AI1 (Figure 54 a), extends, due to an increase of temperature in spring and fall that causes better temperature for growth, above the T_{base}. The extension of *GSL* is related in particular to an anticipation of the beginning, more than to a late in the end of *GS*. AR6 sees a larger extension of *GS* with respect to AR5, with equal scenarios.

This is a common result of other studies. (Bellini, Moriondo, Dibari, Leolini, et al., 2023), using MODIS images of vegetation, show that in the last 20 years the *GS* anticipated the beginning for the increase of temperature. The correlation with temperature is not linear, like here, due to the influence of other conditions, like precipitation and snow cover.

Longer *GSL* contributes to the increase of total productivity Y_y [t/y], AI5 (Figure 54 e), because of the longer time for growth and the chances for more growth cycles.

However, the excessive increase of temperature, and of heat waves frequency, AI2 (Figure 54 b), is a limitation for growth, in particular in *LowAlt*, in both *P1* and *P2*. This could explain the reduction of productivity in *LowAlt*, shown in paragraph 6.5.1. Comparing to the CR period, when no heat waves happen, in the future the number of days with *T* larger than T_{cutoff} will potentially increase a lot. In *LowAlt* the frequency of hot days will increase significantly, especially in *P2*. But also in *HighAlt* for worse scenarios, i.e. SSPs 7.0 and 8.5, at the end of the century heat waves will be present.

AI3 (Figure 54 c) and AI4 (Figure 54 d) are related and coherent with variation of precipitation during spring and summer (Table 23). Indeed, a decrease of precipitation, AI4, is in line with a reduction of the number of days with intense precipitation, AI3. Small reduction in cumulated precipitation during *GS* can be generally seen, with some exceptions for *P2* and 4.5 scenario. AI4 shows more significant reduction with respect to CR period in the number of days with intense precipitation, for all the scenarios, decades and altitude areas.

AI6 (Figure 54 f) is the *ET* efficiency, namely the ratio ET_{eff}/ET_{max}, and it is an indication of fulfilment of water requirements. The increase of *T* causes an increase of ET_{max}, but here ET_{eff} increases more than ET_{max}, in response to the longer *GS* (AI1) and the decrease of extreme precipitation events (AI3), so to a more regular distribution of precipitation during the *GS*. For this reason AI6 increases in *P1* and *P2* in both *LowAlt* and *HighAlt*, in spite of the general decrease of precipitation during *GS*. This happens principally in *HighAlt*, where more soil humidity is present, also due to the increasing snow melt and lower temperature. The increase of this index AI6 is an indication of the better use of available water with respect to CR period.

AI7 (Figure 54 g) is the relative *ET*, i.e. the ratio ET_{eff}/P_{GS}. It increases in both *HighAlt* and *LowAlt* in *P1* and *P2*. This is an indication again of the major use of precipitation to fulfil *ET* requirements for plants' growth, resulting again in an increase of productivity (AI5).

AI8 (Figure 54 h) is specific water footprint, namely the ratio ET_{eff}/Y, and it may increase or decrease depending on the combination of ET_{eff} and *Y*. In *HighAlt* AI8 decreases for all scenarios both in *P1* and *P2*, while in *LowAlt* a potential increase is shown in *P1* and a decrease in *P2*.

Comparing AR5 and AR6 projections, relatively to AI6 no differences could be seen. However, a larger increase in *ET* efficiency is expected in *HighAlt* with respect to *LowAlt*. On the contrary, considering AI7, a larger increase is projected by AR6 scenarios, both in *HighAlt*

and *LowAlt*. Considering no marked differences in precipitation quantity during *GS* (Table 23, and Figure 54 d) based on AR, this means a larger increase of ET_{eff} for AR6.

Considering AI8, AR5 projections show an increase in *LowAlt* and a decrease in *HighAlt*, with the exception of ECHAM6.0, while AR6 GCMs project a decrease in both *LowAlt* and *HighAlt*.

In spite of the increase of ET_{eff}, highlighted by AI6 and AI7 in particular for AR6 and in *HighAlt* for both AR5 and AR6, the large increase of productivity in *HighAlt* (AI5), especially for AR6, explains the reduction of specific water footprint (AI8). On the contrary, the decrease of productivity in *LowAlt* explains the reduction of AI8 in this altitude area.

a)

b)

c)

d)

e)

f)

g)

h)
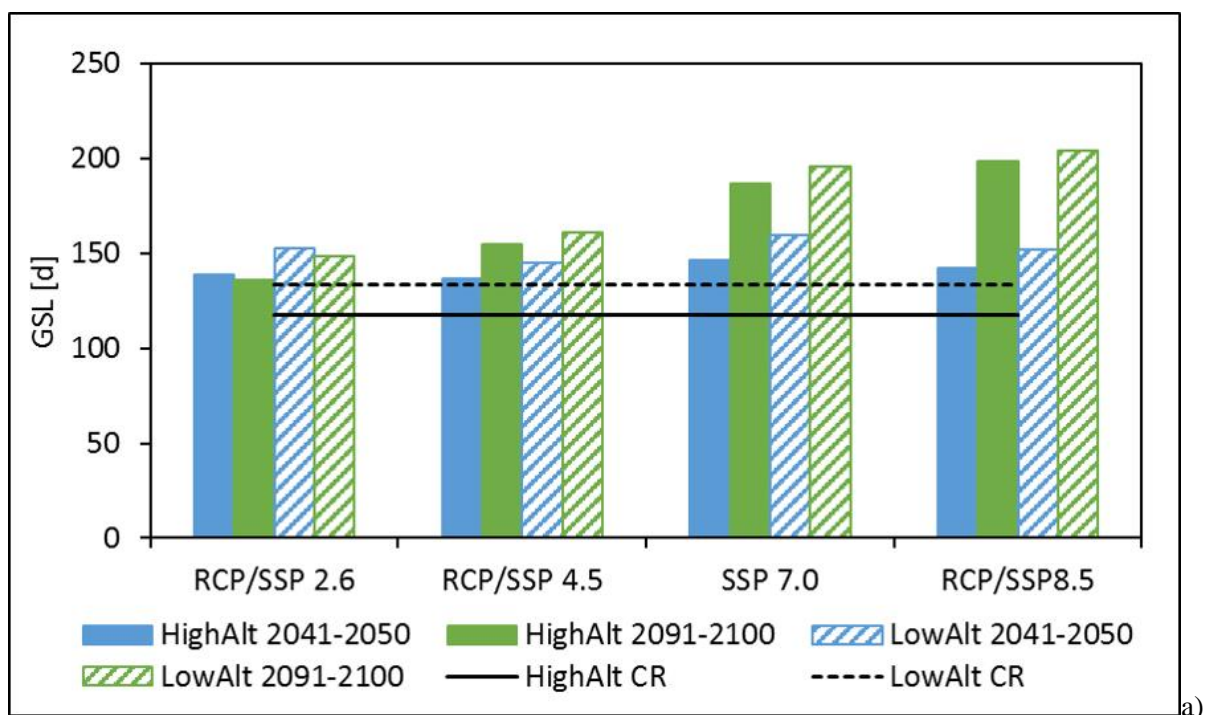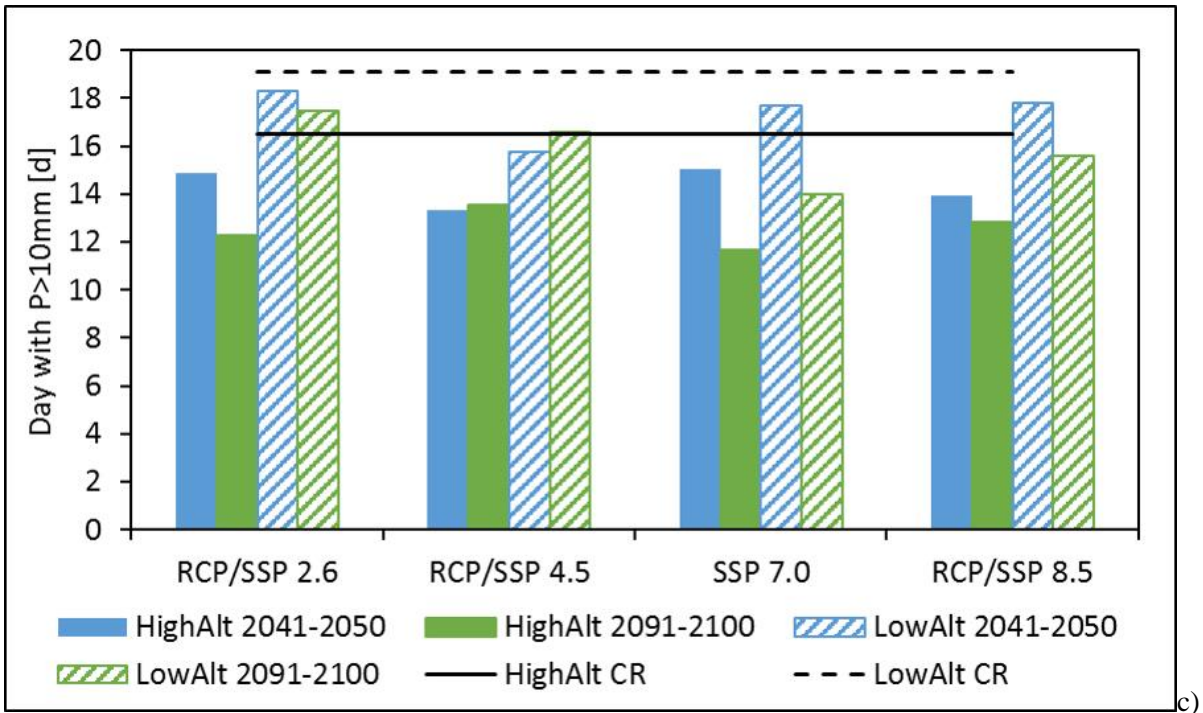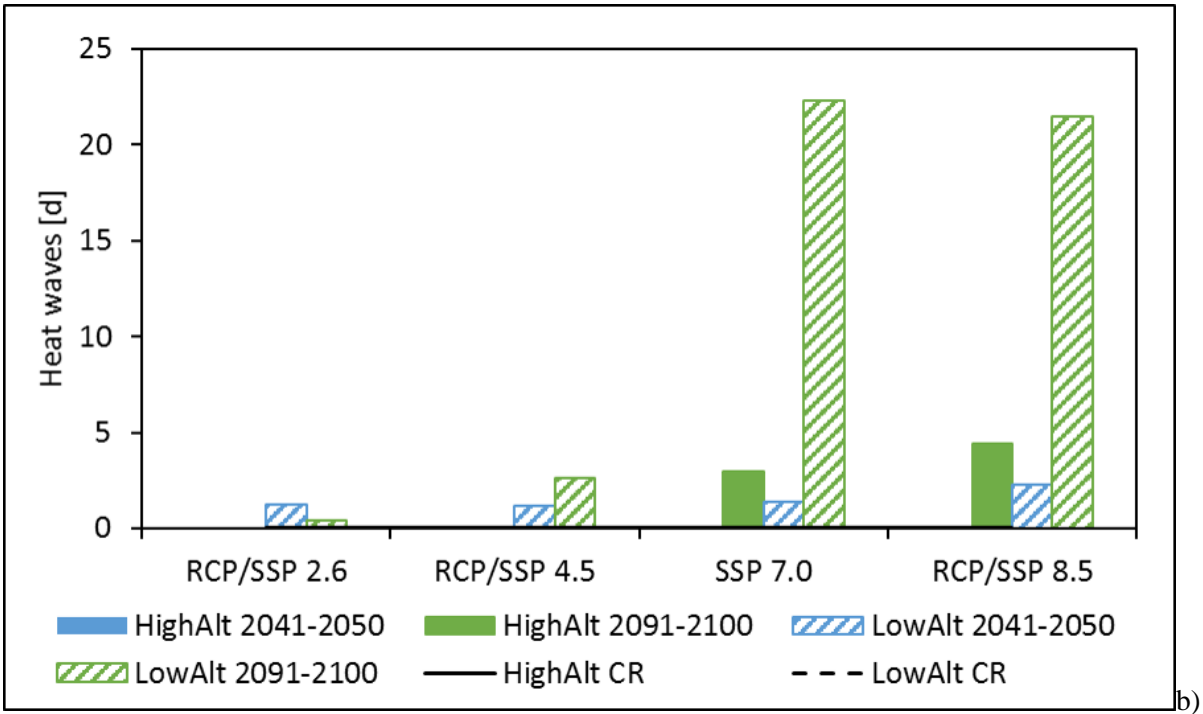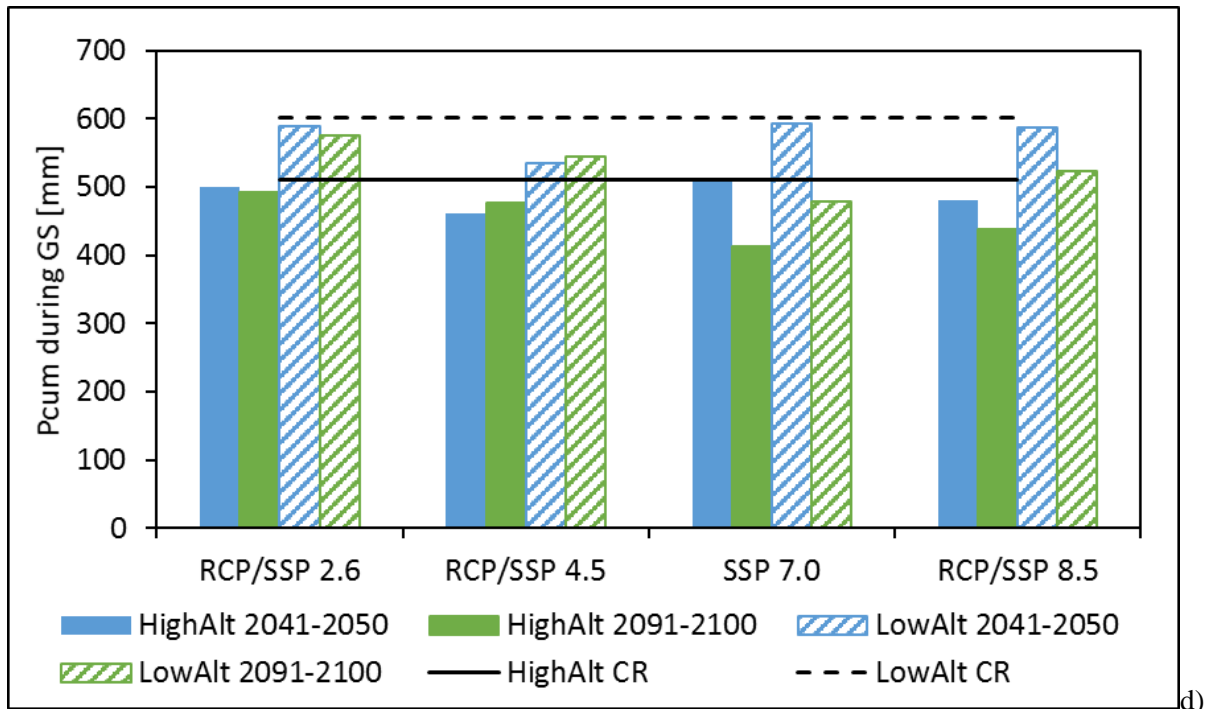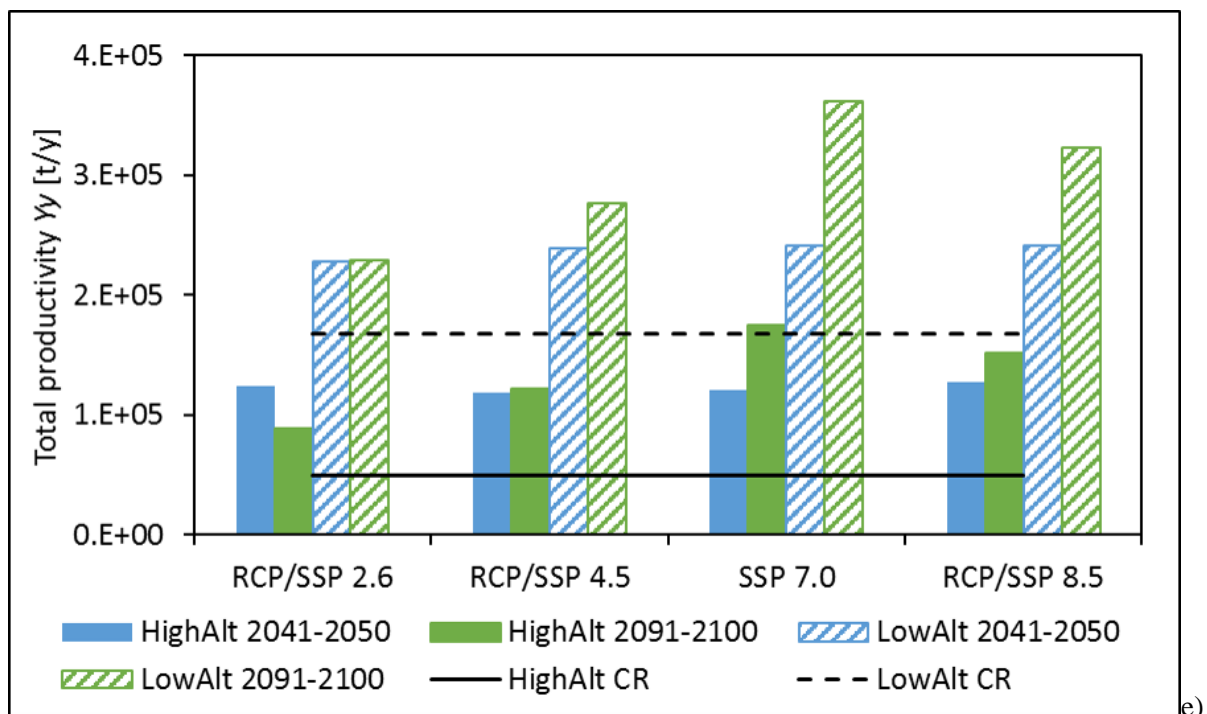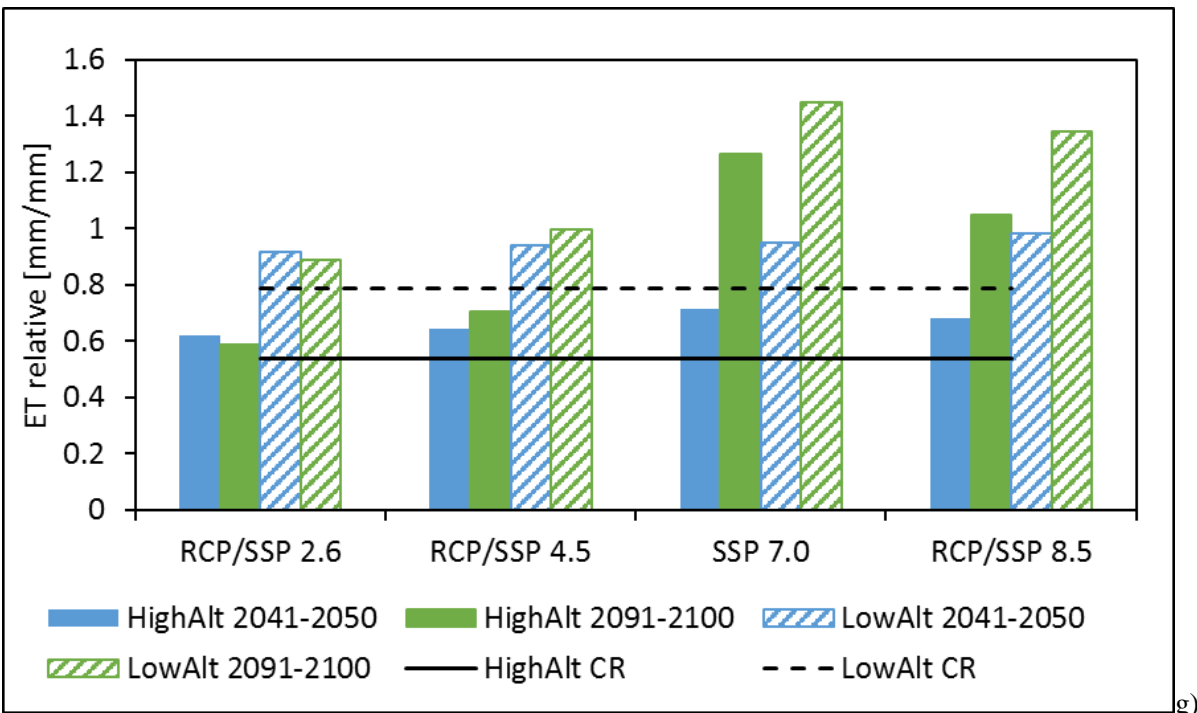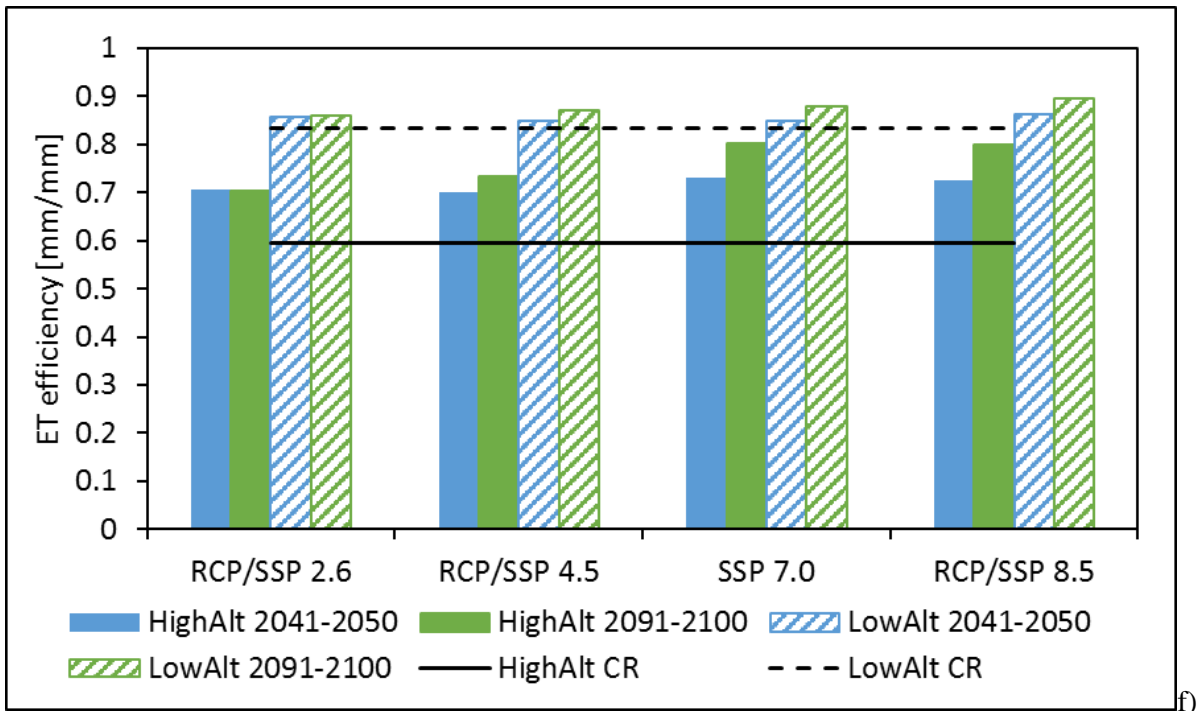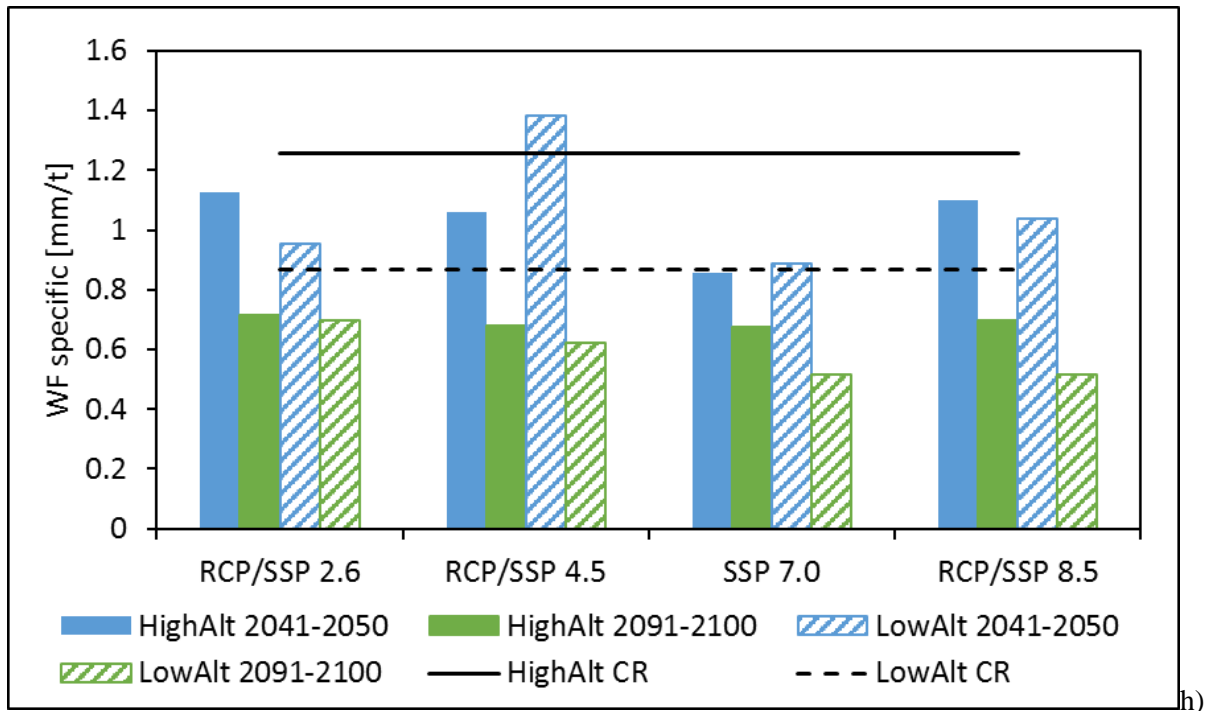
Figure 54: Future projections and comparison with CR period of agroclimatic indices AIs in Valtellina study area. For each scenario (coupled RCPs and SSPs) the average is done between GCMs. In the graphs the results for *HighAlt* (plain color) and *LowAlt* (lines) and for *P1* (blue) and *P2* (green) are reported. AIs are: AI1 growth season length (a), AI2 heat waves frequency (b), AI3 number of days with P larger than 10 mm (c), AI4 cumulated P during *GS* (d), AI5 total productivity (e), AI6 evapotranspiration efficiency (f), AI7 relative evapotranspiration (g), AI8 specific water footprint (h).

6.6.2   Gran Paradiso National Park

In Figure 55 the results of agroclimatic indices are reported for the study area of Gran Paradiso National Park. Figure 55 a represents AI2, the frequency of heatwaves. Here, it is possible to see an occurrence of heatwaves only for the SSP 8.5, in practice, only for *P2* (2091-2100) in both *LowAlt* and *HighAlt*, but with a higher frequency in *HighAlt*, differently from Valtellina case study. The increase of temperature, without an excessive increase causing heatwaves, guarantees optimal temperatures for the vegetation and the large increase of productivity without a decrease, especially in *LowAlt*. This is related to higher altitude with respect to Valtellina valley, but also to the lower threshold altitude between *HighAlt* and *LowAlt*, for this reason *HighAlt* is characterised by lower altitude belt.

For what concerns precipitation, AI3 and AI4 (Figure 55 b and c), a decrease is always seen for all the SSPs, for both *P1* and *P2* and *HighAlt* and *LowAlt*, and the decrease of days with intense precipitation (AI3) coherently decreases with the cumulated precipitation during the growing season (AI4). The results of AI3 and AI4 are in line with projections of

precipitation shown in Table 25, in particular for the summer season. The cumulated precipitation, and the number of days with intense precipitation, decrease more in *P2* than in *P1* for all SSPs with the exception of SSP 2.6 where the decrease in *P2* is lower than in *P1*. Moreover they decrease more for SSP 8.5 than for SSP 7.0 than for SSP 4.5 than for SSP 2.6.

ET efficiency (ET_{eff}/ET_{max}), AI6 (Figure 55 e), has the same behaviour of AI3 and AI4, so it decreases with respect to CR period in both *LowAlt* and *HighAlt* and decreases more for *P2* than for *P1*, with the exception of SSP 2.6, and decreases more for SSP 8.5 than for other SSPs. This is related to the increase of ET_{max} for the increase of temperature, but to the decrease of available water from precipitation for the effective evapotranspiration ET_{eff}.

The AI7 (Figure 55 f), relative *ET* (ET_{eff}/P), shows an increase for all SSPs both in *P1* and *P2* and *HighAlt* and *LowAlt*, with respect to CR period, with the exception of SSP 8.5 for *LowAlt* in *P1* and *P2* and *HighAlt* in *P2*, and SSP 7.0 for *LowAlt* in *P2*. In *LowAlt* the increase is larger and the decrease is smaller in *P1* than in *P2*. On the contrary, in *HighAlt* the increase is higher in *P2*. Only exception are for SSP 2.6 in *LowAlt* and *HighAlt* and for SSP 8.5 for *HighAlt*. Generally, this means that with respect to CR period, more water is used from precipitation to satisfy the evapotranspiration needs. This could mean also that less snow is available on soil and could not be used during the *GS* as available water for growth. The decrease of AI7 is an indication of a larger reduction of ET_{eff} with respect to the decrease of *P*, and it is an indication of the reduced consumption of water for growth.

The results of AI6 and AI7 are different in *GPNP* with respect to *Valt* area, where the two indices increases in all the scenarios with respect to the CR period. Here in *GPNP*, in some cases, a reduction in the consumption of water for vegetation growth, or a lack of available water, can be seen, differently from *Valt* area. The values larger of 1 in *Valt* for AI7 are an indication of the consumption of water from snow melt and glacier melt.

The AI8 (Figure 55 g), specific water footprint (ET_{eff}/Y), decreases here for all the scenarios with respect to the CR period, with very low values in *HighAlt*. It is different from *Valt* where in *LowAlt* in some cases an increase is projected and where sometimes the values are larger than 1. This is a further indication of the small consumption of water for the vegetation growth.

a)

b)

c)

d)

e)

f)

g)
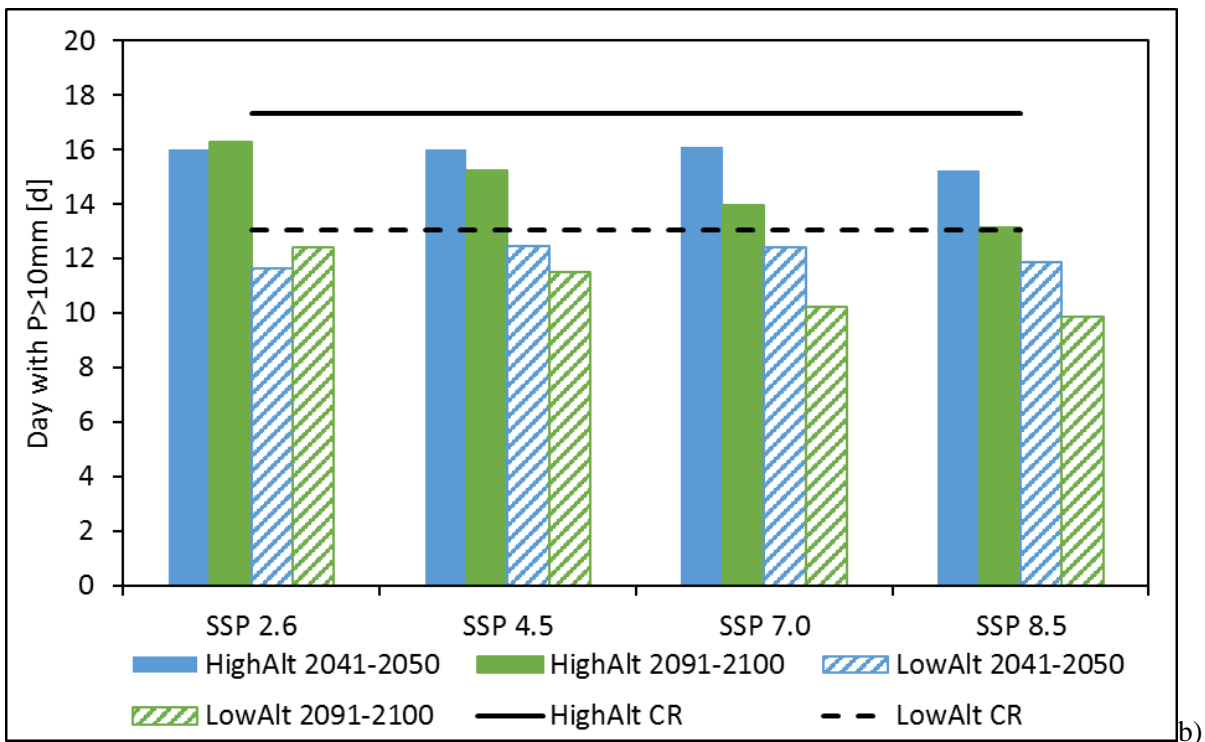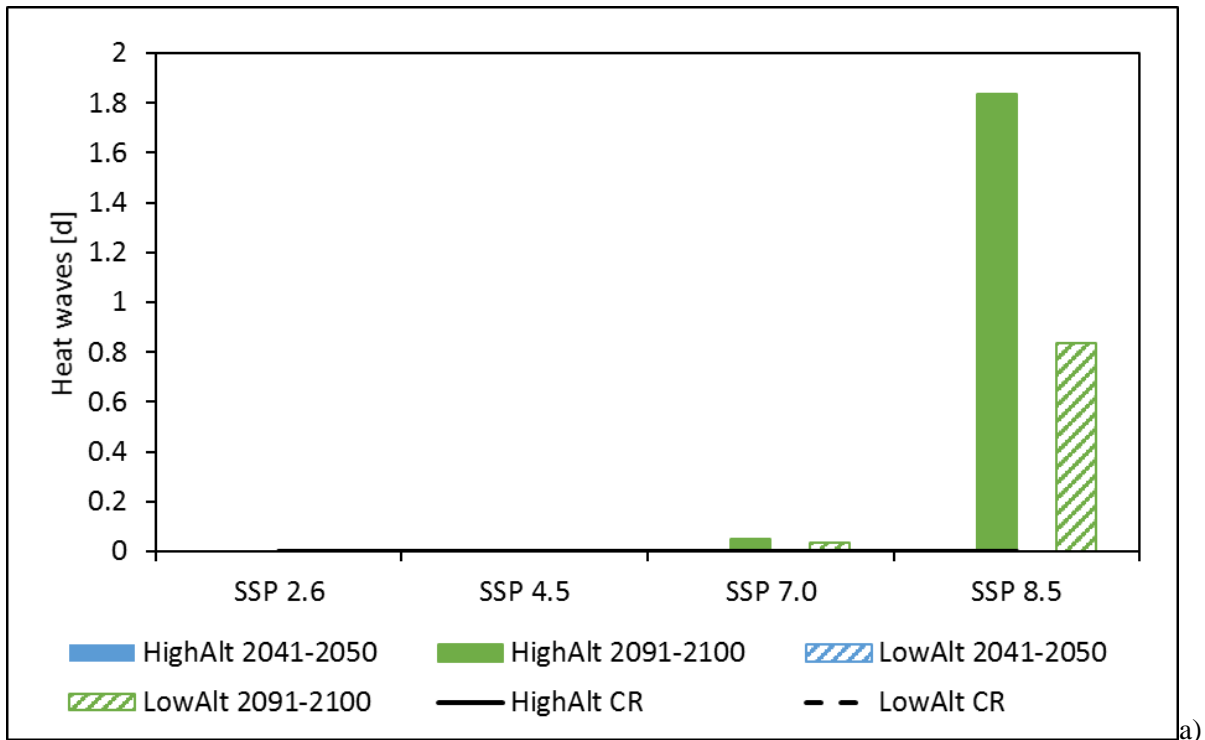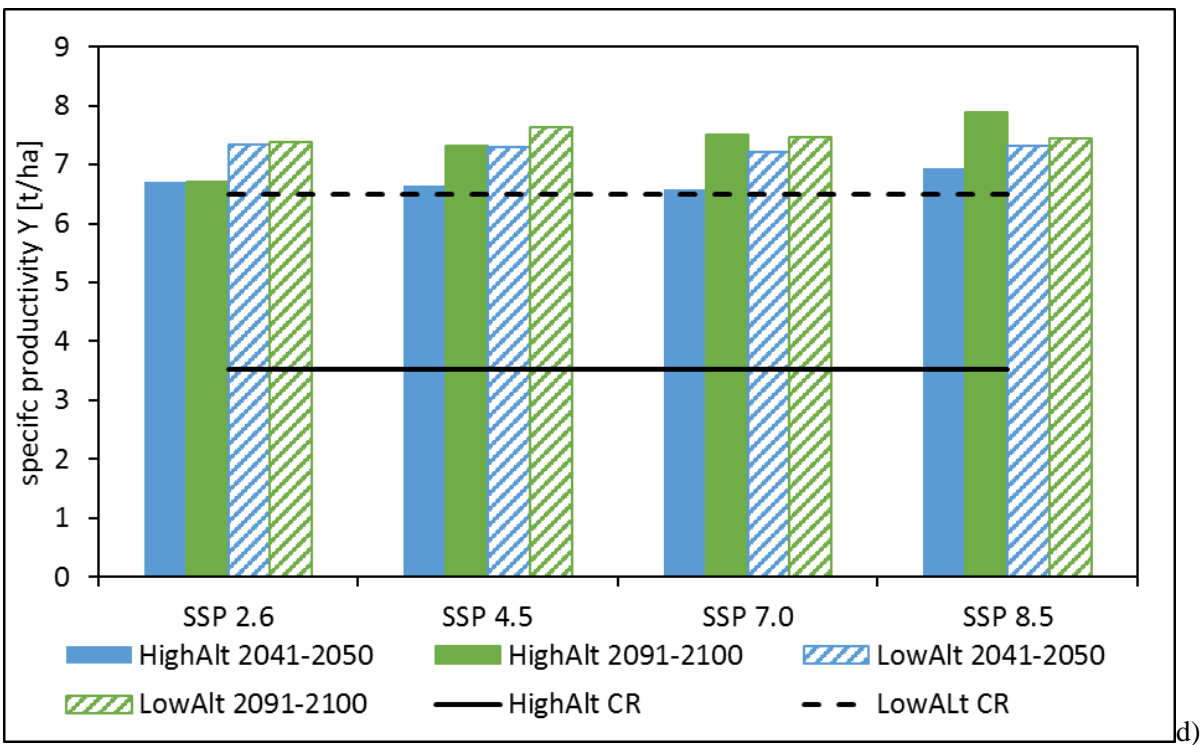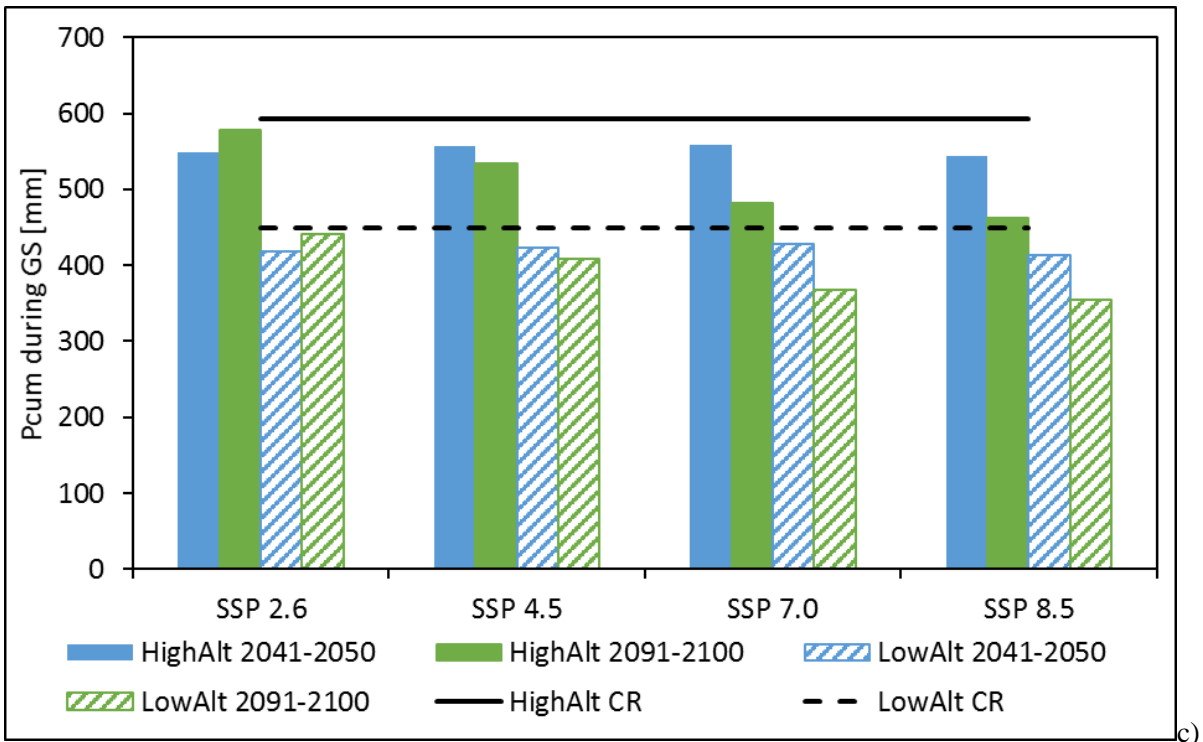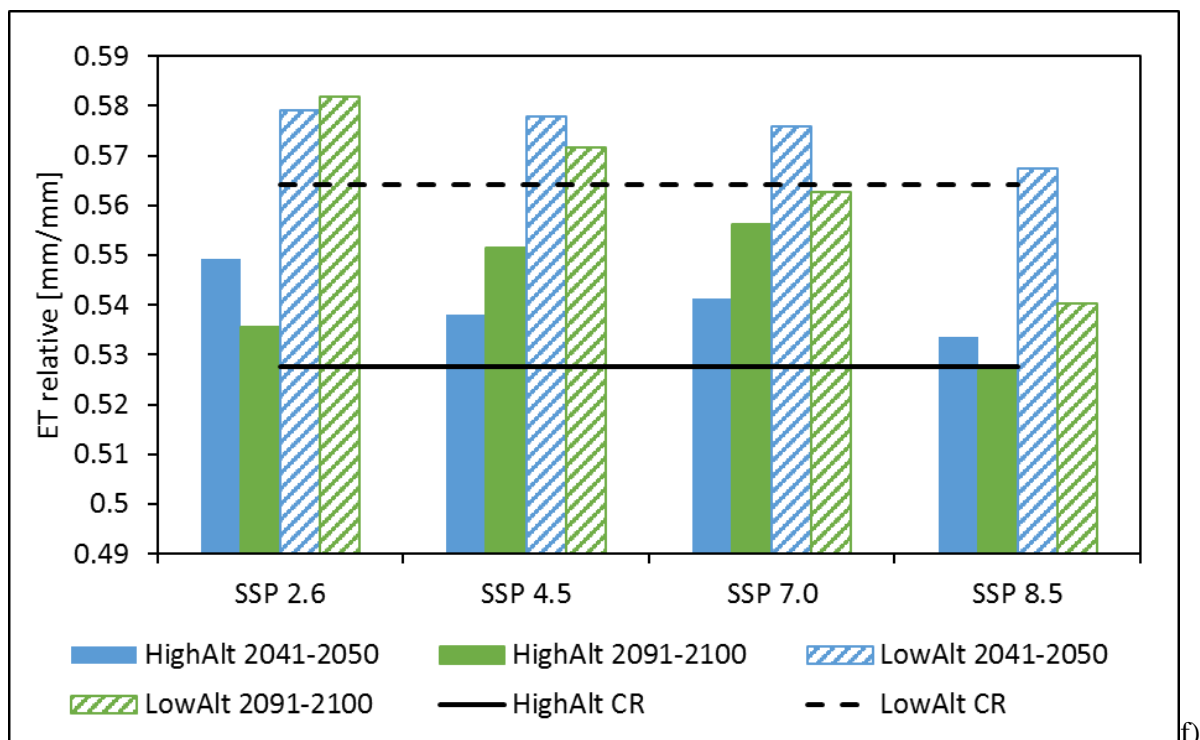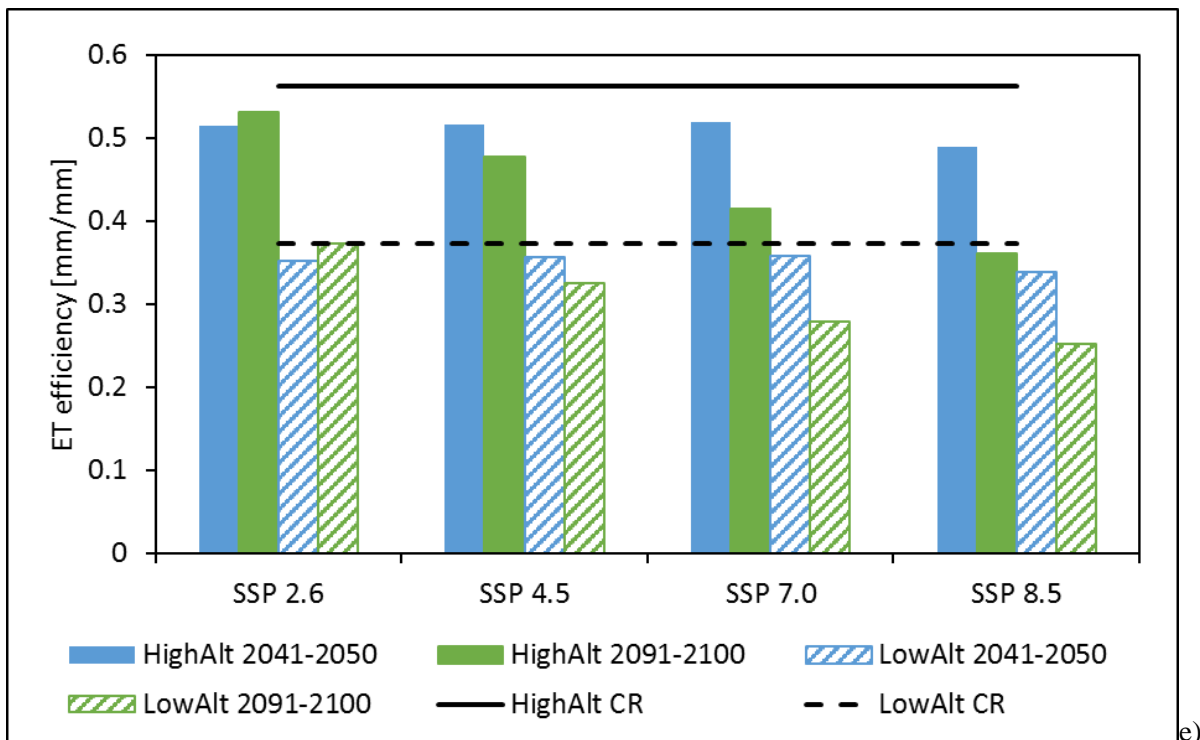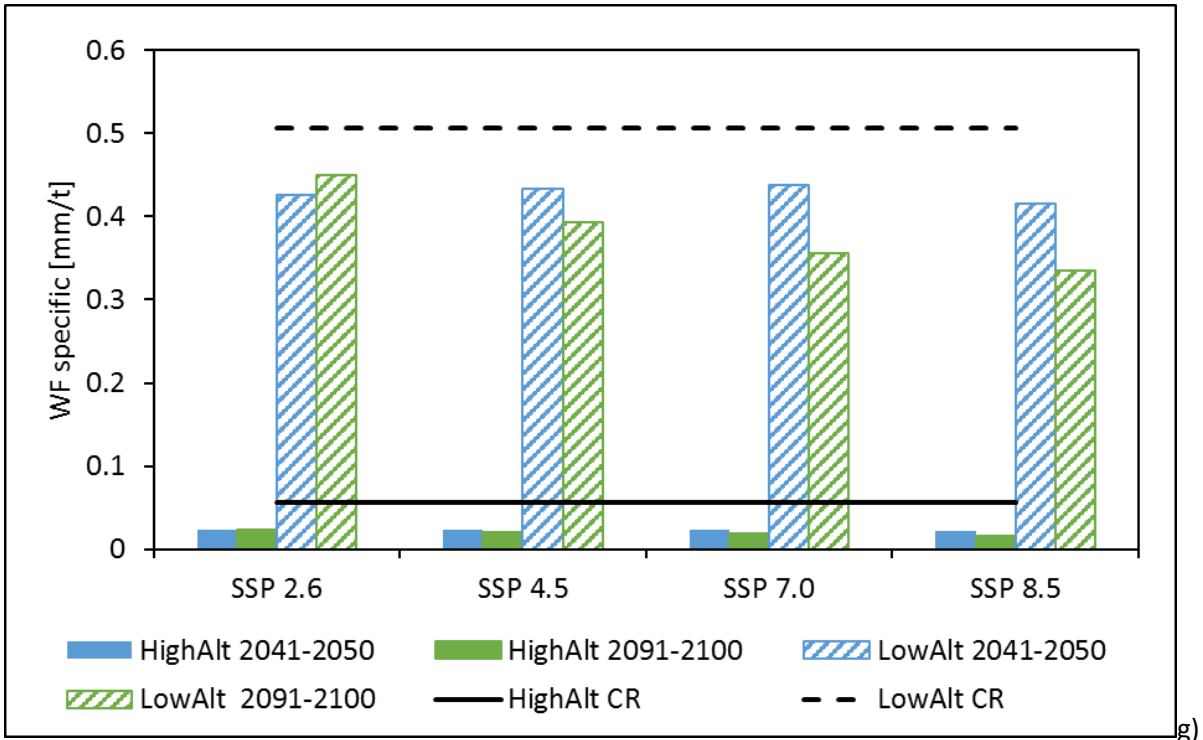
Figure 55: Future projections and comparison with CR period of agroclimatic indices AIs in Gran Paradiso National Park study area. For each SSP scenario the average is done between GCMs. In the graphs the results for *HighAlt* (plain color) and *LowAlt* (lines) and for *P1* (blue) and *P2* (green) are reported. AIs are: AI2 heat waves frequency (a), AI3 number of days with P larger than 10 mm (b), AI4 cumulated P during GS (c), AI5 total productivity (d), AI6 evapotranspiration efficiency (e), AI7 relative evapotranspiration (f), AI8 specific water footprint (g).

7 CONCLUSION

The principal outcome of the thesis work is the simulation of pasture growth in a wide area, with the possibility of considering the inter-specific competition. Even though it is at the expense of a detailed simulation of vegetation growth and of all the mechanisms that influence the biomass growth, the use of a distributed model, able to describe accurately the climate and the hydrology of a large alpine area, guarantees the simulation of pasture behaviour in a notable number of cells and, as a consequence, it is possible to find differences within a territory.

This could be an important information for the planning of alpine areas, whose economy depends for a considerable part on activities in pasture areas, to have a general overview of the future projections of pasture productivity in a valley or a region.

From the results of the simulation under climate projections, it is possible to highlight an increase of productivity in *HighAlt*, with similar values in two case study areas, Valtellina valley and Gran Paradiso National Park. In *LowAlt GPNP* presents lower values in terms of productivity with respect to *Valt*, but it is principally related to the higher average altitude of the considered area in *GPNP* with respect to *Valt*. Moreover in *Valt*, under 1100 m asl, a reduction in productivity is expected.

Generally, more suitable temperatures for growth are projected in *HighAlt*, while in *LowAlt* the excessive increase of temperature and of heat waves frequency causes a limitation to growth. The reduction of precipitation in Valtellina in *HighAlt* causes an increase of evapotranspiration and of *ET* efficiency (AI6), so more water from precipitation is used by vegetation to satisfy potential evapotranspiration and no water lack is found. In *GPNP* low values of *ET* efficiency (AI6) and of *ET* relative (AI7) highlight a probable lack of water and precipitation to satisfy the necessity.

It is confirmed also in other studies (see e.g. (Dibari et al., 2021)) that the increase of temperature can increase the productivity, especially in *HighAlt*, while the drought periods and the reduction of precipitation are causes of the potential reduction of pasture productivity.

The results of projections about inter-specific competition show an increase of more abundant species in both *LowAlt* and *HighAlt*. This is a sign of the reduction in biodiversity and species richness expected for the future (Dibari et al., 2021). Species that are more resistant to high temperature and drought condition, will be more inclined in colonizing pasture area. It is important to simulate the inter-specific competition to understand which species will be more abundant in the pasture areas because, in addition to the projected increase in total productivity,

the nutritional value and the liking of a species could influence the actual value of a pasture area for the animal feed consumption.

For example the increase of *Nardus stricta* at the expense of *Festuca rubra*, in *GPNP*, but in general also the increase in productivity in *HighAlt* in *Valt*, could be a problem for the usage of the pasture because of the low nutritional value of this species. As reported above, the presence of *Nardus stricta* is a consequence of the impoverishment of a pasture area. So, in spite of the increase of productivity, a larger share of *Nardus stricta* at the expense of other species is not a valuable consequence of climate change.

Another useful outcome of the study is the definition of agroclimatic indices that helps the analysis of the results and a deepened understanding of the reasons for a decrease/increase, more or less defined, of productivity. The definition of AIs basing on variables of climate and water availability gives the possibility to link directly the changes in pasture productivity with the climate projections, in this way it is easier to identify the causes of growth limitation, to find solutions, like irrigation or upward shift in pasture usage.

BIBLIOGRAPHY

Addimando, N., Nana, E., & Bocchiola, D. (2015). Modeling pasture dynamics in a mediterranean environment: case study in Sardinia, Italy. *Journal of Irrigation and Drainage Engineering*, *141*(5), 04014063. https://doi.org/10.1061/(ASCE)IR.1943-4774.0000818

Aili, T., Soncini, A., Bianchi, A., Diolaiuti, G., D'Agata, C., & Bocchiola, D. (2019). Assessing water resources under climate change in high-altitude catchments: a methodology and an application in the Italian Alps. *Theoretical and Applied Climatology*, *135*(1–2), 135–156. https://doi.org/10.1007/s00704-017-2366-4

Angus, J. F., Cunningham, R. B., Moncur, M. W., & Mackenzie, D. H. (1980). Phasic development in field crops I. Thermal response in the seedling phase. *Field Crops Research*, *3*, 365–378. https://doi.org/10.1016/0378-4290(80)90042-8

Arnell, N. W., & Freeman, A. (2021). The effect of climate change on agro-climatic indicators in the UK. *Climatic Change*, *165*(1–2), 1–26. https://doi.org/10.1007/s10584-021-03054-8

Arpa Lombardia. (2020a). *Portale Dati Idrologici*. https://www.arpalombardia.it/Pages/Acque-Superficiali/Quantita/Webgis.aspx?firstlevel=Quantità

Arpa Lombardia. (2020b). *Richiesta Dati Misurati | Tema meteorologia*.

Arpa Valle d'Aosta. (2020). *No Title*. https://www.arpa.vda.it/it/

Barcella, M., & Gusmeroli, F. (2018). *La gestione delle superfici pascolive. Linee guida per la gestione dei pascoli a nardo*.

Barnett, T. P., Adam, J. C., & Lettenmaier, D. P. (2005). Potential impacts of a warming climate on water availability in snow-dominated regions. *Nature*, *438*(7066), 303–309. https://doi.org/10.1038/nature04141

Baroni, C., Gennaro, S., Salvatore, M. C., Ivy-Ochs, S., Christl, M., Cerrato, R., & Orombelli, G. (2021). Last Lateglacial glacier advance in the Gran Paradiso Group reveals relatively drier climatic conditions established in the Western Alps since at least the Younger Dryas. *Quaternary Science Reviews*, *255*, 106815. https://doi.org/10.1016/J.QUASCIREV.2021.106815

Baroni, C., Salvatore, M. C., Alderighi, L., Gennaro, S., Zanoner, T., Carton, A., Zorzi, F., Giardino, M., Bertotto, S., & Perotti, L. (2015). The changing Italian glaciers. *Nextdata-Climate and Environmental Changes in the Italian Mountains*.

Battaglini, L., Bovolenta, S., Gusmeroli, F., Salvador, S., & Sturaro, E. (2014). Environmental

sustainability of Alpine livestock farms. *Italian Journal of Animal Science*, *13*(2), 431–443. https://doi.org/10.4081/ijas.2014.3155

Battaglini, L., Mimosi, A., Ighina, A., Lussiana, C., Malfatto, V. M., & Bianchi, M. (2003). Sistemi zootecnici alpini e produzioni legate al territorio. *Convegno SoZooAlp Il Sistema Delle Malghe Alpine: Aspetti Agro-Zootecnici, Paesaggistici e Turistici*, 42–52.

Bellini, E., Moriondo, M., Dibari, C., Bindi, M., Staglianò, N., Cremonese, E., Filippa, G., Galvagno, M., & Argenti, G. (2023). VISTOCK: A simplified model for simulating grassland systems. *European Journal of Agronomy*, *142*, 126647. https://doi.org/10.1016/J.EJA.2022.126647

Bellini, E., Moriondo, M., Dibari, C., Leolini, L., Staglianò, N., Stendardi, L., Filippa, G., Galvagno, M., & Argenti, G. (2023). Impacts of Climate Change on European Grassland Phenology: A 20-Year Analysis of MODIS Satellite Data. *Remote Sensing*, *15*, 218. https://doi.org/10.3390/rs15010218

Benestad, R. E., Hanssen-Bauer, I., & Chen, D. (2008). Empirical-statistical downscaling. *World Scientific Publishing Company*, 1–215. https://doi.org/10.1142/6908

Beniston, M. (2003). Climatic change in mountain regions: a review of possible impacts. *Climatic Change*, *59*(1), 5–31. https://doi.org/10.1023/A:1024458411589

Beniston, M., & Stoffel, M. (2014). Assessing the impacts of climatic change on mountain water resources. *Science of the Total Environment*, *493*, 1129–1137. https://doi.org/10.1016/j.scitotenv.2013.11.122

Bernués, A., Rodríguez-Ortega, T., Alfnes, F., Clemetsen, M., & Eik, L. O. (2015). Quantifying the multifunctionality of fjord and mountain agriculture by means of sociocultural and economic valuation of ecosystem services. *Land Use Policy*, *48*, 170–178. https://doi.org/10.1016/j.landusepol.2015.05.022

Beukes, P. C., Palliser, C. C., Macdonald, K. A., Lancaster, J. A. S., Levy, G., Thorrold, B. S., & Wastney, M. E. (2008). Evaluation of a whole-farm model for pasture-based dairy systems. *Journal of Dairy Science*, *91*(6), 2353–2360. https://doi.org/10.3168/jds.2007-0728

Bocchiola, D. (2014). Long term (1921-2011) hydrological regime of Alpine catchments in Northern Italy. *Advances in Water Resources*, *70*, 51–64. https://doi.org/10.1016/j.advwatres.2014.04.017

Bocchiola, D. (2015). Impact of potential climate change on crop yield and water footprint of rice in the Po valley of Italy. *Agricultural Systems*, *139*, 223–237. https://doi.org/10.1016/j.agsy.2015.07.009

Bocchiola, D., Brunetti, L., Soncini, A., Polinelli, F., & Gianinetto, M. (2019). Impact of climate change on agricultural productivity and food security in the Himalayas: a case study in Nepal. *Agricultural Systems*, *171*, 113–125. https://doi.org/10.1016/j.agsy.2019.01.008

Bocchiola, D., Diolaiuti, G., Soncini, A., Mihalcea, C., D'Agata, C., Mayer, C., Lambrecht, A., Rosso, R., & Smiraglia, C. (2011). Prediction of future hydrological regimes in poorly gauged high altitude basins: the case study of the upper Indus, Pakistan. *Hydrology and Earth System Sciences*, *15*, 2059–2075. https://doi.org/10.5194/hess-15-2059-2011

Bocchiola, D., & Groppelli, B. (2010). Spatial estimation of snow water equivalent at different dates within the Adamello Park of Italy. *Cold Regions Science and Technology*, *63*(3), 97–109. https://doi.org/10.1016/j.coldregions.2010.06.001

Bocchiola, D., Mihalcea, C., Diolaiuti, G., Mosconi, B., Smiraglia, C., & Rosso, R. (2010). Flow prediction in high altitude ungauged catchments: A case study in the Italian Alps (Pantano Basin, Adamello Group). *Advances in Water Resources*, *33*(10), 1224–1234. https://doi.org/10.1016/j.advwatres.2010.06.009

Bocchiola, D., Nana, E., & Soncini, A. (2013). Impact of climate change scenarios on crop yield and water footprint of maize in the Po valley of Italy. *Agricultural Water Management*, *116*, 50–61. https://doi.org/10.1016/j.agwat.2012.10.009

Bocchiola, D., & Rosso, R. (2007). The distribution of daily snow water equivalent in the central Italian Alps. *Advances in Water Resources*, *30*(1), 135–147. https://doi.org/10.1016/j.advwatres.2006.03.002

Bocchiola, D., & Soncini, A. (2017). Pasture modelling in mountain areas: the aase of Italian Alps, and Pakistani Karakoram. *Agricultural Research & Technology: Open Access Journal*, *8*(3), 1–8. https://doi.org/10.19080/artoaj.2017.08.555736

Bocchiola, D., Soncini, A., Senese, A., & Diolaiuti, G. (2018). Modelling hydrological components of the Rio Maipo of Chile, and their prospective evolution under climate change. *Climate*, *6*(3), 57. https://doi.org/10.3390/cli6030057

Bombelli, G. M., Soncini, A., Bianchi, A., & Bocchiola, D. (2019). Potentially modified hydropower production under climate change in the Italian Alps. *Hydrological Processes*, *33*(17), 2355–2372. https://doi.org/10.1002/hyp.13473

Boschetti, M., Bocchi, S., & Brivio, P. A. (2007). Assessment of pasture production in the Italian Alps using spectrometric and remote sensing information. *Agriculture, Ecosystems and Environment*, *118*(1–4), 267–272. https://doi.org/10.1016/j.agee.2006.05.024

Botter, M., Zeeman, M., Burlando, P., & Fatichi, S. (2021). Impacts of fertilization on grassland

productivity and water quality across the European Alps under current and warming climate: insights from a mechanistic model. *Biogeosciences*, *18*(6), 1917–1939. https://doi.org/10.5194/BG-18-1917-2021

Briner, S., Elkin, C., & Huber, R. (2013). Evaluating the relative impact of climate and economic changes on forest and agricultural ecosystem services in mountain regions. *Journal of Environmental Management*, *129*, 414–422. https://doi.org/10.1016/j.jenvman.2013.07.018

Briner, S., Elkin, C., Huber, R., & Grêt-Regamey, A. (2012). Assessing the impacts of economic and climate changes on land-use in mountain regions: A spatial dynamic modeling approach. *Agriculture, Ecosystems and Environment*, *149*, 50–63. https://doi.org/10.1016/j.agee.2011.12.011

Brunetti, M., Lentini, G., Maugeri, M., Nanni, T., Simolo, C., & Spinoni, J. (2009). 1961–1990 high-resolution Northern and Central Italy monthly precipitation climatologies. *Advances in Science and Research*, *3*(1), 73–78. https://doi.org/10.5194/asr-3-73-2009

Calanca, P., Deléglise, C., Martin, R., Carrère, P., & Mosimann, E. (2016). Testing the ability of a simple grassland model to simulate the seasonal effects of drought on herbage growth. *Field Crops Research*, *187*, 12–23. https://doi.org/10.1016/J.FCR.2015.12.008

Carletti, F., Michel, A., Casale, F., Burri, A., Bocchiola, D., Bavay, M., & Lehning, M. (2022). A comparison of hydrological models with different level of complexity in Alpine regions in the context of climate change. *Hydrology and Earth System Sciences*, *26*(13), 3447–3475. https://doi.org/10.5194/hess-26-3447-2022

Casale, F., & Bocchiola, D. (2022). Climate change effects upon pasture in the Alps: the case of Valtellina Valley, Italy. *Climate 2022, Vol. 10, Page 173*, *10*(11), 173. https://doi.org/10.3390/CLI10110173

Casale, F., Bombelli, G. M., Monti, R., & Bocchiola, D. (2020). Hydropower potential in the Kabul River under climate change scenarios in the XXI century. *Theoretical and Applied Climatology*, *139*(3–4), 1415–1434. https://doi.org/10.1007/s00704-019-03052-y

Casale, F., Fuso, F., Giuliani, M., Castelletti, A., & Bocchiola, D. (2021). Exploring future vulnerabilities of subalpine Italian regulated lakes under different climate scenarios: bottom-up vs top-down and CMIP5 vs CMIP6. *Journal of Hydrology: Regional Studies*, *38*, 100973. https://doi.org/10.1016/J.EJRH.2021.100973

Centro Funzionale Regione Autonoma Valle d'Aosta. (2020). *Portale Dati*. https://cf.regione.vda.it/portale_dati.php

Cherchi, A., Fogli, P. G., Lovato, T., Peano, D., Iovino, D., Gualdi, S., Masina, S., Scoccimarro,

E., Materia, S., Bellucci, A., & Navarra, A. (2019). Global Mean Climate and Main Patterns of Variability in the CMCC-CM2 Coupled Model. *Journal of Advances in Modeling Earth Systems*, *11*(1), 185–209. https://doi.org/10.1029/2018MS001369

Cho, M. A., Skidmore, A., Corsi, F., van Wieren, S. E., & Sobhan, I. (2007). Estimation of green grass/herb biomass from airborne hyperspectral imagery using spectral indices and partial least squares regression. *International Journal of Applied Earth Observation and Geoinformation*, *9*(4), 414–424. https://doi.org/10.1016/j.jag.2007.02.001

Confalonieri, R. (2014). CoSMo: a simple approach for reproducing plant community dynamics using a single instance of generic crop simulators. *Ecological Modelling*, *286*, 1–10. https://doi.org/10.1016/j.ecolmodel.2014.04.019

Confortola, G., Soncini, A., & Bocchiola, D. (2013). Climate change will affect hydrological regimes in the Alps. *Revue de Géographie Alpine*, *101*(3). https://doi.org/10.4000/rga.2176

Consorzio dell'Adda. (2020). *Dati Idrologici*. https://www.addaconsorzio.it/dati-idrologici/

Copernicus Land Monitoring Service. (2012). *Corine Land Cover*. https://land.copernicus.eu/pan-european/corine-land-cover/clc-2012

Coppola, E., Verdecchia, M., Giorgi, F., Colaiuda, V., Tomassetti, B., & Lombardi, A. (2014). Changing hydrological conditions in the Po basin under global warming. *Science of the Total Environment*, *493*, 1183–1196. https://doi.org/10.1016/j.scitotenv.2014.03.003

Corbari, C., Ravazzani, G., Martinelli, J., & Mancini, M. (2009). Elevation based correction of snow coverage retrieved from satellite images to improve model calibration. *Hydrology and Earth System Sciences*, *13*(5). https://doi.org/10.5194/hess-13-639-2009

Cullen, B. R., Johnson, I. R., Eckard, R. J., Lodge, G. M., Walker, R. G., Rawnsley, R. P., & McCaskill, M. R. (2009). Climate change effects on pasture systems in south-eastern Australia. *Crop and Pasture Science*, *60*(10), 933–942. https://doi.org/10.1071/CP09019

D'Agata, C., Bocchiola, D., Soncini, A., Maragno, D., Smiraglia, C., & Diolaiuti, G. (2018). Recent area and volume loss of Alpine glaciers in the Adda River of Italy and their contribution to hydropower production. *Cold Regions Science and Technology*, *148*, 172–184. https://doi.org/10.1016/j.coldregions.2017.12.010

D'Agata, C., Diolaiuti, G., Maragno, D., Smiraglia, C., & Pelfini, M. (2020). Climate change effects on landscape and environment in glacierized Alpine areas: retreating glaciers and enlarging forelands in the Bernina group (Italy) in the period 1954–2007. *Geology, Ecology, and Landscapes*, *4*(1), 71–86. https://doi.org/10.1080/24749508.2019.1585658

D'ottavio, P., & Ziliotto, U. (2003). Effect of different management on the production

characteristics of mountain permanent meadows. *Italian Journal of Animal Science*, *2*(sup1), 249–251. https://doi.org/10.4081/ijas.2003.11675976

Dale, V. H., & Polasky, S. (2007). Measures of the effects of agricultural practices on ecosystem services. *Ecological Economics*, *64*(2), 286–296. https://doi.org/10.1016/j.ecolecon.2007.05.009

Danabasoglu, G., Lamarque, J. F., Bacmeister, J., Bailey, D. A., DuVivier, A. K., Edwards, J., Emmons, L. K., Fasullo, J., Garcia, R., Gettelman, A., Hannay, C., Holland, M. M., Large, W. G., Lauritzen, P. H., Lawrence, D. M., Lenaerts, J. T. M., Lindsay, K., Lipscomb, W. H., Mills, M. J., … Strand, W. G. (2020). The Community Earth System Model Version 2 (CESM2). *Journal of Advances in Modeling Earth Systems*, *12*(2), e2019MS001916. https://doi.org/10.1029/2019MS001916

De Silva, M. S., Nachabe, M. H., Šimůnek, J., & Carnahan, R. (2008). Simulating root water uptake from a heterogeneous vegetative cover. *Journal of Irrigation and Drainage Engineering*, *134*(2), 167–174. https://doi.org/10.1061/(ASCE)0733-9437(2008)134:2(167)

Deléglise, C., Dodier, H., Garde, L., François, H., Arpin, I., & Nettier, B. (2019). A method for diagnosing summer mountain pastures' vulnerability to climate change, developed in the French Alps. *Https://Doi.Org/10.1659/MRD-JOURNAL-D-18-00077.1*, *39*(2), D27–D41. https://doi.org/10.1659/MRD-JOURNAL-D-18-00077.1

Denaro, S., Castelletti, A., Giuliani, M., & Characklis, G. W. (2018). Fostering cooperation in power asymmetrical water systems by the use of direct release rules and index-based insurance schemes. *Advances in Water Resources*, *115*, 301–314. https://doi.org/10.1016/j.advwatres.2017.09.021

Dibari, C., Argenti, G., Moriondo, M., Bindi, M., Michalk, D. L., Millar, G. D., Badgery, W. B., & Broadfoot, K. M. (2013). Data Integration and Modelling for the Assessment of Future Climate Change Impacts on Natural Pasturelands of the Alps. In D. L. Michalk, G. D. Millar, W. B. Badgery, & K. M. Broadfoot (Eds.), *XXII Interantional Grassland Congress* (pp. 1317–1318). New South Wales Department of Primary Industry.

Dibari, C., Costafreda-Aumedes, S., Argenti, G., Bindi, M., Carotenuto, F., Moriondo, M., Padovan, G., Pardini, A., Staglianò, N., Vagnoli, C., & Brilli, L. (2020). Expected changes to alpine pastures in extent and composition under future climate conditions. *Agronomy*, *10*(7), 926. https://doi.org/10.3390/agronomy10070926

Dibari, C., Pulina, A., Argenti, G., Aglietti, C., Bindi, M., Moriondo, M., Mula, L., Pasqui, M., Seddaiu, G., & Roggero, P. P. (2021). Climate change impacts on the Alpine, Continental

and Mediterranean grassland systems of Italy: A review. *Italian Journal of Agronomy*, *16*(3), 1843.

Diolaiuti, G., Bocchiola, D., D'agata, C., & Smiraglia, C. (2012). Evidence of climate change impact upon glaciers' recession within the Italian Alps: the case of Lombardy glaciers. *Theoretical and Applied Climatology*, *109*(3), 429–445. https://doi.org/10.1007/s00704-012-0589-y

Diolaiuti, G., Maragno, D., D'Agata, C., Smiraglia, C., & Bocchiola, D. (2011). Glacier retreat and climate change: documenting the last 50 years of alpine glacier history from area and geometry changes of dosdè piazzi glaciers (Lombardy Alps, Italy). *Progress in Physical Geography*, *35*(2), 161–182. https://doi.org/10.1177/0309133311399494

Döscher, R., Acosta, M., Alessandri, A., Anthoni, P., Arsouze, T., Bergman, T., Bernardello, R., Boussetta, S., Caron, L. P., Carver, G., Castrillo, M., Catalano, F., Cvijanovic, I., Davini, P., Dekker, E., Doblas-Reyes, F. J., Docquier, D., Echevarria, P., Fladrich, U., … Zhang, Q. (2022). The EC-Earth3 Earth system model for the Coupled Model Intercomparison Project 6. *Geoscientific Model Development*, *15*(7), 2973–3020. https://doi.org/10.5194/GMD-15-2973-2022

Duratorre, T., Bombelli, G. M., Menduni, G., & Bocchiola, D. (2020). Hydropower potential in the Alps under climate change scenarios. The Chavonne Plant, Val D'Aosta. *Water*, *12*(7), 2011. https://doi.org/10.3390/w12072011

Earthdata. (2019). *ASTER Global Digital Elevation Model v003*. https://www.earthdata.nasa.gov/news/new-aster-gdem

Egarter Vigl, L., Tasser, E., Schirpke, U., & Tappeiner, U. (2017). Using land use/land cover trajectories to uncover ecosystem service patterns across the Alps. *Regional Environmental Change*, *17*(8), 2237–2250. https://doi.org/10.1007/s10113-017-1132-6

Erfini, R. (2017). *Analisi dello stato gestionale dei prati della Val Grosina e delle potenzialità foraggere del Comune di Grosio*. Università degli Studi di Milano.

European Environemntal Agency. (2009). Regional climate change and adaptation. *Report EEA No. 8/2009*, *8*(8), 148.

Eyring, V., Bony, S., Meehl, G. A., Senior, C., Stevens, B., Stouffer, R. J., & Taylor, K. E. (2015). Overview of the Coupled Model Intercomparison Project Phase 6 (CMIP6) experimental design and organisation. *Geoscientific Model Development Discussions*, *9*(5), 1937–1958. https://doi.org/10.5194/gmdd-8-10539-2015

Faccioni, G., Sturaro, E., Ramanzin, M., & Bernués, A. (2019). Socio-economic valuation of abandonment and intensification of Alpine agroecosystems and associated ecosystem

services. *Land Use Policy*. https://doi.org/10.1016/j.landusepol.2018.10.044

Fatichi, S., Ivanov, V. Y., & Caporali, E. (2012). A mechanistic ecohydrological model to investigate complex interactions in cold and warm water-controlled environments: 1. Theoretical framework and plot-scale analysis. *Journal of Advances in Modeling Earth Systems*, *4*(2), 5002. https://doi.org/10.1029/2011MS000086

Fatichi, S., Pappas, C., & Ivanov, V. Y. (2016). Modeling plant–water interactions: an ecohydrological overview from the cell to the global scale. *Wiley Interdisciplinary Reviews: Water*, *3*(3), 327–368. https://doi.org/10.1002/WAT2.1125

Fatichi, S., Zeeman, M. J., Fuhrer, J., & Burlando, P. (2014). Ecohydrological effects of management on subalpine grasslands: From local to catchment scale. *Water Resources Research*, *50*(1), 148–164. https://doi.org/10.1002/2013WR014535

Filippa, G., Cremonese, E., Galvagno, M., Bayle, A., Choler, P., Bassignana, M., Piccot, A., Poggio, L., Oddi, L., Gascoin, S., Costafreda-Aumedes, S., Argenti, G., & Dibari, C. (2022). On the distribution and productivity of mountain grasslands in the Gran Paradiso National Park, NW Italy: A remote sensing approach. *International Journal of Applied Earth Observation and Geoinformation*, *108*, 102718. https://doi.org/10.1016/J.JAG.2022.102718

Fragnière, Y., Gremaud, J., Pesenti, E., Bétrisey, S., Petitpierre, B., Guisan, A., & Kozlowski, G. (2022). Mapping habitats sensitive to overgrazing in the Swiss Northern Alps using habitat suitability modeling. *Biological Conservation*, *274*, 109742. https://doi.org/10.1016/J.BIOCON.2022.109742

Fuso, F., Casale, F., Giudici, F., & Bocchiola, D. (2021). Future hydrology of the cryospheric driven Lake Como catchment in Italy under climate change scenarios. *Climate*, *9*(1), 8. https://doi.org/10.3390/cli9010008

García-Franco, J. L., Gray, L. J., & Osprey, S. (2020). The American monsoon system in HadGEM3 and UKESM1. *Weather and Climate Dynamics*, *1*(2), 349–371. https://doi.org/10.5194/wcd-1-349-2020

Gent, P. R., Danabasoglu, G., Donner, L. J., Holland, M. M., Hunke, E. C., Jayne, S. R., Lawrence, D. M., Neale, R. B., Rasch, P. J., Vertenstein, M., Worley, P. H., Yang, Z. L., & Zhang, M. (2011). The community climate system model version 4. *Journal of Climate*, *24*(19), 4973–4991. https://doi.org/10.1175/2011JCLI4083.1

Geoportale SCT. (2008). *Modello Digitale del Terreno*. https://geoportale.regione.vda.it/download/dtm/

Geoportale SCT. (2012). *Catasto ghiacciai della Valle d'Aosta*.

http://catastoghiacciai.partout.it/

Groppelli, B., Bocchiola, D., & Rosso, R. (2011). Spatial downscaling of precipitation from GCMs for climate change projections using random cascades: A case study in Italy. *Water Resources Research*, *47*(3). https://doi.org/10.1029/2010WR009437

Groppelli, B., Soncini, A., Bocchiola, D., & Rosso, R. (2011). Evaluation of future hydrological cycle under climate change scenarios in a mesoscale Alpine watershed of Italy. *Natural Hazards and Earth System Science*, *11*(6), 1769–1785. https://doi.org/10.5194/nhess-11-1769-2011

Gusmeroli, F. (2003). Il piano di pascolamento: strumento fondamentale per una corretta gestione del pascolo. *Convegno SoZooAlp Il Sistema Delle Malghe Alpine: Aspetti Agro-Zootecnici, Paesaggistici e Turistici*, 27–41.

Gusmeroli, F., Corti, M., Orlandi, D., Pasut, D., & Bassignana, M. (2005). Produzione e prerogative qualitative dei pascoli alpini : riflessi sul comportamento al pascolo e l'ingestione. *Convegno SoZooAlp L'alimentazione Della Vacca Da Latte Al Pascolo: Riflessi Zootecnici, Agroambientali e Sulla Tipicità Delle Produzioni*, 7–28.

Haeberli, W., & Beniston, M. (1998). Climate change and its impacts on glaciers and permafrost in the Alps. *Ambio*, 258–265. https://doi.org/10.2307/4314732

Haldemann, C., & Fuhrer, J. (2005). Interactive effects of CO2 and O3 on the growth of Trisetum flavescens and Trifolium pratense grown in monoculture or a bi-species mixture. *Journal of Crop Improvement*, *13*, 275–289. https://doi.org/10.1300/J411v13n01_13

Hazeleger, W., Wang, X., Severijns, C., Ştefănescu, S., Bintanja, R., Sterl, A., Wyser, K., Semmler, T., Yang, S., van den Hurk, B., van Noije, T., van der Linden, E., & van der Wiel, K. (2012). EC-Earth V2.2: description and validation of a new seamless earth system prediction model. *Climate Dynamics*, *39*(11), 2611–2629. https://doi.org/10.1007/s00382-011-1228-5

Hock, R. (2003). Temperature index melt modelling in mountain areas. *Journal of Hydrology*, *282*(1–4), 104–115. https://doi.org/10.1016/S0022-1694(03)00257-9

Huber, R., Briner, S., Peringer, A., Lauber, S., Seidl, R., Widmer, A., Gillet, F., Buttler, A., Le, Q. B., & Hirschi, C. (2013). Modeling social-ecological feedback effects in the implementation of payments for environmental services in pasture-woodlands. *Ecology and Society*, *18*(2). https://doi.org/10.5751/ES-05487-180241

Insua, J. R., Utsumi, S. A., & Basso, B. (2019a). Assessing and modeling pasture growth under different nitrogen fertilizer and defoliation rates in Argentina and the United States. *Agronomy Journal*, *111*(2), 702–713. https://doi.org/10.2134/AGRONJ2018.07.0438

Insua, J. R., Utsumi, S. A., & Basso, B. (2019b). Estimation of spatial and temporal variability of pasture growth and digestibility in grazing rotations coupling unmanned aerial vehicle (UAV) with crop simulation models. *PLOS ONE*, *14*(3), e0212773. https://doi.org/10.1371/JOURNAL.PONE.0212773

Istat. (2020). *Dati Agricoltura | Coltivazioni foraggere*. https://www.istat.it/it/agricoltura?dati

Johnson, I. R. (2008). *Biophysical pasture model documentation: model documentation for DairyMod, EcoMod and the SGS Pasture Model*.

Johnson, I. R., Chapman, D. F., Snow, V. O., Eckard, R. J., Parsons, A. J., Lambert, G. M., & Cullen, B. R. (2008). DairyMod and EcoMod: biophysical pasture-simulation models for Australia and New Zealand. *Australian Journal of Experimental Agriculture*, *48*, 621–631. https://doi.org/10.1071/EA07133

Kataoka, T., Tatebe, H., Koyama, H., Mochizuki, T., Ogochi, K., Naoe, H., Imada, Y., Shiogama, H., Kimoto, M., & Watanabe, M. (2020). Seasonal to decadal predictions with MIROC6: description and basic evaluation. *Journal of Advances in Modeling Earth Systems*, *12*(12), e2019MS002035. https://doi.org/10.1029/2019MS002035

Kurtogullari, Y., Rieder, N. S., Arlettaz, R., & Humbert, J. Y. (2020). Conservation and restoration of Nardus grasslands in the Swiss northern Alps. *Applied Vegetation Science*, *23*(1), 26–38. https://doi.org/10.1111/AVSC.12462

Life Pastoralp. (2019). *Pastures vulnerability and adaptation strategies to climate change impacts in the Alps Deliverable C . 1 Report on future climate scenarios for the two study areas*.

Liu, L., & Basso, B. (2017). Spatial evaluation of switchgrass productivity under historical and future climate scenarios in Michigan. *GCB Bioenergy*, *9*(8), 1320–1332. https://doi.org/10.1111/GCBB.12417

LP DAAC. (2020). *MODIS/Terra Leaf Area Index/FPAR 8-Day L4 Global 500 m SIN Grid (MOD15A2H v006)*. https://lpdaac.usgs.gov/products/mod15a2hv006/

Martinec, J. (1975). Snowmelt - runoff model for stream flow forecasts. *Hydrology Research*, *6*(3), 145–154. https://doi.org/https://doi.org/10.2166/nh.1975.0010

Martinec, J., & Rango, A. (1986). Parameter values for snowmelt runoff modelling. *Journal of Hydrology*, *84*(3–4), 197–219. https://doi.org/10.1016/0022-1694(86)90123-X

Maruffi, L., Stucchi, L., Casale, F., & Bocchiola, D. (2022). Soil erosion and sediment transport under climate change for Mera River, in Italian Alps of Valchiavenna. *Science of The Total Environment*, *806*, 150651. https://doi.org/10.1016/J.SCITOTENV.2021.150651

Mastrotheodoros, T., Pappas, C., Molnar, P., Burlando, P., Hadjidoukas, P., & Fatichi, S.

(2019). Ecohydrological dynamics in the Alps: insights from a modelling analysis of the spatial variability. *Ecohydrology*, *12*(1), 1–18. https://doi.org/10.1002/eco.2054

Mastrotheodoros, T., Pappas, C., Molnar, P., Burlando, P., Manoli, G., Parajka, J., Rigon, R., Szeles, B., Bottazzi, M., Hadjidoukas, P., & Fatichi, S. (2020). More green and less blue water in the Alps during warmer summers. *Nature Climate Change 2020 10:2*, *10*(2), 155–161. https://doi.org/10.1038/s41558-019-0676-5

Mauritsen, T., Bader, J., Becker, T., Behrens, J., Bittner, M., Brokopf, R., Brovkin, V., Claussen, M., Crueger, T., Esch, M., Fast, I., Fiedler, S., Fläschner, D., Gayler, V., Giorgetta, M., Goll, D. S., Haak, H., Hagemann, S., Hedemann, C., … Roeckner, E. (2019). Developments in the MPI-M Earth System Model version 1.2 (MPI-ESM1.2) and Its Response to Increasing CO2. *Journal of Advances in Modeling Earth Systems*, *11*(4), 998–1038. https://doi.org/10.1029/2018MS001400

Mazzocchi, C., Ruggeri, G., & Sali, G. (2018). The role of tourists for pastures resilience and agriculture sustainability in the Alps: a multivariate analysis approach. *Intervento Presentato Al 7. Convegno Evidence-Based Policies to Face New Challenges for Agri-Food Systems Tenutosi a Conegliano Nel 2018.*

McCall, D. G., & Bishop-Hurley, G. J. (2003). A pasture growth model for use in a whole-farm dairy production model. *Agricultural Systems*, *76*(3), 1183–1205. https://doi.org/10.1016/S0308-521X(02)00104-X

Mishra, S. K., & Singh, V. P. (2003). SCS-CN Method. In: Soil Conservation Service Curve Number (SCS-CN) Methodology. *Springer Science & Business Media*, *42*, 84–146. https://doi.org/10.1007/978-94-017-0147-1_2

Monks, D., SadatAsilan, K., & Moot, D. (2009). Cardinal temperatures and thermal time requirements for germination of annual and perennial temperate pasture species. *38th Agronomy Society Conference*. https://doi.org/10.13140/2.1.1455.4242

Monteiro, A. T., Fava, F., Hiltbrunner, E., Della Marianna, G., & Bocchi, S. (2011). Assessment of land cover changes and spatial drivers behind loss of permanent meadows in the lowlands of Italian Alps. *Landscape and Urban Planning*, *100*(3), 287–294. https://doi.org/10.1016/J.LANDURBPLAN.2010.12.015

Moot, D. J., Scott, W. R., Roy, A. M., & Nicholls, A. C. (2000). Base temperature and thermal time requirements for germination and emergence of temperate pasture species. *New Zealand Journal of Agricultural Research*, *43*(1), 15–25. https://doi.org/https://doi.org/10.1080/00288233.2000.9513404

Morgese, S. (2022). *Dinamica dei sistemi pascolivi multispecie montani in risposta ai*

cambiamenti climatici: il Gran Paradiso. Politecnico di Milano.

Movedi, E., Bellocchi, G., Argenti, G., Paleari, L., Vesely, F., Staglianò, N., Dibari, C., & Confalonieri, R. (2019). Development of generic crop models for simulation of multi-species plant communities in mown grasslands. *Ecological Modelling*, *401*, 111–128. https://doi.org/10.1016/j.ecolmodel.2019.03.001

Nana, E., Corbari, C., & Bocchiola, D. (2014). A model for crop yield and water footprint assessment: Study of maize in the Po valley. *Agricultural Systems*, *127*, 139–149. https://doi.org/10.1016/j.agsy.2014.03.006

National Snow and Ice Data Center. (2019). *MODIS/Terra Snow Cover Daily L3 Global 500m SIN Grid, Version 61 (MOD10A1)*. https://nsidc.org/data/mod10a1/versions/61#anchor-1

National Snow and Ice Data Center. (2020). *GLIMS: Global Land Ice Measurements from Space | GLIMS Glacier Database*. https://www.glims.org/

Nobakht, M., Beavis, P., O'Hara, S., Hutjes, R., & Supit, I. (2019). *Agroclimatic Indicators Product User Guide and Specification*.

Ohmura, A. (2001). Physical basis for the temperature-based melt-index method. *Journal of Applied Meteorology*, *40*(4), 753–761. https://doi.org/10.1175/1520-0450(2001)040<0753:PBFTTB>2.0.CO;2

Orsenigo, S. (2018). *I nardeti e l'habitat prioritario 6230*. Linee guida per la gestione dei pascoli a nardo*.

Parajka, J., & Blöschl, G. (2008). The value of MODIS snow cover data in validating and calibrating conceptual hydrologic models. *Journal of Hydrology*, *358*(3–4), 240–258. https://doi.org/10.1016/j.jhydrol.2008.06.006

Paul, F., Rastner, P., Azzoni, R. S., Diolaiuti, G., Fugazza, D., Le Bris, R., Nemec, J., Rabatel, A., Ramusovic, M., Schwaizer, G., & Smiraglia, C. (2020). Glacier shrinkage in the Alps continues unabated as revealed by a new glacier inventory from Sentinel-2. *Earth System Science Data*, *12*(3), 1805–1821. https://doi.org/10.5194/essd-12-1805-2020

Peel, M. C., Finlayson, B. L., & McMahon, T. A. (2007). Updated world map of the Köppen-Geiger climate classification. *Hydrology and Earth System Sciences*, *11*(5), 1633–1644. https://doi.org/10.5194/hess-11-1633-2007

Piani, C., Haerter, J. O., & Coppola, E. (2010). Statistical bias correction for daily precipitation in regional climate models over Europe. *Theoretical and Applied Climatology*, *99*(1–2), 187–192. https://doi.org/10.1007/s00704-009-0134-9

Piseddu, F., Martin, R., Movedi, E., Louault, F., Confalonieri, R., & Bellocchi, G. (2022). *Simulation of Multi-Species Plant Communities in Perturbed and Nutrient-Limited*

Grasslands: Development of the Growth Model ModVege. https://doi.org/10.3390/agronomy12102468

Raup, B., Racoviteanu, A., Khalsa, S. J. S., Helm, C., Armstrong, R., & Arnaud, Y. (2007). The GLIMS geospatial glacier database: a new tool for studying glacier change. *Global and Planetary Change*, *56*(1–2), 101–110. https://doi.org/10.1016/J.GLOPLACHA.2006.07.018

Rivington, M., Matthews, K. B., Buchan, K., Miller, D. G., Bellocchi, G., & Russell, G. (2013). Climate change impacts and adaptation scope for agriculture indicated by agro-meteorological metrics. *Agricultural Systems*, *114*, 15–31. https://doi.org/10.1016/j.agsy.2012.08.003

Rosso, R. (1984). Nash Model Relation to Horton Order Ratios. *Water Resources Research*, *20*(7), 914–920. https://doi.org/10.1029/WR020i007p00914

Rosso, R. (2004). Mappatura dell'indice di assorbimento e del massimo volume specifico di ritenzione potenziale del terreno. *ARPA Lombardia*.

Rottler, E., Kormann, C., Francke, T., & Bronstert, A. (2019). Elevation-dependent warming in the Swiss Alps 1981–2017: features, forcings and feedbacks. *International Journal of Climatology*, *39*(5), 2556–2568. https://doi.org/10.1002/joc.5970

Ruelle, E., Hennessy, D., & Delaby, L. (2018). Development of the Moorepark St Gilles grass growth model (MoSt GG model): a predictive model for grass growth for pasture based systems. *European Journal of Agronomy*, *99*, 80–91. https://doi.org/10.1016/J.EJA.2018.06.010

Sabatini, S., Argenti, G., Staglianò, N., & Targetti, S. (2008). *Caratterizzazione delle risorse pascolive in un ' area delle Alpi orientali in relazione ad alcuni parametri ecologici e gestionali. 1*.

Saxton, K. E., Rawls, W. J., Romberger, J. S., & Papendick, R. I. (1986). Estimating generalized soil water characteristics from texture. *Soil Science Society of America Journal*, *50*(4), 1031–1036. https://doi.org/https://doi.org/10.2136/sssaj1986.03615995005000040039x

Singh, P., Kumar, N., & Arora, M. (2000). Degree-day factors for snow and ice for Dokriani Glacier, Garhwal Himalayas. *Journal of Hydrology*, *235*(1–2), 1–11. https://doi.org/10.1016/S0022-1694(00)00249-3

Soncini, A., & Bocchiola, D. (2011). Assessment of future snowfall regimes within the italian alps using general circulation models. *Cold Regions Science and Technology*, *68*(3), 113–123. https://doi.org/10.1016/j.coldregions.2011.06.011

Soncini, A., Bocchiola, D., Azzoni, R. S., & Diolaiuti, G. (2017). A methodology for

monitoring and modeling of high altitude Alpine catchments. *Progress in Physical Geography*, *41*(4), 393–420. https://doi.org/10.1177/0309133317710832

Soncini, A., Bocchiola, D., Confortola, G., Bianchi, A., Rosso, R., Mayer, C., Lambrecht, A., Palazzi, E., Smiraglia, C., & Diolaiuti, G. (2015). Future hydrological regimes in the Upper Indus Basin: a case study from a high-altitude glacierized catchment. *Journal of Hydrometeorology*, *16*(1), 306–326. https://doi.org/10.1175/JHM-D-14-0043.1

Stendardi, L., Dibari, C., Bassignana, M., Bindi, M., Brilli, L., Choler, P., Cremonese, E., Filippa, G., Piccot, A., & Argenti, G. (2022). Pasture areas in the Gran Paradiso National Park. *Journal of Maps*, 1–12. https://doi.org/10.1080/17445647.2022.2120835

Stevens, B., Giorgetta, M., Esch, M., Mauritsen, T., Crueger, T., Rast, S., Salzmann, M., Schmidt, H., Bader, J., Block, K., Brokopf, R., Fast, I., Kinne, S., Kornblueh, L., Lohmann, U., Pincus, R., Reichler, T., & Roeckner, E. (2013). Atmospheric component of the MPI-M earth system model: ECHAM6. *Journal of Advances in Modeling Earth Systems*, *5*(2), 146–172. https://doi.org/10.1002/jame.20015

Stocker, T. F., Qin, D., Plattner, G.-K., Tignor, M. M. B., Allen, S. K., Boschung, J., Nauels, A., Xia, Y., Bex, V., Midgley, P. M., Alexander, L. V., Allen, S. K., Bindoff, N. L., Breon, F.-M., Church, J. A., Cubasch, U., Emori, S., Forster, P., Friedlingstein, P., … Wuebbles, D. (2013). *Climate change 2013. The physical science basis. Working Group I contribution to the Fifth Assessment Report of the Intergovernmental Panel on Climate Change - Abstract for decision-makers; Changements climatiques 2013. Les elements scientifiques. Contrib*.

Stöckle, C. O., Nelson, R., Donatelli, M., Yan, Y., Ferrer, F., Evert, F. Van, Mccool, D., Martin, S., Mulla, D., Bechini, L., & Deabaeke, P. (1994). *Cropping Systems Simulation Model User's Manual*. Washington State University Biological System Engineering Department.

Stucchi, L., Bombelli, G. M., Bianchi, A., & Bocchiola, D. (2019). Hydropower from the Alpine cryosphere in the era of climate change: the case of the Sabbione storage plant in Italy. *Water 2019, Vol. 11, Page 1599*, *11*(8), 1599. https://doi.org/10.3390/W11081599

Taylor, K. E., Stouffer, R. J., & Meehl, G. A. (2012). An overview of CMIP5 and the experiment design. *Bulletin of the American Meteorological Society*, *93*(4), 485–498. https://doi.org/10.1175/BAMS-D-11-00094.1

Tubiello, F. N., Soussana, J. F., & Howden, M. S. (2007). Crop and pasture response to climate change. *Proceedings of the National Academy of Sciences of the United States of America*, *104*(50), 19686–19690. https://doi.org/10.1073/pnas.0701728104

Valt, M., Chiambretti, I., & Dellavedova, P. (2014). Fresh snow density on the Italian Alps.

Geophysical Research Abstracts, 9715.

Van Der Wal, R., Madan, N., Van Lieshout, S., Dormann, C. F., Langvatn, R., & Albon, S. D. (2000). Trading forage quality for quantity? Plant phenology and patch choice by Svalbard reindeer. *Oecologia*, *123*(1), 108–115. https://doi.org/10.1007/s004420050995

van Oijen, M., Barcza, Z., Confalonieri, R., Korhonen, P., Kröel-Dulay, G., Lellei-Kovács, E., Louarn, G., Louault, F., Martin, R., Moulin, T., Movedi, E., Picon-Cochard, C., Rolinski, S., Viovy, N., Wirth, S. B., & Bellocchi, G. (2020). Incorporating biodiversity into biogeochemistry models to improve prediction of ecosystem services in temperate grasslands: Review and roadmap. *Agronomy*, *10*(2), 1–24. https://doi.org/10.3390/agronomy10020259

Wanner, A., Pröbstl-Haider, U., & Feilhammer, M. (2021). The future of Alpine pastures – Agricultural or tourism development? Experiences from the German Alps. *Journal of Outdoor Recreation and Tourism*, *35*, 100405. https://doi.org/10.1016/J.JORT.2021.100405

Zeeman, M. J., Mauder, M., Steinbrecher, R., Heidbach, K., Eckart, E., & Schmid, H. P. (2017). Reduced snow cover affects productivity of upland temperate grasslands. *Agricultural and Forest Meteorology*, *232*, 514–526. https://doi.org/10.1016/j.agrformet.2016.09.002

Zhu, Z., Bi, J., Pan, Y., Ganguly, S., Anav, A., Xu, L., Samanta, A., Piao, S., Nemani, R., & Myneni, R. (2013). Global Data Sets of Vegetation Leaf Area Index (LAI)3g and Fraction of Photosynthetically Active Radiation (FPAR)3g Derived from Global Inventory Modeling and Mapping Studies (GIMMS) Normalized Difference Vegetation Index (NDVI3g) for the Period 1981 to 2011. *Remote Sensing*, *5*(2). https://doi.org/10.3390/rs5020927

Ziliotto, U., Scotton, M., & Da Ronch, F. (2003). I pascoli alpini: aspetti ecologici e vegetazionali. *Convegno SoZooAlp Il Sistema Delle Malghe Alpine: Aspetti Agro-Zootecnici, Paesaggistici e Turistici*, 11–26.